การตรึงเอนไซม์ฮอสแรดิชเปอร์ออกซิเดสบนนาโนคอมพอสิต
ของซิลเวอร์และซิลิกาชนิดเมโซพอร์

นางสาว วิไลวรรณ ช่วยยก

วิทยานิพนธ์นี้เป็นส่วนหนึ่งของการศึกษาตามหลักสูตรปริญญาวิศวกรรมศาสตรดุษฎีบัณฑิต
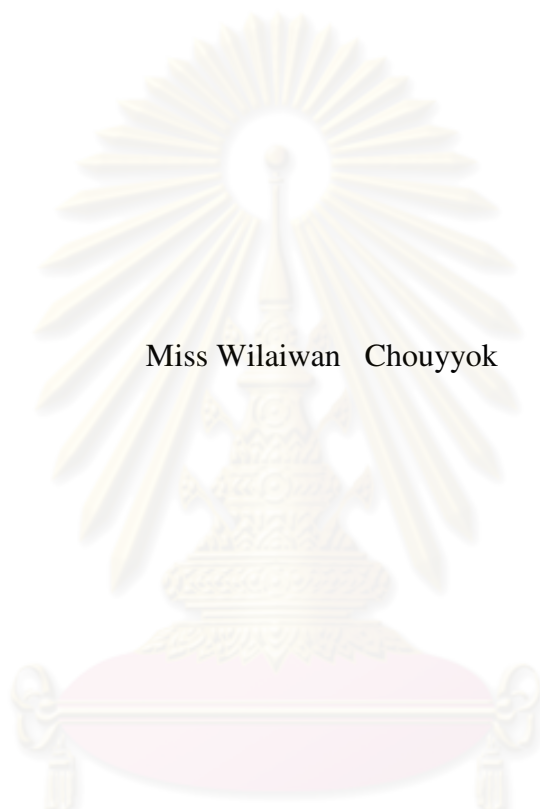สาขาวิชาวิศวกรรมเคมี   ภาควิชาวิศวกรรมเคมี
คณะวิศวกรรมศาสตร์   จุฬาลงกรณ์มหาวิทยาลัย
ปีการศึกษา 2551
ลิขสิทธิ์ของจุฬาลงกรณ์มหาวิทยาลัย

THE IMMOBILIZATION OF HORSERADISH PEROXIDASE ON
Ag/MESOPOROUS SILICA NANOCOMPOSITE

Miss Wilaiwan   Chouyyok

A Dissertation Submitted in Partial Fulfillment of the Requirements

for the Degree of Doctor of Engineering Program in Chemical Engineering

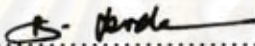Department of Chemical Engineering

Faculty of Engineering

Chulalongkorn University

Academic year 2008

Thesis Title	THE IMMOBILIZATION OF HORSERADISH PEROXIDASE ON Ag/MESOPOROUS SILICA NANOCOMPOSITE
By	Miss Wilaiwan Chouyyok
Field of Study	Chemical Engineering
Advisor	Associate Professor Seeroong Prichanont, Ph.D.
Co-Advisor	Assistant Professor Joongjai Panpranot, Ph.D.
	Chanchana Thanachayanant, Ph.D.

Accepted by the Faculty of Engineering, Chulalongkorn University in Partial Fulfillment of the Requirements for the Doctoral Degree

.... Dean of the Faculty of Engineering

(Associate Professor Boonsom Lerdhirunwong, Dr.Ing.)

THESIS COMMITTEE
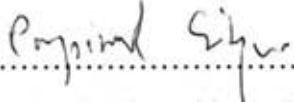
.... Chairman

(Associate Professor Muenduen Phisalaphong, Ph.D.)

.... Advisor

(Associate Professor Seeroong Prichanont, Ph.D.)

.... Co-Advisor

(Assistant Professor Joongjai Panpranot, Ph.D.)

.... Co-Advisor

(Chanchana Thanachayanant, Ph.D.)

.... Examiner

(Assistant Professor Bunjerd Jongsomjit, Ph.D.)

.... External Examiner

(Pornpimol Sritongkham, Ph.D.)

วิไลวรรณ ช่วยยก : การตรึงเอนไซม์ฮอสแรดิชเปอร์ออกซิเดสบนนาโนคอมพอสิตของ ซิลเวอร์และซิลิกาชนิดเมโซพอร์ (THE IMMOBILIZATION OF HORSERADISH PEROXIDASE ON Ag/MESOPOROUS SILICA NANOCOMPOSITE) อ. ที่ปรึกษา วิทยานิพนธ์หลัก : รศ. ดร. สีรุ้ง ปรีชานนท์, อ.ที่ปรึกษาวิทยานิพนธ์ร่วม : ผศ.ดร. ฐูงใจ ปั้นประณต, ดร. ชัญชนา ธนชยานนท์, 144 หน้า

วัสดุตรึงมีโซพอร์มีการนำไปใช้ศึกษาอย่างกว้างขวางในการตรึงเอนไซม์ และกำลังมีการประยุกต์ใช้ในงานไบโอเซนเซอร์เพิ่มขึ้น ด้วยคุณสมบัติ ที่น่าสนใจของวัสดุมีโซพอร์ งานวิจัยนี้จึงมีเป้าหมายที่จะศึกษาถึงอิทธิพลของวัสดุตรึงและพัฒนาต่อเพื่อให้เป็นวัสดุตรึงที่มีคุณสมบัติที่ดีสำหรับการตรึง เอนไซม์ และ นำไปใช้ในงานไบโอเซนเซอร์ ดังนั้นในส่วนแรกของงานวิจัยนี้ จึงศึกษาชนิดของวัสดุตรึงและภาวะในการตรึงเอนไซม์ ต่อการตรึงรูป เอนไซม์ฮอสแรดิชเปอรอกซิเดส (HRP, E.C. 1.11.1.17) โดยศึกษาอิทธิพลของพีเอชขณะตรึงรูปและคุณสมบัติรูพรุนของซิลิกาชนิดมีโซพอร์ ได้แก่ MCM-41, SBA-15, and MCF โดย MCM-41 และ SBA-15 เป็นรูปทรงแท่ง มีเส้นผ่านศูนย์กลางเฉลี่ย 32 และ 54 Å ตามลำดับ ในขณะที่ MCF มีรูปทรงกลมและ โครงกรอบขนาด 148 Å โดยปริมาณของหมู่ซิลานอล (silanol groups) ของวัสดุเหล่านี้มีปริมาณใกล้เคียงกัน ที่พีเอชในการตรึงรูปเท่ากับ 6 และ 8 พบว่า ปริมาณHRP ตรึงรูปอยู่บนวัสดุตรึงทุกชนิดเกือบ 100% และปริมาณการหลุดระของเอนไซม์จากวัสดุตรึงทุกชนิดมีน้อยสำคัญ อย่างไรก็ตามพบว่า MCF ซึ่งมี ขนาดรูพรุนใหญ่ที่สุด ทำให้ปริมาณที่ดูดซับและปริมาณการหลุดระของเอนไซม์มีค่าสูงสุดที่พีเอชเท่ากับ 10 กิจกรรมของเอนไซม์ตรึงรูป HRP มีค่าสูงสุด และต่ำสุดเมื่อตรึงรูปที่ พีเอช 8 และ 6 ตามลำดับ กิจกรรมของ HRP ตรึงรูป มีค่าเพิ่มขึ้นเมื่อขนาดรูพรุนของวัสดุมีขนาดใหญ่ขึ้น ดังนี้ MCM-41 < SBA-15 < MCF โดย HRP ที่ตรึงรูปที่พีเอช 8 มีเสถียรภาพในการเก็บรักษาสูงที่สุด (ทั้งที่อุณหภูมิ 4 องศาเซลเซียสและอุณหภูมิห้อง) แต่ให้ผลตรงกันข้ามกับค่าที่ พีเอช 6 นอกจากนี้ HRP ตรึงรูปบนวัสดุตรึง MCF มีเสถียรภาพในการเก็บรักษามากที่สุดด้วย การค้นพบนี้จึงเป็นประโยชน์ในการใช้งานด้าน ตัวเร่ง ปฏิกิริยาชีวภาพและไบโอเซนเซอร์

เพื่อเป็นการช่วยเพิ่มการถ่ายเทอิเล็กตรอน จึงทำการศึกษาการสังเคราะห์ซิลเวอร์ขนาดนาโนในวัสดุตรึง MCF และคาดว่าซิลเวอร์ขนาดนาโน จะช่วยเพิ่มให้คุณสมบัติของเอนไซม์ตรึงรูปดีขึ้น อย่างไรก็ตามการตรึงเอนไซม์ในวัสดุรูพรุนควรจะคำนึงถึงการถ่ายเทมวลสาร ดังนั้นซิลิกานาโนในพาวเดอร์ จึงใช้ในการศึกษาอิทธิพลของการถ่ายเทมวลสารต่อการตรึงเอนไซม์ควบคู่ไปพร้อมกับวัสดุตรึง MCF เพื่อความสะดวกในการสังเคราะห์ ซิลิกาขนาดนาโนใน จึงถูกใช้เป็นแบบจำลองในการรองรับซิลเวอร์ขนาดนาโนใน ดังนั้นงานวิจัยในส่วนที่สองจึงทำการศึกษาภาวะในการเตรียม Ag/SiO₂ นาโนคอมพอสิตด้วย วิธีการอัลตร้าซาว จากการสังเคราะห์ พบว่าเวลาในการดูดซับของซิลเวอร์ไอออนและความเข้มข้นของซิลเวอร์ในเครทมีอิทธิพลต่อจำนวนซิลเวอร์ขนาดนา โนอย่างมีนัยสำคัญ ใน ขณะที่มีผลต่อขนาดของซิลเวอร์ขนาดนาโนเพียงเล็กน้อยเท่านั้น เป็นที่น่าสนใจ ที่ขนาดและการกระจายของขนาดของซิลเวอร์ ขนาดนาโนแสดงให้เห็นชัดเจนว่าเวลาในการวีดิวซ์สามารถควบคุมขนาดของซิลเวอร์ขนาดนาโนได้ นอกจากนี้ยังพบว่าสาร 3-(aminopropyl) trialkoxysilane ซึ่งใช้ในการปรับพื้นผิวของวัสดุตรึงก็สามารถให้อิเล็กตรอนกับซิลเวอร์ไอออนได้ จากที่คาดว่าขนาดของซิลเวอร์ขนาดนาโนอาจจะมีผล ต่อการตรึงรูปเอนไซม์หรือการประยุกต์ทางด้านไบโอเซนเซอร์ซึ่งเป็นเป้าหมายของงานวิจัยนี้ ดังนั้นภาวะในการสังเคราะห์ที่ให้ความแตกต่างของขนาด ของซิลเวอร์ขนาดนาโนใน จึงถูกนำไปใช้ในการสังเคราะห์ Ag/MCF โดย Ag/MCF จะถูกสังเคราะห์ด้วยที่เวลาในการวีดิวซ์ 2 และ 8 ชั่วโมง และคงความ เข้มข้นของซิลเวอร์ในเครท ที่ 2000 ppm และเวลาในการดูดซับ 12 ชั่วโมง

ประสบความสำเร็จในการสังเคราะห์ Ag/MCF ที่ภาวะในการสังเคราะห์เดียวกับ Ag/SiO₂ พบว่าเวลาทั้งสองของการวีดิวซ์ให้ขนาดเฉลี่ยของ ซิลเวอร์ขนาดนาโนซึ่งเกาะอยู่ในรูพรุนของ MCFใกล้เคียงกัน คือ 5 nm การประยุกต์ใช้งานสำหรับการตรึงรูปเอนไซม์นั้น วัสดุตรึงที่แตกต่างกันของชนิด MCF และของชนิดซิลิกานาโนในพาวเดอร์ใช้ในการตรึงรูปเอนไซม์ HRP ซึ่งพบว่าวัสดุตรึงที่แตกต่างกันชนิด MCF ซึ่งมีพื้นที่ผิวมากจังคงมีบทบาทในการดูด ซับปริมาณเอนไซม์ ได้สูงถึงเกือบ 100 % อย่างไรก็ตามกิจกรรมของเอนไซม์ตรึงรูปยังคงมีค่าต่ำ ประมาณ 35 เปอร์เซนต์เมื่อเทียบกับเอนไซม์อิสระ ในทาง กลับกันเอนไซม์ตรึงรูปบนวัสดุที่แตกต่างชนิดซิลิกานาโนในพาวเดอร์ให้กิจกรรมสูงสุด ถึง 98% อย่างไรก็ตามพบว่าซิลเวอร์ขนาดนาโนในยับยั้งการทำงาน ของเอนไซม์บนวัสดุตรึงทั้งสองชนิดอย่างมีนัยสำคัญ นอกจากนี้ยังพบว่าการหลุดระของเอนไซม์ตรึงรูปยังคงสังเกตได้จากวัสดุตรึงเหล่านี้ สำหรับการใช้ ในงานไบโอเซนเซอร์ พบว่าซิลเวอร์ขนาดนาโนในมีบทบาทสำคัญในการเพิ่มอัตราการถ่ายเทอิเล็กตรอนที่พื้นผิวหน้าของอิเล็กโทรด โดยสามารถเพิ่มกระแส บนวัสดุตรึง MCFและ บนซิลิกานาโนในพาวเดอร์ จาก -2.9 μA เป็น -3.4 μA และ-2.0 μA เป็น - 3.4 μA ตามลำดับ จากผลการทดลองนี้เป็นการบ่งบอกว่า Ag/MCF และ Ag/SiO₂ เหมาะสมสำหรับการใช้งานหรือพัฒนาต่อเพื่อเป็นตัวรองรับสำหรับไบโอเซนเซอร์

ภาควิชา ....วิศวกรรมเคมี........ ลายมือชื่อนิสิต ....

สาขาวิชา ....วิศวกรรมเคมี........ ลายมือชื่อ อ. ที่ปรึกษาวิทยานิพนธ์หลัก.....................

ปีการศึกษา ....2551........ ลายมือชื่อ อ. ที่ปรึกษาวิทยานิพนธ์ร่วม.....................

ลายมือชื่อ อ. ที่ปรึกษาวิทยานิพนธ์ร่วม.....................

4771838021: MAJOR CHEMICAL ENGINEERING
KEYWORDS : ENZYME IMMOBILIZATION/ HORSERADISH PEROXIDASE/ MESOPOROUS SILICA /SILVER NANOPARTICLE/ NANOCOMPOSITE /SILVER NANOSIZE SNYTHESIS/ ULTRASONICATION/ BIOSENSOR

WILAIWAN CHOUYYOK: THE IMMOBILIZATION OF HORSERADISH PEROXIDASE ON Ag/MESOPOROUS SILICA NANOCOMPOSITE. ADVISOR: ASSOC. PROF. SEEROONG PRICHANONT, Ph.D., CO-ADVISORS: ASST. PROF. JOONGJAI PANPRANOT, Ph.D., CHANCHANA THANACHAYANANT, Ph.D., 144 pp.

The ordered mesoporous materials (OMMs) have been widely investigated for enzyme immobilization, and also growing in biosensor applications. With interesting feathers of OMMs, this thesis was aimed to investigate the influence of OMMs, as well as to develop OMMs to be the good carrier for enzyme immobilization and biosensor application. Therefore, the suitable OMMs and pH for immobilization were studied in the first part of this thesis. MCM-41, SBA-15, and MCF, were simultaneously investigated for the immobilization of horseradish peroxidase (HRP; E.C. 1.11.1.7). MCM-41 and SBA-15 were rod-like with respective average pore diameters of 32, and 54 Å, while that of MCF with spherical cell and frame structure was 148 Å. Moreover, these materials synthesized were of identical surface functional groups and similar contents of free silanol groups. At immobilization pH 6 and 8 almost 100% HRP loadings were obtained and in significant leaching were observed for all types of supports. However, MCF was found to give both the highest enzyme loading and leaching at pH 10. Maximum and minimum HRP activities were obtained at respectively immobilization pH 8, and 6. Activities of immobilized HRP increased with support pore diameters in the order: MCM-41 < SBA-15 < MCF. HRP immobilized at pH 8 gave the highest storage stability (both at 4°C and room temperature), and in opposition to pH 6. In addition, HRP immobilized in MCF was found to be the most stable under storage. The finding should be useful for the creation of biocatalysts and biosensors. Therefore, MCF was further developed to aim as a biocarrier for biosensor application in this work.

Silver nanoparticle was synthesized on MCF to enhance the electron transfer and it was expected to improve the properties of immobilized HRP. However, in the enzyme immobilization onto the pore of carrier, the mass transfer must be considered. Therefore, silica nanopowder was used in parallel to investigate mass transfer affecting HRP immobilization with MCF. For convenience, silica nanopowder was used as a model as a support of silver nanoparticles. Therefore, the synthesis conditions of Ag/SiO$_2$ nanocomposite by ultrasonication method were investigated in the second part of this thesis. Following the synthesis, the results showed that the adsorption time and silver precursor concentration significantly affected the number of silver nanoparticles. On the other hand, those synthesis parameters only slightly affected on the size of silver nanoparticles. Interestingly, the particle size and size distribution of the nanoparticles clearly showed that they could be controlled by the reduction time. Moreover, the functionalization reagent, (3-aminopropyl) trialkoxysilane was also found to act as an electron donor for the silver precursor. Since the sizes of silver nanoparticles were speculated to affect enzyme immobilization and biosensor application as the aim of this work. The synthesis conditions which showed the distinct size of silver nanoparticles were further used to synthesize Ag/MCF. Therefore, Ag/MCF was carried out under varying reduction time of 2 and 8 h, and fixing the silver nitrate concentration of 2000 ppm and adsorption time of 12 h.

Ag/MCF was achieved to synthesize in similar conditions as Ag/SiO$_2$. The average size of silver nanoparticles which were attached inside the pore of MCF of both reduction times was similar at 5 nm. For enzyme based application, the different MCF supports and different silica nanopowder support were used to immobilize HRP. It was found that, the large surface area of different MCF support play an important role in enzyme loading; almost 100% of HRP was immobilized. However, less activity of immobilized HRP was obtained, around 35% when compared to free enzyme. On the other hand, different silica nanopowder support provided the higher activity of immobilized HRP. The highest activity of immobilized HRP was obtained from MSPs; it was up to 98% when compared to free enzyme. It was found that the silver nanopartilces inhibited the activity of immobilized HRP. The enzyme leaching from both types of supports were still observed. For biosensor application, silver nanoparticles play an important role in electron transfer. Silver nanoparticles enhanced the currents of immobilized HRP at electrode surface modified with MCF and silica nanopowder from -2.9 µA to -3.4 µA, and -2.0 to -3.4 µA, respectively. This indicates that Ag/MCF and Ag/SiO$_2$ is suitable to further application or develop as the receptor of biosensor.

Department	Chemical Engineering	Student's Signature
Field of Study	Chemical Engineering	Advisor's Signature
Academic Year	2008	Co-Advisor's Signature
		Co-Advisor's Signature

ACKNOWLEDGEMENTS

CONTENTS

LIST OF TABLES

LIST OF FIGURES

CHAPTER I

INTRODUCTION

In recent years, the development and application of mesoporous materials have been a core research of porous material. Mesoporous materials have the pore diameter 2-50 nm, which is the subset of nanostructured materials. They possess unique surface, structural, and bulk properties [1]. Resulting in their important uses in many fields such as environmental separation, clean energy production and storage, catalysis and photocatalysis, sensor and actuators, biological application including biosensor, and biomarker [1].

The mesoporous materials have been investigated for immobilization of enzyme for many years. Normally, enzyme immobilization aims to recover or reuse the expensive enzyme. Recently, the immobilization of enzyme on mesoporous materials advances to apply to biological field for other aims, such as for increasing the amount of adsorbed enzyme on the electrode surface of biosensor. Among these materials, the ordered mesoporous materials (OMMs) offer the many advantages for enzyme immobilization. Their pore diameters is in the range of nanometers (1-300 Å), which is matched to the size of many biomolecules [1-2]. Ordered mesoporous materials provide high surface area and pore volume to permit the high enzyme loading, and also the substrate and product diffusion through the pores. The ordered structure and controllable pore properties offer the real possibility for enzyme immobilization. In particular, the surface properties can be modified by functionalization to improve the immobilized enzyme properties with pore space retaining [3]. Additionally, they stable to chemical and mechanical, and resistant to enzyme attack [4].

MCM-41, SBA-15 and MCF are ordered mesoporous material based silica, as well known as mesoporous silicates, that has been widely studied for biomolecular immobilization [4-13] MCM-41 and SBA-15 possess the cylindrical hexagonal

structure while MCF has spherical cells and frame structure. Due to different template and/or synthesis conditions, these mesoporous silicates are of different pore sizes, surface areas, and surface charges. Thus, different immobilized enzyme activities and stability on these supports are undoubtedly expected.

It was found that enzyme immobilization on mesoporous silicates can be simply achieved by physical adsorption which has the least effect on enzyme structures compared to other methods such as covalent bonding [6]. In addition, the existence of silanol groups on mesoporous silicas surface possibly helps enhancing physical adsorption of enzymes via hydrogen bonding [7]. It is generally reported that factors influencing enzyme immobilization are a pore diameter [4-5, 7, 14], and surface characteristics of mesoporous silicates [5, 10-12]. Specifically, excellent thermal stability and high enzyme activities can be obtained when average support pore diameter matches that of enzyme molecular size.

Horseradish peroxidase (HRP, EC 1.11.1.7) was used as a model enzyme in this study due to its wide applications. HRP is a catalyst for oxidative reactions of many chemicals, for instance, phenols and polyphenols (i.e. phenolic acid, flavonoids, and tannins) [12, 13, 14]. Therefore, it has been used to verify contaminants in food and waste water from oil industry, paints, polymer, and drug factories [15], and to indicate the amounts of antioxidant compounds in food and beverages [16-17]. For HRP immobilization on mesoporous silicates, Diaz and Bulkus [6] reported that the amount of various proteins adsorbed on MCM-41 depended on their molecular sizes, thus HRP with relatively large molecular diameter was less adsorbed. Moreover, it was found that the amount of adsorbed HRP was higher on the supports synthesized from cationic surfactant (FSM-16 and MCM-41) than on nonionic surfactant (SBA-15) [2]. Some other factors such as pH [7, 11] and ionic strength [11, 18] of enzyme solution were also found to affect the degree of enzyme bonding on silica surface. For example, the maximum degree of protein bonding was observed at a pH closed to the protein's isoelectric point. However, the effect of pH on enzyme immobilization on Mesoporous silicates with different pore characters is still unclear.

Furthermore, as mention above that research of enzyme immobilization is growing to various applications. In this study, we aimed to apply the enzyme immobilization to biosensor field. However, it is well known that silica based material is a semiconductor, which is not a good material for electron transferring. Therefore, to improve the electron transfer rate at electrode surface of biosensor, noble metals nanoparticles such as gold and silver are promising nanomaterials for adding into carriers. Additionally, they can also increase enzyme loading because noble metals and protein have good adsorption interaction. However, there are only a few researched publications that applied noble metals into mesoporous silica in nanocomposites form as bioreceptor [19, 20].

Ultrasonication has been used in material synthesis, including the metal nanoparticles and nanocomposites [21-23]. There are several advantages to using this method. It is simple method, and the synthesized mechanism is well known. It provides a pure phase because water is the only electron donor. The size and morphology of the nanoparticles were then easier to control [21]. Ultrasound radiation yielded smaller particles, higher specific surface [23-24], and more uniform distribution dispersion of the nanoparticles [25]. Additionally, it provides a narrower size distribution than the thermal method [21]. However, the effects of operating conditions of Ag/mesoporous silica nanocomposite, such as the effects of silver precursor adsorption time, and ultrasonic irradiation time have been not published.

This dissertation was divided into 6 chapters starting with this introduction. The second chapter covers the knowledge related to the background of formation and characterization of mesoporous silica material, method and parameter of enzyme immobilization, and biosensor. The influential parameters of enzyme immobilization as another core technology employed in this study are also described. The third chapter contains the literature review of the field of enzyme immobilization on mesoporous silica materials. The influences of functionalization of mesoporous silica materials with organosilanes, and the methods of metal nanoparticles synthesis on mesoporous silica materials, and biosensor application were reviewed. The fourth

chapter explains the experimental procedures and the techniques use to synthesize the nanomaterials, enzyme immobilization and the analytical methods.

Chapter 5 contains the 3 parts of the results and discussions. Part 1 covers the immobilization of HRP on various mesoporous silicas (MCM-41, SBA-15, and MCF) with the adsorption method. Influential parameters to enzyme immobilization which were surface properties under various pH of enzyme solution and pore size with different mesoporous silicas are studied. Suitable support was selected based on loading, leaching, activity, and storage stability of immobilized enzyme.

Part 2 describes the use of silica nanopowder to model how the selected support is developed to improve the electron transfer rate by adding silver nanoparticles. To investigate effects of operating conditions on synthesized Ag/SiO$_2$ nanocomposite in order to understand the mechanism and be able to tailor-made the required nanocomposite characteristics. To our knowledge, no other work has investigated effects of silver precursor adsorption time, and ultrasonic irradiation time on the syntheses of Ag/SiO$_2$ nanocomposites. The results from this work was be useful for controlling silver nanoparticles on selected support nanocomposite (Ag/mesoporous silica) characteristics using synthesizing conditions.

Lastly, part 3 describes the synthesis of Ag/mesoporous silica following the conditions of Ag/SiO$_2$ from part 2. The conclusion the discussion by covering the HRP immobilization on Ag/SiO$_2$, Ag/mesoporous nanocomposite, and compares it with the absence of silver nanoparticles. The pore character and surface properties on loading, leaching, activity, and storage stability of immobilized enzyme were investigated. The biosensor application of electrode modified HRP immobilized Ag/SiO$_2$ and Ag/mesoporous silica nanocomposite were shown in the end.

Finally, Chapter 6 concludes the results of these experiments.

1.1 Objectives

1. To investigate the influence of various mesoporous silica supports on HRP immobilization
2. To develop mesoporous silica with good characteristics for bioreceptor application by adding silver nanoparticles

1.2 Scopes

1. To study structure and physical characteristic of MCM-41, SBA-15 and MCF

    1.1 structure and particle size were characterized by X-Ray Diffraction (XRD)

    1.2 pore size, pore volume and surface area were measured by adsorption and desorption of Nitrogen with Brunauer-Emmett-Teller (BET)

    1.3 pore structure and arrangement were obtained from Transmission Electron Microscopy (TEM)

2. To study the influence of immobilization parameters; pH and pore size. The good result can be considered from loading, leaching, activity and storage stability of immobilized enzyme

3. To study preparation conditions and characteristic of Ag/SiO_2

    - The effect of adsorption time of silver precursor

    - The effect of concentration of silver precursor

    - The effect of reduction time

    - The Ag/SiO2 was identified by UV-Vis spectrophotometer, the structure and shape of silver nanoparticles were characterized by XRD and TEM, the surface properties were measured by zetasizer nano

4. The Ag/MCF was synthesized in a similar condition as the conditions to synthesize Ag/SiO_2

5. Comparison of Ag/SiO_2 and Ag/MCF on enzyme immobilization can be based on loading, leaching, activity, and storage stability of immobilized enzyme, and current of biosensor

1.3 Expected benefits

1. To obtain the immobilized HRP on Ag/MPS which high activity and stability
2. To obtain a good feature of HRP bioreceptors

CHAPTER II

THERORETICAL BACKGROUND

In this chapter, related topics to the work carried out in this study are presented. The properties of HRP were introduced. The formation and properties of ordered mesoporous silica materials, and the methods for charateration were discussed briefly. Moreover, enzyme immobilization as another core technology employed in this study along with its influential parameters is also discussed in this chapter. As this study is aimed at development of bioreceptor in biosensor, introduction to biosensor is considered necessary and will be discussed at the end.

2.1 Horseradish peroxidase

Horseradish peroxidase (HRP, EC 1.11.1.7) is an oxidation enzyme which can be isolated from horseradish root and also obtained from other sources, such as bacteria, mold, plants, and animals [26]. The molecular weight of HRP molecule is approximate 44 KDa [2], and its approximate size is 64 and 37 Å of the long and short axes, respectively [27]. The other important properties are given in Table 2.1.

Table 2.1 The properties of soluble HRP [28]

Properties	
Structure	Glycoprotein with one mole of Protohaemin
Inhibitors	Cyanide, sulfide, fluoride, azide
Optimum pH	6.0-7.0
Optimum temperature	45 ℃
pH stability	5-10 (25 ℃, 20 h)
Thermal stability	Below 50 ℃ (pH 6, 10 min)

The reaction of HRP to analysis phenol (pyrogallol) [28]

$$2\text{Pyrogallol} + 3\text{H}_2\text{O}_2 \xrightarrow{\text{HRP}} \text{Purpurogallin} + 5\text{H}_2\text{O} + \text{CO}_2 \qquad (2.1)$$

HRP has been used to detected H_2O_2 in clinical analysis, verify phenol, and polyphenol in food and in waste water from factories [18, 29-30]. The HRP is also applied to polymer synthesis especially for phenolic resin synthesis, diagnostic assays, nucleic acid analysis, biosensors, bioremediations, and other biotechnological processes [31].

2.2 The ordered mesoporous silica materials

The International Union of Pure and Applied Chemistry (IUPAC) proposed to classify the porous material by using the internal pore width (diameter) as a criteria. They subdivided porous materials into 3 types; micropore (diameter <2 nm), mesopore (diameter 2-50 nm), and macropore (diameter >50 nm). Therefore, mesoporous materials are classified as nanoporous materials due to their diameters are in the range of nano size (1-100 nm) [1].

In early 1990s, the ordered mesoporous silica material (OMMs) with uniform pore sizes in mesoporous range, high surface area (~1000 m^2/g), and large pore volume (~ 1 cm^3/g) were recovered [32-33]. They have shown advantageous properties as carriers for immobilization of biomolecules, such as ordered, uniform, and adjustable pore sizes, large surface area, chemical and mechanical stability, and resistance to microbial attack [18, 34]. These materials possess affinities suitable for the physical adsorption of molecules, for example through hydrogen bonding, and may also be used as reactive points for the attachment of tethering functional groups [35]. Additionally, their pore sizes are suitable for the protein molecules and can accommodate enzymes within their long channels. Thus, they provide a higher density of enzyme loading and facilitate transport of substrate and product. [4, 18, 34]. Moreover, the open pore structure can be modified with organosilane groups to create a high potential entrapment of protein molecules [18].

Among these OMMs materials, FSM-16, MCM-41, MCM-48, SBA-15, and MCF have been extensively investigated for enzyme immobilization [2, 7, 35]. The pore size of FSM-16 and MCM-41 are essentially similar such as highly uniform, hexagonally arranged, on dimensional cylindrical pore [2, 32]. Moreover, their surface properties are also similar since they are both synthesized by using the cationic surfactant as a template [2]. MCM-48 possesses a three-dimensional bicontinuous cubic pore structure, while SBA-15 has similar pore structure as that of FSM-16 and MCM-41, but of SBA-15 are much bigger pore sizes of around 6-15 nm. Lastly, MCFs are synthesized from the protocol of SBA-15 by adding the oil in water and then use as template. In this research, MCM-41, SBA-15, and MCF with different pore sizes, pore structures, and surface properties were used to immobilize HRP. As a result, the details of synthesis parameters and their properties are given more in the sections below.

2.2.1   MCM-41

MCM-41 is a member of M41S which is divided into 3 groups depending on shape and size of the pores; (1) MCM-41 which has a hexagonal array, (2) MCM-48 with a cubic pore structure, and (3) MCM-50 with a lamellar structure. MCM-41 was discovered by the members of Mobile Corporation in 1992 [36]. It displays an ordered structure with uniform cylindrical mesopores arranged into hexagonal which has the pore thickness of 1-1.5 nm and the pore diameter range of 1.5-10 nm. MCM-41 has a large specific surface area of approximately 1,000 m^2g-1 [33]. These properties make MCM-41 interesting to be used as a support material for heterogeneous catalysts. However, MCM-41 is instable with mineralizing agents, i.e. hydroxide and fluoride ions. Due to these agents, MCM-41 is instable in aqueous solution with pH higher than 8. Their pore structures and sizes depend on various conditions (1) choice of template i.e. the length of the hydrophobic chain , hydrophilic head group, and counter ion, (2) choice of the swelling reagent i.e. 1,3,5-trimethylbenzene (TMB), and (3) reaction conditions i.e. pH, temperature, and composition.

The formation of M41S

The formation of M41S has been explained by Zhao et al. [37] as show in Figure 2.1. The structure and shape of M41S depends on the concentration of the surfactant used. At lower concentration, the surfactant energetically exists as monomolecule. With the concentration increasing, surfactant molecules aggregate together, and then form circular micelles in order to decrease the system entropy. The initial concentration threshold at which monoatomic molecules aggregate to form isotropic micelles is known as CMC (critical micellization concentration). As the concentration increases, hexagonal close packed array appears, producing the hexagonal phase. The next step in the process is the coalescence of the adjacent, mutually parallel cylinders to produce the lamellar phase. In some cases, the cubic phase is generally believed to consist of complex interwoven networks of rod-shaped aggregates [37].

Additionally, the formation of silica on rod-shaped of surfactant was shown as Figure 2.2 [38]. They proposed that there were 2 possible path ways for silica formation on the surfactant structure. In the first path way, silica molecules condense around ordered surfactant structure. While in the second path way, silica formed during the surfactant formation leading to form the ordered surfactant. The second path way has more possible tendency since it was found that Table 2.2 [39] different M41S structures are formed by varying the silicate concentration while maintaining constant surfactant concentration. Moreover, at high pH, silica exists as a complex mixture of molecular and polyanionic species. Therefore, the silicate anions participate in the surfactant organization process.
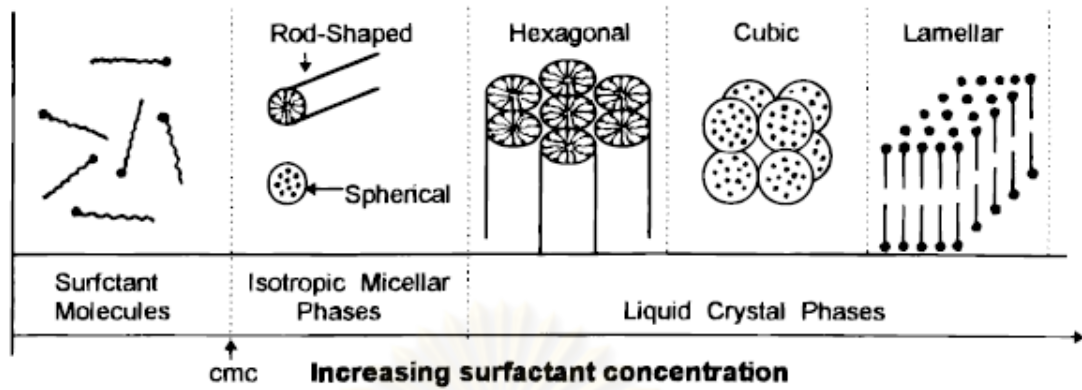
Figure 2.1 The formation of M41S with various surfactant concentrations [37]
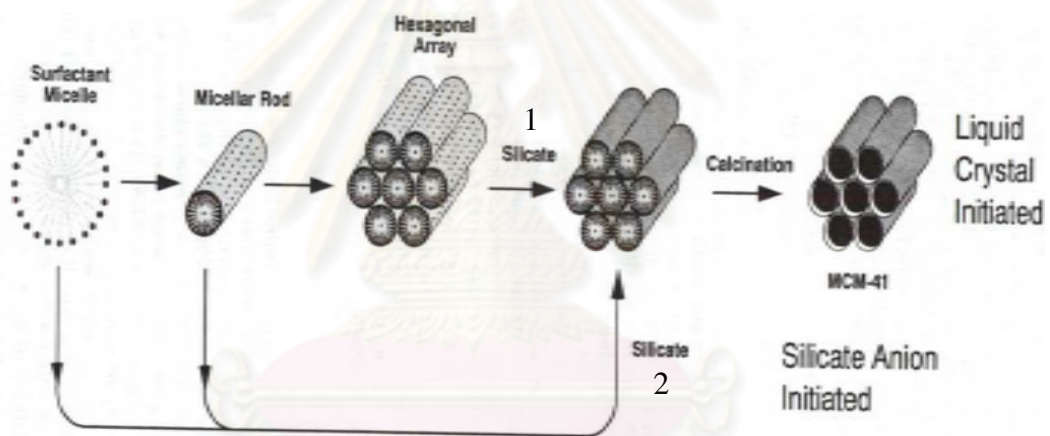
Figure 2.2 The formation path way of MCM-41 [38]

Table 2.2 Correlation between M41S and surfactant/silica mole ratios [39]

Surfactant/silica	M41S structure
<1.5	Hexagonal structure (MCM-41)
1.0-1.5	Cubic structure (MCM-48)
1.2-2.0	Thermally unstable materials
2.0	Cubic octamer [(CTMA)SiO$_2$.5]

2.2.2 SBA-15

SBA-15 is a family of highly ordered mesoporous silica structure. It has been synthesized by using nonionic triblock copolymer surfactant which has a category of poly(alkylene oxide) i.e. PEO-PPO-PEO [poly(ethylene oxide)-poly(proplylene oxide)-poly(ethylene oxide), P123] as a template. This polymer displays excellent interfacial stabilization properties such as mesostructural ordering, amphiphilic character, low-cost, commercially available, nontoxic, and biodegradable. SBA-15 has been prepared under acidic condition at room temperature. Nonionic triblock copolymer forms hexagonal mesoporous structure at these conditions. The pore diameter and wall thickness of SBA-15 are in the range of 40-120 Å [40] and 31-64 Å, respectively. Comparing with MCM-41, SBA-15 provides higher resistance and stability to thermal and pressure due to its thick pore wall [41]. Pore sizes and pore wall thickness of SBA-15 depend on temperature and thermal reaction time as shown in Table 2.3.

Table 2.3 The properties of SBA-15 prepared from poly(alkylene oxide) [41]

Block copolymer	Reaction temperature (°C)	d(100) (Å)	BET surface area (m^2/g)	Pore size (Å)	Pore volume (cm^3/g)	Wall thickness (Å)
EO$_5$PO$_{70}$EO$_5$	35	118(117)	630	100	1.04	35
EO$_{20}$PO$_{70}$EO$_{20}$	35	104(95.7)	690	47	0.56	64
EO$_{20}$PO$_{70}$EO$_{20}$	35, 80*	105(97.5)	780	60	0.80	53
EO$_{20}$PO$_{70}$EO$_{20}$	35, 80*[a]	103(99.5)	820	77	1.03	38
EO$_{20}$PO$_{70}$EO$_{20}$	35,90*	108(105)	920	85	1.23	36
EO$_{20}$PO$_{70}$EO$_{20}$	35,100*	105(104)	850	89	1.17	31
EO$_{17}$PO$_{55}$EO$_{17}$	40	97.5(80.6)	770	46	0.70	47
EO$_{20}$PO$_{30}$EO$_{20}$	60	77.6(77.6)	1000	51	1.26	39
EO$_{26}$PO$_{39}$EO$_{26}$	40	92.6(88.2)	960	60	1.08	42
EO$_{13}$PO$_{70}$EO$_{13}$	60	80.6(80.5)	950	59	1.19	34
EO$_{19}$PO$_{33}$EO$_{19}$	60	74.5(71.1)	1040	48	1.15	34

* reaction temperature was at 35 °C for 20 hours and then heating to the higher temperature was done for 24 hours

[a] heating to 80 °C for 48 hours

SBA-15 can be synthesized over a range of reaction compositions and conditions (Table 2.3). At higher reaction temperature or longer reaction time, both large pore sizes and pore volumes are obtained. However, these conditions give a thinner pore walls due to protonation or temperature dependent hydrophilicity of the PEO block of the copolymer under acidic synthesis conditions [41].

Comparing with PPO, PEO of triblock copolymer (PEO-PPO-PEO) has a stronger interaction with silica thus it is the part that attaches to the pore wall of inorganic support. However, when reaction temperature is increased, PEO block becomes more hydrophobic. As results, hydrophobic domain volumes are increased, larger pore size is obtained, and smaller lengths of PEO are segmented by silica wall. Moreover, the pore size of SBA-15 can be extended to 300 Å by increasing hydrophobic volume part of the self-assembled aggregates. This can be achieved by changing the copolymer composition, block size of polymer and adding the swelling agent such as TMB.

2.2.3 MCF

Mesocellular foam (MCF) is prepared by adding TMB in PEO-PPO-PEO triblocked copolymer mesostructure template. The MCF synthesis depends on mass ratios of TMB and surfactant as shown in Figure 2.3. The transition between hexagonal structured SBA-15 to MCF begins at TMB/surfactant mass ratios of 0.2-0.3. At TMB/surfactant mass ratio higher than 0.3, the transition of hexagonal to cubic shape is completed. Figure 2.4 shows the strong effect of TMB/surfactant mass ratios to SBA-15 and MCF formation that is with a small change of TMB/surfactant mass ratios, various pore sizes and structures are obtained.
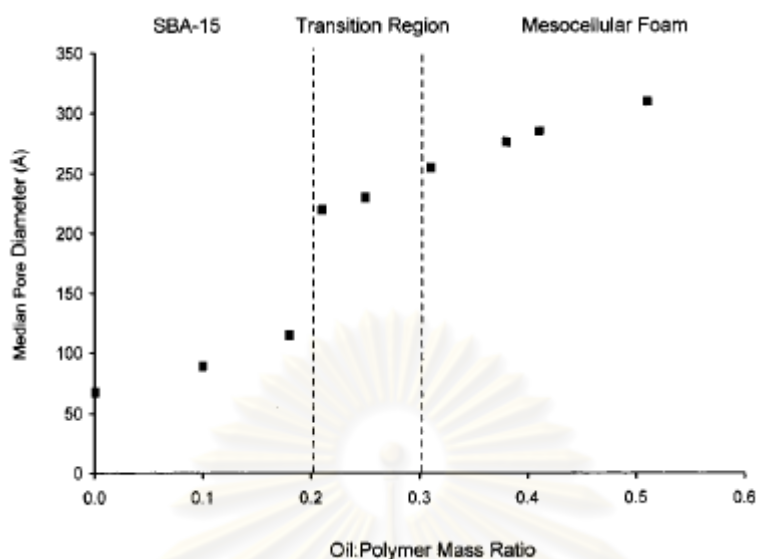
Figure 2.3 The effect of TMB/surfactant ratio on the changing of MCF pore size and shape [40].

In Figure 2.3, as the oil-polymer mass ratios increases to 0.21, the nodes separate into spherical micelles and aggregate to form the mesocellular foamy material. The mesophase change is thought to be driven by the need to decrease micelle surface-to-volume ratio as more oil is added to solution with a fixed amount of polymer.
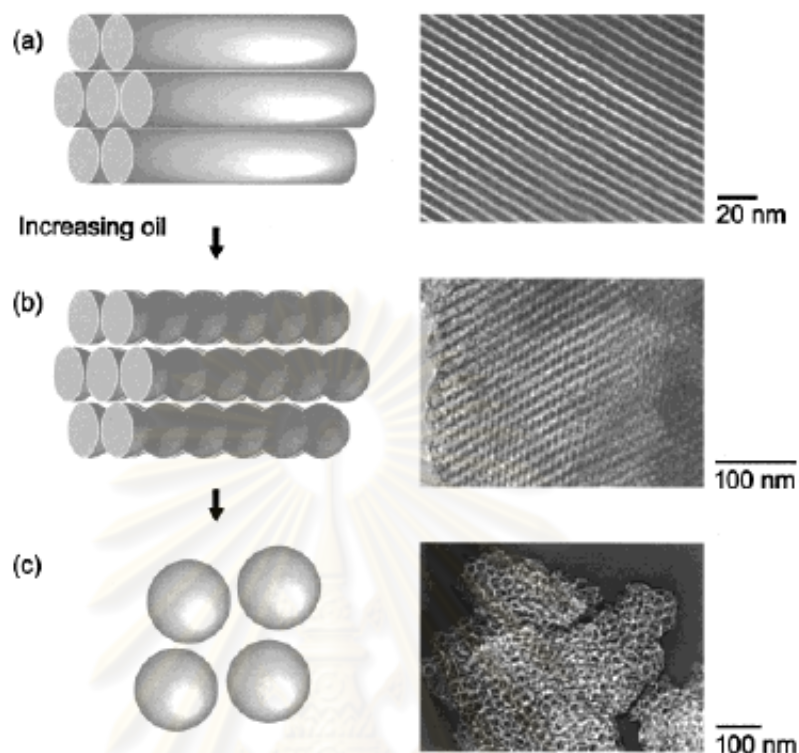
Figure 2.4 Progress of the morphological transition in P123 templated materials swollen by TMB. The proposed schemes show the formation and TEM micrographs of the mesoporous silicas synthesized at oil-polymer mass ratios of (a) 0 (b) 0.21 (c) 0.5 [40].

2.3 The characterization of ordered mesoporous silica materials

2.3.1 X-Ray Diffraction

X-Ray Diffraction (XRD) is one of the most important non-destructive technique for qualitative and quantitative analysis of materials ranging from fluid to solid and powdery crystals. Basically, XRD difractogram is generated from the reflection of an X-ray beam by the parallel and equally spaced atoms that are arranged in atomic planes, as shown in Figure 2.5. The phenomenon is governed by the Bragg's law. In an X-ray diffraction, the angle (θ) is measured as the angle between the arms of the diffractometer as they move. The "n" is the periodicity of the wave and can be any positive integer. The wavelength is incident on the lactic planes and then the

diffraction occurs when the path of rays reflected by the parallel planes (distance between planes, d). The crystals have their own lactic pattern. Therefore, the condition for maximum intensity contained in Bragg's law is used to calculate details about the crystal structure. To identify the structure of sample, the diffractogram of sample is compared diffraction patterns of known materials from a database
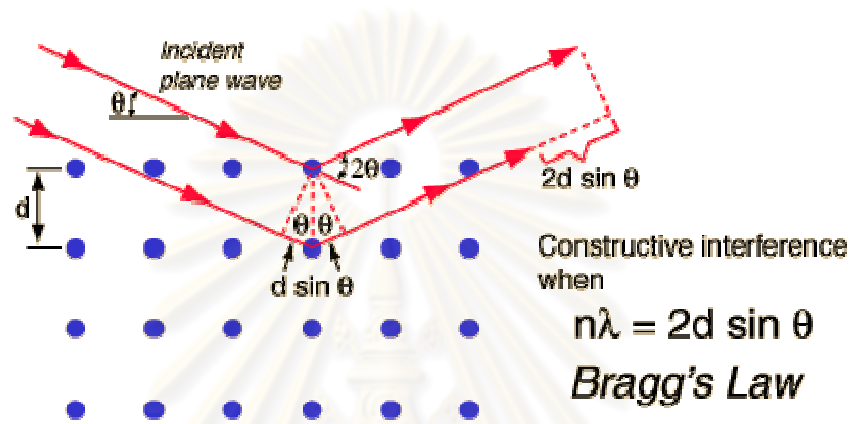
Figure 2.5 The diffractogram [42]

The solid matter is divided into 2 types, amorphous and crystalline. For amorphous materials, the atoms are not arranged in a random way similar to the disorder. In contrast, atoms of crystalline materials are arranged in a regular pattern, and there is as smallest volume element that by repetition in three dimensions describes the crystal.

The XRD technique has been applied to the analysis of solid matters in many fields such as residual stress, texture, thin film, crystallite size and microstain, and structure analysis. In this study, the XRD technique is used to indentify the structure of OMMs and the metal nanomaterial. The position and the relative intensities of the diffraction lines can be correlated to the position of the atoms in the unit cell, and its dimensions. Indexing, structure refinement, and simulation can be obtained with specific computer programs.

2.3.2 Surface and pore size analysis by physisorption

Physical adsorption of gases on solid surface is occurred by the attractive van der Walls interactions of gas molecules to solid surface. The amount of adsorbed gas can be expressed by volume or mass of gas. The gas adsorption isotherms allow to determine surface area, pore size, pore size distribution, pore volume, and porosity.

Brunauer Emmett and Teller (BET) method is a well-known rule for the physical adsorption of gas molecules on a solid surface. It is the basic important technique for analysis the specific surface area of a material. This method was published by Stephen Brunauer, Paul Hugh Emmett, and Edward Teller In 1938.

The concept of the theory is an extension of the Langmuir theory, which is a theory for monolayer molecular adsorption, to multilayer adsorption with the following hypotheses: (a) gas molecules physically adsorb on a solid in layers infinitely; (b) there is no interaction between each adsorption layer; and (c) the Langmuir theory can be applied to each layer.

The total surface area (S_{total}) and a specific surface (S) area are evaluated by the following equation.

$$S_{BET,total} = \frac{(\upsilon_m N_s)}{V} \qquad (2.2)$$

$$S_{BET} = \frac{S_{total}}{a} \qquad (2.3)$$

Where N is Avogadro's number, S is adsorption cross section, υ_m is molar volume of adsorbent gas, and a is molar weight of adsorbed species.

Classification of adsorption isotherm by BET

The types of sorption isotherm were classified into 6 different shapes of the 6 isotherms by IUPAC as shown in Figure 2.6 [43]. The classification reveals the influence of the interaction between fluid-wall and fluid-fluid interaction, and pore space affects the shape of adsorption isotherms.
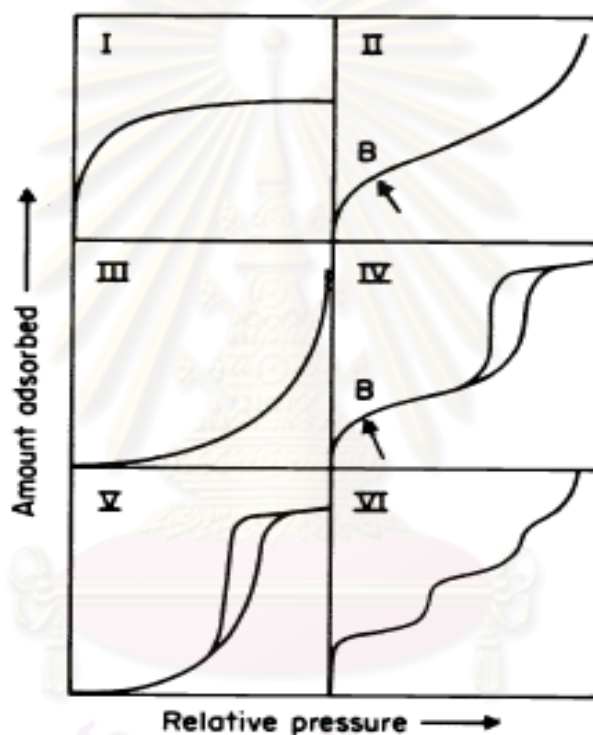
Figure 2.6 The IUPAC classification of adsorption isotherms for gas–solid Equilibrium.

In this classification, type I isotherm is given by the monolayer adsorption, the interaction between molecules of adsorbate-adsorbent is not occurred. The microporous adsorbent having relatively small external surfaces is the member of this type, such as activated carbons, molecular sieve zeolites and certain porous oxides. Type II isotherm is the normal form of isotherm obtained with a non-porous or macroporous adsorbent. It represents unrestricted monolayer-multilayer adsorptions with strong nitrogen-adsorbent interaction. Type III isotherm also describes

adsorption on macroporous adsorbents. The interaction between adsorbate-adsorbent is weak, then the adsorbate-adsorbate interactions play an important role to this isotherm. It is not common, but there are a number of systems (e .g. nitrogen on polyethylene). Type IV isotherm is its hysteresis loop, which is associated with capillary condensation taking place in mesopores. The initial part of the Type IV isotherm is attributed to monolayer-multilayer adsorption since it follows the same path as the corresponding part of a Type II isotherm obtained with the given adsorptive on the same surface area of the adsorbent in a non-porous form. Type IV isotherms are given by many mesoporous industrial adsorbents. The Type V isotherm is uncommon; it is related to the Type III isotherm in that the adsorbate-adsorbent interaction is weak, but is obtained with certain porous adsorbents. The Type VI isotherm, in which the sharpness of the steps depends on the system and the temperature, represents stepwise multilayer adsorption on a uniform non-porous surface.

2.3.3 Fourier Transform Infrared (FTIR)

Fourier Transform Infrared (FTIR) is an important technique for identification the presence of certain functional groups in a molecule or in a compound. The absorption spectrum of sample is obtained by allowing the infrared radiation passes through a sample. Some of the infrared radiation is absorbed by the sample and some of it is passed through (transmitted). The resulting spectrum represents the molecular absorption and transmission, creating a molecular fingerprint of the sample. Therefore, the intensity and spectral position of infrared absorptions allow identifying the functional groups and chemical reactions, and can be used to determine the quality of consistency of sample or amount of compound in the mixture.

2.3.4 Transmission electron microscopy (TEM)

Transmission electron microscopy (TEM) is a microscopy technique where by a beam of electrons is transmitted through an ultra thin interested sample. The electron beam interacts with the sample as it transmitted through, and then an image is formed. It is a major analysis method, which used in both physical and biological

sciences. TEM is the most powerful method to determine size and shape distributions of nanoparticles [44]. However, extensive sample preparation that is often required can cause preparation effects.

2.3.5 Zeta potential

Zeta potential is the potential difference between the dispersion particles and the stationary layer of fluid attached to the dispersed particle. It depends on the charge and size of particle and the concentration of ion in the solution. Then, the pH of suspension strongly influences the net charge of the colloid particle because the ion concentration in the solution is changed following the pH. At the high pH which is the high alkali, the particles tend to be more negative charges. While at the low pH, acid will cause the particles build up of the positive charges. Generally, a zeta potential versus pH curve will be positive at low pH and negative at high pH. Where the curve passes through the zero zeta potential, we called pH at this point "isoelectric point" (pI).

The value of zeta potential is related to the stability of colloidal dispersions. It indicates the degree of repulsion between the similar charges on the adjacent particles. When the particles are small enough, the repulsion is high, which provides the high zeta potential (positive or negative). As a consequence a high stability of the solution or dispersion is obtained. When the potential is low, the less repulsion between the charges occurs. There is no force to prevent the particles from diffusing close to each other. The short distance between particles results in the attractive van der Waals force dominates, therefore the colloids tend to aggregate. The zeta potential value relates the stability of colloid has been given by ASTM as Table 2.4.

Table 2.4 The correlation of zeta potential and stability of colloid [45].

Zeta Potential [mV]	Stability behavior of the colloid
from 0 to ±5	Rapid coagulation or flocculation
from ±10 to ±30	Incipient instability
from ±30 to ±40	Moderate stability
from ±40 to ±60	Good stability
more than ±61	Excellent stability

2.3.6 Plasmon adsorption of metal nanoparticle

The surface plasmon resonance is an oscillation of the surface plasma electrons induced by the electromagnetic field such as in radio waves, microwaves, infrared, visible light, ultraviolet, X-rays, and gamma rays . Under the influence of an electrical field, there is a plasmon excitation of the electrons at the particle surface. This is called resonance which is achieved by a given wavelength and angle, results in an optical absorption. This phenomenon called the plasmon absorption or plasma resonance absorption [44].

This phenomenon is the basis of many standard tools for measuring adsorption of material onto planar metal (typically gold and silver) surfaces or onto the surface of metal nanoparticles. The characteristics of this adsorption such as the shape, intensity and position of the peak, relate to the particular metal nanoparticle; the nature structure, topology, and the cluster system [44]. The adsorption frequency is related to the particular metal, the intensity of the peak is related to the amount of particle, the absorption wavelength is related to the particle shape. This method has been used to study of cluster nucleation and growth mechanisms [44]. Additionally, the optical properties of metal nanopartilces embedded in an insulting host differ substantially from the optical properties of bulk metals.

The adsorption peak of surface plasmon express in 2 factors, these are the spectral position (position of maximum peak) and the relative intensity. Both factors depend on various physical parameters such as the particle size and shape distribution, the interaction between metals, the interaction of metal particles and surrounding medium, and the interaction of metal and other compound.

2.4 Method of enzyme immobilization on mesoporous materials

It is known that enzyme immobilizations have been widely studied to fix the drawbacks of using free enzyme such as high cost. The advantages of enzyme are enable to reuse and easier to separation. This can reduce the cost of enzyme and the purification process. The immobilization method seriously influence on the properties of immobilized enzyme: for example, activity, stability, deactivation, and regeneration of immobilized enzyme. Thus, the selection of enzyme immobilization strategy should be considered carefully. Immobilization method may be evaluated from support material properties and application conditions. The major methods of immobilization are summarized in Figure 2.7.
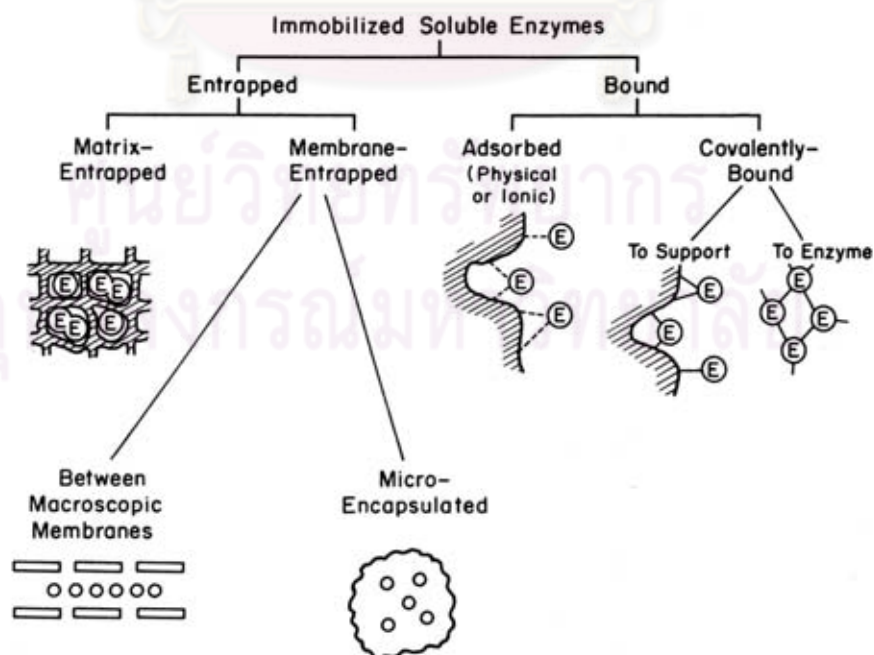
Figure 2.7 Major immobilization methods [46]

2.4.1 Entrapment

Entrapment is the physical enclosure of enzyme in a small space where the substrate is able to penetrate. The immobilized enzyme is protected from damaging environment. Normally, polymer and sol-gel method is used to entrap the enzyme, so the shrinkage or swelling problem is often found, resulting in the leaching of enzyme. Another drawback of this method is the large barrier of diffusion, as a consequence, the long reaction time is needed for the transportation of substrate or production.

Encapsulation is type of entrapment method, which is often applied in biological field. This method using the continuous film or polymeric material to enclose the enzyme in the pore space, where the size of the pore opening is smaller than the diameter of the pore space [32]. This method does not require the any interaction between enzyme and support. The strong mass transfer resistance for the reactant and product is also the problem in this method.

2.4.2   Surface immobilization

OMMs offer great properties for enzyme immobilization with surface technique. OMM has large surface area containing silanol groups which can be directly attached by enzyme and functionalized with various chemical groups. There are two major methods to immobilize enzyme on a surface of support material: adsorption and covalent binding.

Adsorption is the attachment of enzyme on the surface of support particles by weak physical forces, such as van der Waals or dispersion forces. The active site of the adsorbed enzyme is usually unaffected, and nearly full activity is retained upon adsorption. However, the leaching of enzyme is a common problem in this case. The interaction can be improved by modifying the enzyme or support surface to enable hydrogen boding to occur [32], or by adjusting pH of immobilized solution to form the electrostatic interaction. Additionally, good adsorption can be acquired by adjusting the environment during the immobilization such as pH, solvent,

23

temperature, and ion concentration. There are many advantages of using the OMMs for enzyme adsorption such as high enzyme loading as a result of the high specific area of OMMs. The enzyme stability and activity enable to improve because of the tailorable mesopores properties. The high ordered pore structure and uniform surface offer the predictable of enzyme behavior. Adsorption is the easiest way to immobilize enzyme on support because it is simple and no further treatment of the support is needed. Just by mixing enzyme and support then a link is formed. There are various supporting materials that can be employed for enzyme adsorption, for examples alumina, silica, porous glass, ceramics, and clay.

Covalent binding is the connection of enzyme and surface of the support with covalent bond formation. Enzyme and support surface bind together with the help of chemical linker containing functional groups, such as amines, thiols, carboxylic, and alkyl chloride [47]. The advantage of this method is that enzyme leaching is minimized due to enzyme permanently binding to the functional group. However, this strong binding can blocks active site of enzyme, which results in inactivation of some of immobilized enzymes.

2.5 Important parameters on activity of immobilized enzyme

Many factors correspond to activity of enzyme in immobilized state. Several of them which are considered prominent in this study are discussed in sections below.

2.5.1 The interactions between immobilized enzyme and support surface by adsorption method

The three-dimensional structure of an enzyme is not very stable; due to this it can be changed in different particular environments. The resulting enzyme always adsorbs on different surfaces by different mechanisms and interactions [48]. The interaction between enzyme and solid surface depends on environment such as the pH of buffer solution, which influences the structure and charge of enzyme, and

functional group on the support surface. The possibly interaction between surface of OMMs and HRP molecular is given in the paragraphs that follow.

Normally, enzyme molecule consists of various types of amino acids. The amino acids which have the hydrophobic groups will be gathering together at inner three-dimensional structure of the enzyme molecules. While other amino acids which have the hydrophilic groups, including the charge on functional group and the polar groups, are outer around the molecule of enzyme. Therefore, if the adsorption occurred at hydrophobic group, enzyme and support will be interacted by weak interaction of van der Walls, hydrogen bond or hydrophobic force. On the other hand, if the adsorption is occurred between hydrophilic groups and the support surface, they will be interacted by the electrostatic interaction.

1. Van der Waals interaction

Van der Waals is the attractive or repulsive force between molecules, or between part of the same molecule including between surface. It is the relatively weak compare to the other interactions such as electrostatic or covalent bonds, but it plays a fundamental role in the many fields such as the supramolecular chemistry, structural biology, polymer science, nanotechnology, surface science, and condensed matter physics. They also used to explain the solubility of organic molecules in polar and non polar media. Example, at the low molecular weight of alcohols, the properties of the polar hydroxyl group dominate, the alcohols can be dissolved in water. At higher molecular weight of alcohols, the properties of the nonpolar hydrocarbons chains(s) dominate, resulting in the less solubility. Therefore, van der Waals forces grow with the length of the nonpolar part of the molecules.

2. Hydrogen bond

Hydrogen bond is the attractive force between one electronegative atom and hydrogen covalently bonded to another electronegative atom. The high eletronegative atoms are bonded to nitrogen, oxygen or fluorine, while hydrogen is the low

electronegativity. This interaction results from a dipole-dipole force between the molecules. Therefore, hydrogen bond is a strong type of dipole-dipole force, but this bond is weaker than covalent, or ionic bonds. Therefore, in enzyme immobilization field, hydrogen bond occurs by amino groups (NH_2) or carboxylic groups (COOH) of enzyme are bound to the function groups such as NH_2, OH of support surface.

3. Electrostatic interaction

The electrostatic interaction is occurred by the different charges of enzyme and solid surface. The charges on the surface of enzyme molecule depend on isoeletric point (pI) of that enzyme and the pH of buffer solution. The electrostatic conditions often favor adsorptions of enzyme at a solid surface [49]. However, the electrical charge of the enzyme affects its structural stability, which may also affect its adsorption properties. Not only electrostatic interactions that influence the bind of enzyme and support, hydrophobic interaction are also found significant in many cases [49].

4. Hydrophobic interaction

Hydrophobic interaction is interaction between organic molecules or between nonpolar molecules. The enzymes often change conformation on adsorption to a hydrophobic surface in order to expose hydrophobic residues to the surface. This probably leads the surface denaturation of the enzyme [50]. Even though, the support surface with hydrophobic properties has a labile structure in contrast to bulk water, it also can be dispersed easily in the water by mechanical force. This drives adsorption to occur spontaneously.

2.5.2 Effects of mass transfer on immobilized enzyme reaction

It is well known that activity of immobilized enzyme has been limited by mass transfer. Immobilized enzyme does not freely contact with substrate in solution, which is in contrast to that of free enzyme. There are two types of mass transfer

limitation in a system involving immobilized enzyme; external and internal. External mass transfer barrier occurs when enzyme is immobilized on the outside surface of support. For enzyme immobilized inside the pore of a carrier, internal mass transfer becomes important. The extent of mass transfer effect on enzyme activity varies considerably and used to be determined empirically by doing a specific experiment for each immobilized enzyme application.

1. The effect of external mass transfer resistance

The external mass transfer resistance is considered in cases that enzyme is immobilized on nonporous support. The mass transport from bulk solution to support surface and reaction at the immobilized enzyme position is emphasized. The old traditional model, called the *Nernst diffusion layer* is used to explain this mechanism as shown below

$$N_s \quad = \quad k_s(S_0 - S) \quad\quad\quad (2.4)$$

Here, S and S_0 are the substrate concentrations at the interface and in the bulk solution, respectively, k_s is the mass-transfer coefficient. The mass-transfer coefficient is a function of physical properties as well as hydrodynamic conditions near the interface.

2. The effect of internal mass-transfer resistance

In this case, enzyme is typically immobilized on the internal surface of porous supports. The substrate diffuses from the bulk solution to support surface, and then to the immobilized enzyme in the pore. The effective diffusion coefficient (D_{es}) is used to explain the internal mass-transfer resistance which relates to the support properties as the following [51].

1. Some of the particle cross section is occupied by solid and hence not available for diffusive transport (parameter : particles porosity ε_p)

2. The pore network is complex and entangled so diffusion occurs only in allowed, frequently changing directions (parameter :tortuosity factor τ)

3. Pores may have very small diameter, similar to substrate molecular dimension (restricted diffusion situation; parameter : K_p/K_r)

The effective diffusion coefficient for substrate may be written as a function of the support properties as shown below

$$D_{es} = D_{s0} \cdot \frac{\varepsilon_p}{\tau} \cdot \frac{K_p}{K_r} \tag{2.5}$$

Where D_{e0} is the substrate diffusivity in the bulk solution, ε_p is the porosity parameter, tortuosity factor values are usually assumed to be in the range of 1.4-7, the restricted diffusion occurs is obtained from the crude estimate by equation below.

$$\frac{K_p}{K_r} \cong \left(1 - \frac{r_{substrate}}{r_{pore}} \right)^4 \tag{2.6}$$

Where $r_{substrate}$ and r_{pore} are the radius of substrate molecular and pore respectively.

2.6 Biosensor

A biosensor is an analytical device used in order to determine the concentration of substances and other parameters of biological interest [52]. It combines a biological component with a physiochemical detector component which converts a biological response into an electrical signal. The main components of a biosensor are bioreceptors and transducer. Bioreceptors are a biological component which highly specific bind to only one substrate (analyte), which are enzyme, antibody, and DNA. Transducers are devices used to convert a physical or chemical change into a measurable signal. Normally, it is an electronic signal, which its magnitude relates to the concentration of a specific chemical or set of chemicals.

According to the types of transducer which is quantitate the amount of analyte, the biosensors are classified into 4 types such as electrochemical, optical, piezoelectric, and thermal devices. Electrochemical system was used to study the respond of HRP on phenol detection in this research. Thus, the background of electrochemical will be introduced in the following paragraph.

Electrochemical system is set up by 3 electrodes which are working electrode (WE), reference electrode (RE) and counter electrode (CE). The working electrode consists of biomolecular which is immobilized into support and then trapped by polymer on the electrode surface. The reaction of interest is occurred at the working electrode. Common materials for working electrodes include glassy carbon, platinum, and gold. The reference electrode is an electrode which has a stable and well-known electrode potential. The most common reference electrode systems used in the aqueous solutions are Ag/AgCl. The counter electrode is used to ensure that current does not run through the reference electrode, which would disturb the potential of reference electrode. It has an opposite in sign to that of the working electrode, but its current and potential are not measured. The counter electrode often has a surface area much larger than that of the working electrode to ensure that the reactions occurring on the working electrode are not surface area limited by the working electrode. The two types of electrochemical transducer will be introduced next.

2.6.1 Voltammetry

Voltammetry is one of the electroanalytical techniques that measure a current as a function of potential. The difference between potentiometry and voltammetry is obtained from 3 electrode system. The potential is applied to the working electrode as a function of time, and then the current is measure as potential varied. The signal in the form of current as a function of potential is called voltammogram.

1. Cyclic voltammetry

Cyclic voltammetry (CV) is an excellent technique for the study of electroactive species. The controlling potential is applied to the working electrode and after it reached the set potential, the potential is scanned in reverse, resulting in a negative scan back to the original potential and thus the cycle is made. Single or multiple cycles can be used on the same surface. This inversion can happen multiple times during a single experiment. The current at the working electrode is plotted versus the applied voltage to give the cyclic voltammogram trace as shown in Figure 2.8 [53]. Cyclic voltammogram shows the anodic peak potential (E_{pa}), anodic peak current (i_{pa}) or oxidation current because the potential is scanned positively, anodic current occurs when the electrode becomes a sufficiently strong oxidant. When the scan direction is switched to negative for reverse scan, the electrode becomes a sufficiently strong reductant. This causes the cathodic peak potential (E_{pc}), the cathodic peak current (i_{pc}) or reduction current occurs. This oxidation peak will usually have a similar shape to the reduction peak.
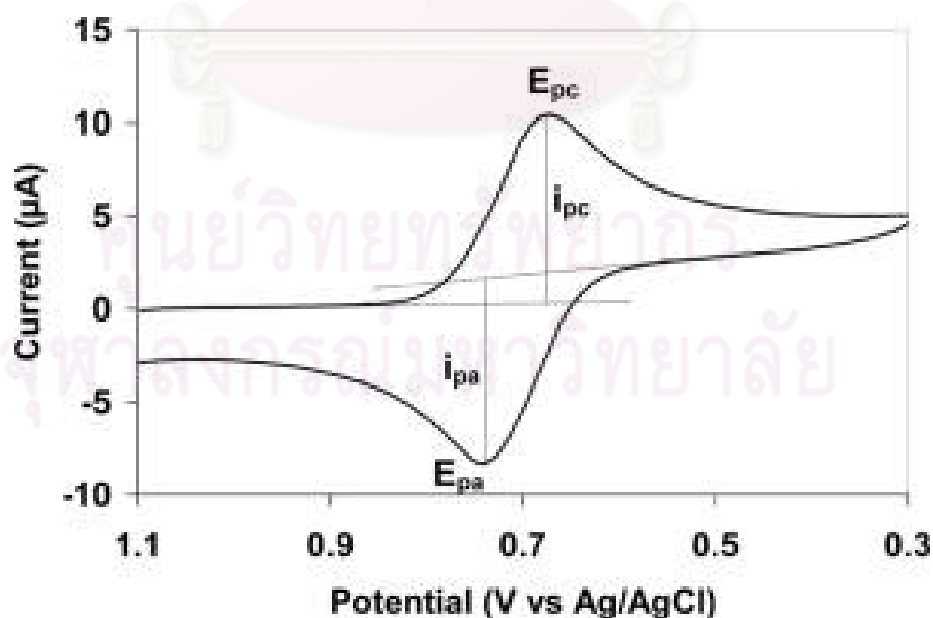
Figure 2.8 Current-potential plot for cyclic voltammetry [53]

2.6.2 Amperometry

In this technique, a constant potential is applied at the working electrode. The analyte is oxidized or reduced by the immobilized biological molecules at the surface of electrode. The measured current is a proportion of the analyte concentrations.

Additionally, the important characteristics of a biosensor are selective, sensitive, and fast response. These requirements may depend mainly on bioreceptor which should contain excess amount of active enzyme. The biosensor should be easy to use like pH electrode. Thus, essential features of desired carrier are: large surface areas and high pore volume to obtain high enzyme loading, small size that can be put in electrode easily, and biocompatible to achieve high activity and stability of enzyme without the maintain problem. Further, carriers should facilitate substrate to immobilized enzyme and electron transfer to transducer with fewer barriers to the analyte solution. Thus, from the desirable characteristics of biosensor, mesoporous silica was chosen as carriers of HRP in this research.

CHAPTER III

LISTERATURE REVIEW

This chapter leads the reader to explore literature in the field of enzyme immobilization on mesoporous silica materials. The enzyme immobilization is very useful for practical applications, i.e. biocatalysis, biosensor, and separation [18]. The immobilized enzyme may show improved stability to the effect of heat and chemical deactivation. Further more, it should be possible to use immobilized enzyme in solvents in place the native enzyme would be insoluble [1]. However, activity of enzyme is reduced by immobilization process. There are many reasons that affect to actvity of immobilized enzyme such as the binding type of enzyme and carrier, and pore diffusion resistance [1, 4]. As a result, many methods of immobilization have been developed to obtain both high stability and activity. In order to improve the immobilization of enzyme and the loading of metal in mesoporous silica, the surface modification by organosilane was also described. Finally, the synthesis of metal-mesoporous nanocomposite; including the type of metals, the synthesized technique and biosensor application; was further review.

3.1 The enzyme immobilization by using ordered mesoporous silica

There are 3 main parameters must to be considered on enzyme immobilization. The enzyme properties at the immobilization and using conditions are the first parameters. The second and thirds parameters are the chemical and mechanical of carrier properties, and the method of enzyme immobilization, respectively.

3.1.1 The enzyme properties

The enzyme properties are the biochemical properties and kinetic parameter [1]. The biochemical properties are the own character and properties of enzyme such molecular weight, size, functional groups, surface charge and purity of enzyme. The kinetic parameters are the specific activity, pH and temperature. The biochemical and kinetic of HRP were introduced in the chapter 2, section 2.1.

3.1.2 Ordered mesoporous silica materials

A suitable carrier is of a critical importance for the activity of immobilized enzyme [1]. The chemical and physical properties such as surface area, functional group, surface charge pore size, morphology and stability of carriers must be considered to making the correct carrier.

In this decade, mesoporous silicas which have the pore diameter in the range of 2-50 nm have shown a good advantage as carrier in bio-immobilization. It has demonstrated good features, such as ordered and uniform size, adjustable pore size, large surface area, chemical and mechanical stability, and resistance to microbial attack [1, 18, 34].

1. <u>The chemical properties</u>

The chemical properties demonstrate surface properties such as the functional groups and surface charge of carriers. The different carrier materials possess the different function groups and charge on their surface. The interaction of the enzyme and carrier depended strongly on the nature of the functional groups that attached to the surface [35]. The interactions may result in the activity, leaching, and stability of immobilized enzyme. The interactions between enzyme and surface of mesoporous silica by adsorption as described in paragraph following.

<u>Hydrogen bond</u>

Hydrogen bond is the attractive force between one electronegative atom and a hydrogen covalently bonded to another electronegative atom. It results from a dipole-dipole force with a hydrogen atom bonded to nitrogen, oxygen or fluorine (thus the name "hydrogen bond". In the case of enzyme immobilization, because of the functional group properties on silica surface, the silanol groups are suitable for the physical adsorption of enzyme molecules by hydrogen bonding. As shown in figure 3.1, the hydrogen bond is occurred by the hydrogen atom of amino groups or carboxylic groups of enzyme bind with the hydrogen atom of silanol groups. However, the hydrogen bond is weak interaction, resulting in the immobilized enzyme is easy to leach. Additionally, Chong and Zhao [4] found that hydrogen bonding caused the penicillin acylase slowly adsorbed into the OMMs [4].
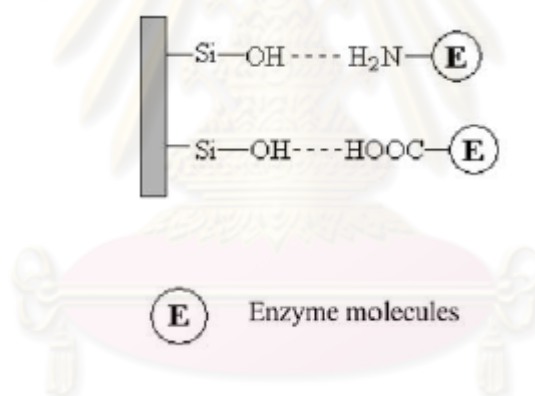
Figure 3.1 Hydrogen bond between enzyme and silica surface [4]

<u>Electrostatic interaction</u>

Electrostatic interaction is the charge action of enzyme and silica surface (Figure 3.3). It depends on many factors (1) charge properties of enzyme and carrier considered from their pI, (silica surface has pI around 2) (2) surface functionalization of silica with chemical [54] (3) template type i.e cat-ionic surfactant provided more negative charges of silanol group on the silica surface. As result, enzyme absorbed

more on silica carrier surface prepared from cat-ionic surfactant than nonionic surfactant [2].

By adjusting pH of enzyme solution during immobilization, net charge difference between enzyme and carrier is obtain, this will affect their electrostatic interaction. Additionally, this interaction depends on pI of enzyme and carrier. Loading and adsorption rate of enzyme on silica material was faster when pH value of enzyme solution was lower than its pI [4]. For example, at pH value of 3.4 highest activity of immobilized Chloroperoxidase (CPO) absorbed on MCF was observed [7]. As this pH, enzyme had a negative net charge while MCF had a positive charge. Resulting in an electrostatic interaction was obtained. However, reduced enzyme activity was observed at lower pH value, due to strong binding of enzyme and MCF which caused inactive of enzyme. CPO was unabsorbed on MCF when enzyme solution with pH 5 was used because both enzyme and MCF had negative charges.

Moreover, ionic strength is one factor that affects to adsorption of enzyme. It was found that the adsorption of enzyme and protein when presented a high amount of ion in buffer solution was reduced [18, 55].
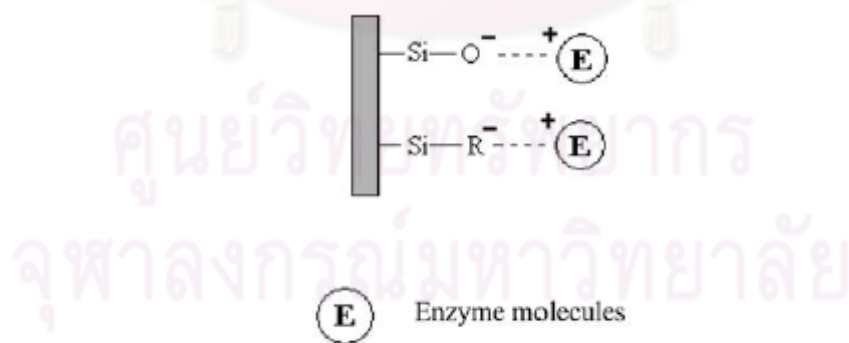
Figure 3.2 Electrostatic interaction between enzyme and silica surface [55]

Hydrophobic interaction

As explained in chapter 2, section 2.5 that hydrophobic interaction is the interaction between organic molecules. The hydrophobic and hydrophilic properties

of carrier surface have more influence to the adsorption of some proteins on mesoporous silicas than electrostatic interaction [55-56]. The hydrophobic properties of silica surface can be improved by functionalization with organosilanes. The hydroxyl groups of silica surface are co-condensation with organosilanes as will be more described later in section 3.2. The hydrophobic interaction between enzyme and silica surface is shown in Figure 3.3. This surface modification can enhance the interaction between enzyme and silica surface and also increase the electrostatic charge of enzyme and silica surface [4].
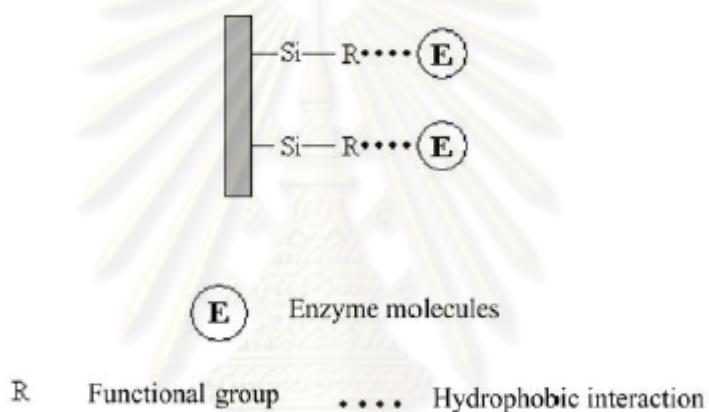
Figure 3.3 Hydrophobic interactions between enzyme and silica surface [4]

2. The effect of functional groups

In recent work, some groups of researchers [3-4, 9] were interested in organosilane materials which present the rich functional groups to provide the essential interactions with the enzyme. The interactions of enzyme and the organosilane modified support materials can be enhanced by physical force (i.e. hydrogen bonding, van der Waals, hydrophobic, and electrostatic interactions) or by chemical bonding with the help of a cross-linker [4].

The functionalization of silica MS 3030 with cotyltriethoxysilane was studied to immobilize lipase from *Candida antarctica B* [57]. The modified mesoporous silica surface supplied a high hydrophobic interaction between surface and enzyme

and then enhanced the stability of the adsorbed enzyme molecule. However, in their research, enzyme with high uptake was inactive because of its accumulation.

Various mesoporous silicas i.e. MCM-41, SBA-15, MCF were functionalized with 3-aminopropyltriethoxysilane and glutaraldehyde for α-amylase immobilization [30]. The 3-aminoproplytriethoxysilane was covalently bonded to silanol groups on the surface of mesoporous silica. Then one of the –CHO groups of gulataraldehyde was coupled with amino group of 3-aminopropyltriethoxysilane. Another -CHO group of glutaraldehyde was free to immobilize with –NH$_2$ group of enzyme by chemical bonding. The specific activity and stability of immobilized α-amylase were highest on the biggest pore sized mesoporous silica (MCF carrier). Moreover, the functionalization of MCF with various organosilanes for immobilization of Glucozamylase by chemical boding was studied by Szymańska et al. [10].

Chong and Zhao [3] studied to functionalized SBA-15 with various organosilanes such as 3-aminoproplyltriethoxysilane (APTES), 3-mercaptoproplylmethoxysilane (MPTMS), phenyltrimethoxysilane (PTMS), vinyltriethoxysilane (VTES), and 4-(triethoxysily)butyronitrile (TSBN) by investigating the effect of organosilanes types and the molar ratios of organosilane to TEOS also. The formation of the mesoporous structure was disrupted by organosilanes as follows VTES<TSBN<PTMS $\cong$ MPTMS<APTES. The lower organosilane/TEOS ratios provided the high surfaces and wide pore diameters of functionalized SBA-15. Thus, they chose the SBA-15 functionalized with 1:20 of organosilane/TEOS ratios to immobilize the enzyme penicillin acylase [9]. From their experimental data, the functionalized SBA-15 showed a significant faster adsorption rate and a higher adsorption capacity than the unmodified SBA-15 because he functionalized-organosilane surface increased hydrophobic interaction between and carrier. The VTES-functionalized mesoporous support was found to be a good potential support for physical immobilization of penicillin acylase because it obtained both of high enzyme loading and activity. However, the organosilanes (MTES, VTES, PETS, and phTES) did not improve the activity of glucose oxidase immobilized in mesoporous gel [58].

3. The physical properties

These features are suitable for the physical adsorption of molecules by hydrogen bonding of enzyme and silanol group on the silica surface. The silanol group can also be used as reactive points for the attachment of tethering functional groups [35]. Moreover, diameter of mesoporous silica is matched by the size of protein molecules. Mesoporous and accommodates enzyme within its long channels. Thus, they provide a high density of enzyme loading and facilitate transport of substrate and product. [4, 18, 34]. Moreover, the open pore structure of mesoporous silica can be modified with organosilane groups to obtain a high potential of entrapment of protein molecules [18].

Pore size of supports and the size of enzyme molecule should be matched to immobilize enzyme with adsorption method. Small pore size of the supports can not allow enzyme molecule to the inside surface of the pore, varying enzyme to be immobilized on the outside surface. On the other hand, higher leaching of immobilized enzyme occurs in the case of large pore size of support. However, the carriers should be sufficiently large for allowing enzyme to pass through easily and to be adsorbed firmly on the surface of pore wall. Thus, adjustable pore size is very useful for enzyme immobilization by adsorption method on mesoporous silica material. Diaz and Balkus [6] found that the immobilized protein on MCM-41 was reduced when the protein molecule was bigger. Moreover, pore size of carrier also influences the equilibrium rate, loading, and leaching of enzyme. The adsorption of penicillin acylase (PA) on a large pore support (SBA-15, $\varnothing$ 90 Å) reaches to the equilibrium faster than small pore support (MCM-41 ,40 Å)[4, 6]. Similarly, the loading of typsin on SBA-15 was much higher than MCM-41 and MCM-48, while the leaching was lower [35]. Takahashi et al. [2] observed that HRP and Subtilisin loading on the large pore of various mesoporous silica supports were higher than small pore but the data of leaching has not been reported.

Shape or morphology of support is a one of many parameters which influences the immobilization of enzyme. Lei et al. [34] found that the carrier with various

structures (Figure 3.1 a-d) obtained different enzyme loading. Enzyme immobilized on a rod shape SBA-15 obtained a higher loading and a faster adsorption rate than con-SBA-15 (conventional SBA-15), macroporous mesoporous membranes (MMM) and mesoporous monoliths (MM), respectively due to the small shape of carrier which allowed enzyme to come to its pore easily and faster. Moreover, carrier with bottle neck shape did not ease enzyme and substrate to come in the pore [7].
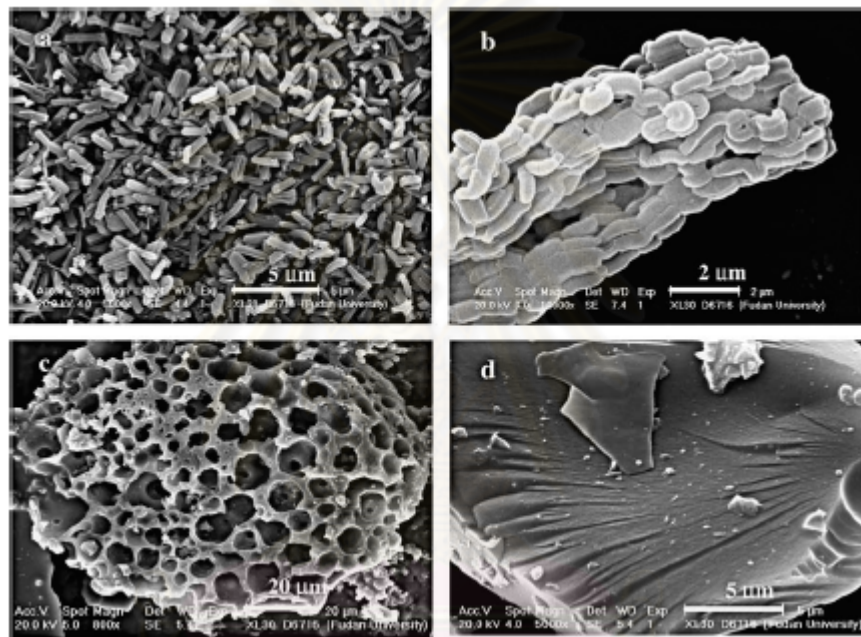
Figure 3.4 Scanning electron micrograph (SEM) of various shapes of silica
(a) rod-SBA-15 (b) con-SBA-15 (c) MMM (d) MM [34]

3.1.3 The enzyme immobilization method

The methods of enzyme immobilization influence the activity of immobilized enzyme as described in chapter 2, section 2. 4 . The methods to immobilized enzyme by using OMMs as the carriers were summarized in Table 3.1

Table 3.1 The enzyme immobilization using ordered mesoporous silica

Support	Method	Enzyme	Analysis	Ref
MCM-41	encapsulation	cytochrome *c* tyrpsin papain horseradish peroxidase	Hydrolysis of BAPNA	6
MCM-41, MCM-48, Al-MCM-41 Nb-TMS1	encapsulation	cytochrome *c*	cyclic votammetry	56
MCM-41	encapsulation	horseradish peroxidase	cyclic votammetry	98
MCM-41	adsorption	penicillin acylase	hydrolysis of phenylacetic acid	8
SBA-15 Modified-SBA-15	adsorption	penicillin acylase	hydrolysis of phenylacetic acid	9
MCF-41	adsorption	trypsin	hydrolysis of BAPNA	18
FSM-16, MCM-41, SBA-15	adsorption	Horseradish peroxidase	oxidation of diaminobenzene	27
SBA-15, MCM-41, MCM-48	adsorption	Trypsin	hydrolysis of BAPNA	35
MCM-41, SBA-15, MCF	adsorption	horseradish peroxidase	phenol	59
MCF	chemical binding	chloroperoxidase	MCD assay	7
MCM-41, SBA-15, MCF	chemical bonding	a-amylase	hydrolysis of starch	30
SBA-15(-COOH)	chemical binding	organophosphorus hydrolase	paraoxon assay	34
SBA-15 (-SH, -Cl, -COOH, etc	chemical binding	trypsin	hydrolysis of BAPNA	35

3.2 Surface modification of mesoporous supports

The surface functionalization/modification of mesoporous material has played an important role in enzyme immobilization as introduced in the section 3.2. It has improved the interaction between enzyme and carriers. Additionally, the functionalized surface is needed for synthesis of metal-silica nanocomposite, which would be given more detail in the section 3.3. There are 2 ways to functionalize the mesoporous materials, the direct-synthesis and grafting. The functionalized surfaces are built in the pore wall of support materials and replace the old surfaces.

3.2.1 Direct-synthesis

The direct-synthesis (also know as co-condensation), is a single step method of surface modification by copolymerization of an organosilane with a silica in the presence of a surfactant template. This approach provides a higher and more uniform surface coverage of organosilane functionalities. Moreover, the surface properties of modified materials are easier to control. However, the structure of mesoporous might be affected by the interaction between organosilane and silica source. Additionally, the trouble of this method is the template removal step which uses solvent extraction. Probably, the template can not be all removed by solvent extraction.

The co-condensation method was used to modified SBA-15 by oganosilanes which had various functional groups such as amino ($-NH_2$), mercapto(SH), phenyl ($-C_6 H_5$), vinyl(C=C) and carboxylic (COOH) [3-4, 9]. The ratios of organosilanes to tetraethyl orthosilicate (TEOS) were investigated by varying the ratio from 1:2-1:20, depending on the type of organosilanes. They found that there were different concentration limitations for different organosilanes that could be co-condensed with TEOS while a good mesoporous structure can be maintained. When the concentration of organosilane was higher than the limitation, the mesostructure no longer exists but a mixed structure of micro and mesostructure was obtained. Among these organosilane groups, they found that APTES which had the amino groups

strongly affected the formation of mesostructure. They explained that amino groups of APTES are easily protonated under the acidic conditions. Then, they would cross-link with the silanol groups of the TEOS. This is resulting in the disruptions of the silicate walls. Additionally, this protonated amine groups can interact with silanol groups, which prevented the interaction of surfactant and silicated to form mesoporous SBA-15.

3.2.2 Post-modification

The post-modification (also known as grafting method) consists of reaction of a suitable organosilane and silanol groups of pore wall surface. The covalent bonding of organosilane and silanol groups is formed as a functional layer inside the pores. The advantage of this method is the preserved structure of mesopore material. However, it had some drawbacks [9]. The pore size and pore volume of mesoporous materials are reduced after functionalization [1, 30]. It is quite difficult to control the loading level and uniformity of functional groups.

The traditional grafting method, the organosilane reaction is carried out using an appropriated solvent under reflux conditions. The accessible surface silanol groups which would interact with organosilane also play a key role in grafting. Recently, Luan et al. [60] reported the convenient method for functionalizing the amino group ($-NH_2$) on pore surface of SBA-15. The functionalizations have been success fully incorporated into the channels of the SBA-15 by an incipient-wetness impregnation procedure at 100ºC for 24 h. The incorporation process is highly convenient, quantitatively controllable, and reaches the maximum molar pecentages of about 13% with respect to silicon in parent silica material. The modified materials still possess the high BET surface area up to 700 m^2/g and well-defined mesoporous structure with pore dimensions less than 7 Å smaller than that of parent SBA-15.

3.3   The metal/mesoporous nanocomposite

As we explained in the chapter 1 that one of the aims of this study was to apply the enzyme immobilization to biosensor field. Thus, the type and method to synthesize metal nanoparticle in/onto the mesoporous material to form metal-silica nanocomposite must be consider and reviewed in this section.

Recently, enzyme immobilizations on metal nanoparticles in sol-gel, polymer and mesoporous silica for biosensor applications have been studied [20, 61-63]. Nanoparticles are advantageous for biosensor application because they have good interaction with the protein and also enhance the electron transfer. Various metals have been studied as bioreceptor of biosensor for enzyme attachment, including silver (Ag), gold (Au), platinum (Pd), and palladium (Pd). The loading of gold nanoparticles in various polymers have been published [64-67].

3.3.1 The metal nanoparticles and biosensor application

1. Silver nanoparticles

Silver is the best conductor among metals, silver nanoparticles may facilitate more efficient electron transfer than gold nanoparticle in biosensor [62]. The silver nanoparticle plays important role in biosensor in 2 ways. It can enhance the conductivity of enzyme electrode and absorb enzyme. The immobilization of glucose oxidase on Ag nanoparticle sol was investigated for the first time by Ren et al. [68]. Ag nanoparticles were added in sol-gel film for preparing a biosensor. The current of enzyme electrode increased with the presence of hydrophobic Ag sol, and time to reach the steady–state current response was reduced. HRP immobilized on silver nanoparticles dropped in sol-gel, biosensor with high sensitivity, quick response to H_2O_2, and good stability [62]. Compared to traditional sol-gel biosensor, Ag nanoparticle containing biosensor exhibited higher sensibility.

However, only few researches have been focused on application of silver nanoparticles and mesoporous silica composites. From literatures, some workers have synthesized silver nanoparticles or nanowires by using mesoporous silica as a template [69-70]. Other researchers have not clearly applied Ag-mesoporous silica composites on enzyme immobilization or any fields [71-72].

2. Gold nanoparticles

Gold nanoparticles are favorite metal which have been investigated for attaching enzyme to biosensor because of their biocompatibility. They can provide an environment that is suitable to enzyme immobilization [65]. The gold nanoparticles were added in chitosan to improve the current of HRP biosensors [65, 73]. Line et al. [73] prepared biosensor by entrapment HRP in colloidal gold nanoparticles which was modified to chitosan membrane while Xu et al. [66] prepared biosensor by entrapment HRP in silica sol-gel followed by linking with chitosan-gold nanopartilce nanocomposites (Figure 3.5). Even though the preparations were different, but both biosensors exhibited fast amperometric and linear response. The gold nanoparticles can also be used directly (without polymers or silica sol-gel) to modify biosensor electrode, for example, by using dithiol [74] and cysteamine [75] to make a connection between electrode and nanoparticles. Glucose oxidase has been immobilized on gold nanoparticles with various methods such as direct adsorption, or covalent linking [74-75].
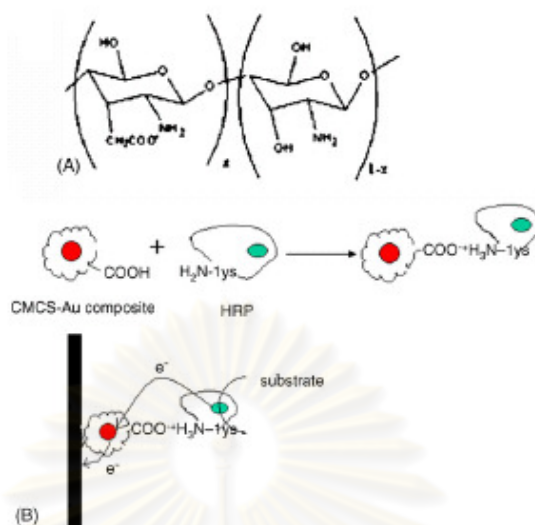
Figure 3.5 The structure of carboxymethylchitosan (A) and the electron transfer
between the electrode and HRP (B) [66]

However, there are just few published reports on gold nanoparticle-
mesoporous silica composite. It is still a novel approach to enzyme immobilization for
biosensor construction. Gold nanoparticles-mesoporous silica composite was
synthesized by a "postsynthesis" procedure for enzyme and protein immobilization
[19-20]. Gold nanoparticles were incorporated into SBA-15 for glucose oxidase
immobilization in biosensor construction by Bai et al. [19]. In their research, gold
nanoparticles/SBA-15 was successfully synthesized with a high and uniform gold
loading. The nanoparticles were formed from $AuCl_4^-$ adsorbed on H_2N-SBA-15 by
$NaBH_4$ reduction. Most of Au nanoparticles are sphere in shape and size was around
3-5 nm although some big ones still can be observed (Figure 3.6). The construction
of the glucose biosensor was shown in Figure 3.7. Briefly, the gold nanoparticles
SBA-15 composite was dropped on Au electrode surface with PVA as a supporting
medium. Then the nanoparticles were functionalized by 2-aminoethanethiol to obtain
-HN_2 groups. Finally, enzyme was immobilized on nanoparticles through the
formation of Schiff bases between –HN_2 of 2-aminoethanethiol and CHO groups of
enzyme. the biosensor exhibited an excellent bioelectrocatalytic response to glucose
with a fast response time less than 7 s, a broad linear range of 0.02-14 mM, high
sensitivity of 6.1 μAM^{-1} cm^{-2} , as well as good long-term stability and reproducibility.
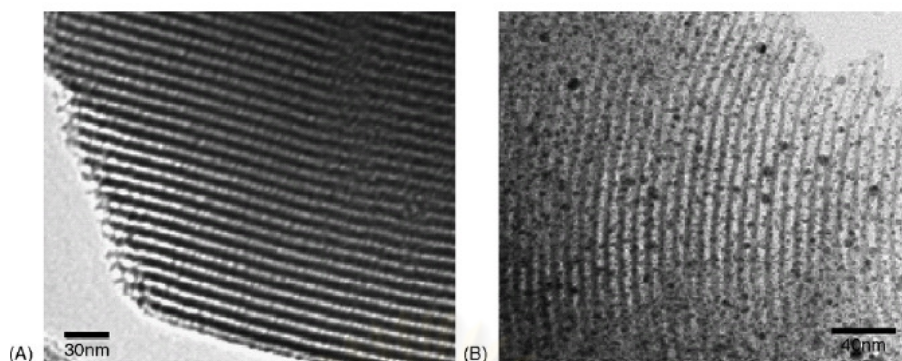
Figure 3.6 TEM images of (A) SBA-15 and (B) gold nanoparticles SBA-15 [19]
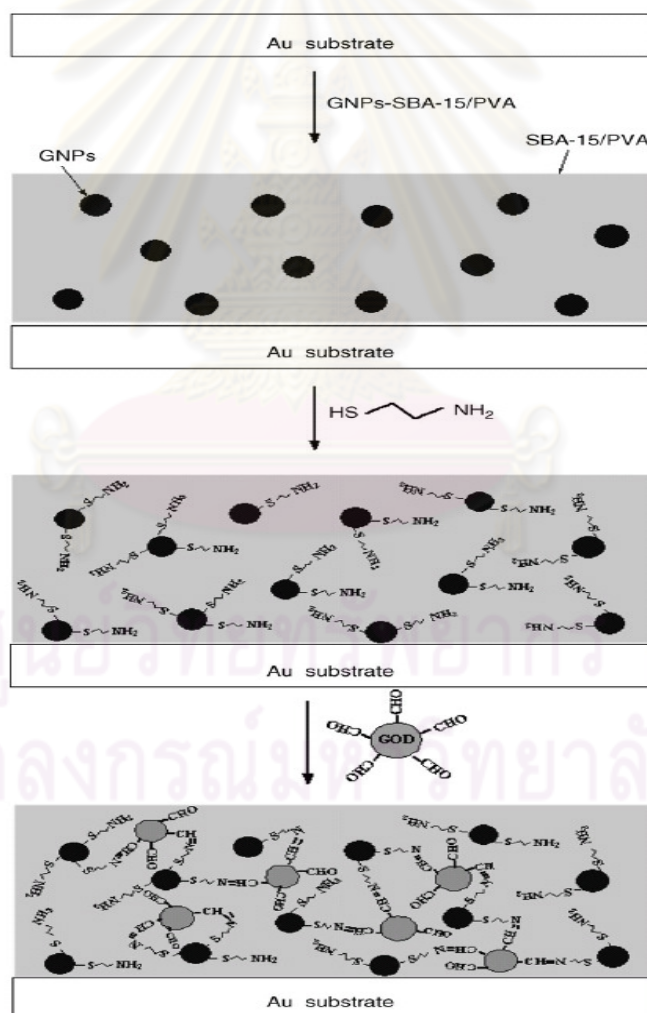
Figure 3.7 Fabrication processes of the Au electrode modified with IO_4^- oxidized-
GOD/GNPs-SBA-15 [19]

Additionally, gold nanopartilces–SBA-15 composite was also used for encapsulation hemoglobin [20]. The HAuCl4 solution was added in SBA-15 which was previously after functionalized with *N*-trimethoxysilylpropyl-*N,N,N*-trimethylammonium chloride (TMSPA). The mixture was combined with NaBH$_4$ to obtain Au-SBA-15. Figure 3.8, was shown TEM image of SBA-15 and Au-SBA-15. The average pore diameter of SBA-15 is about 5.8 nm as shown Figure 3.8 (a). From TEM image, it was clear that Au nanoparticles was incorporated and isolated inside the pore of SBA-15 (Figure 3.8, c). Au nanopaticles are approximately 2-3 nm. The influence of solution pH, structure of mesoporous silicas and gold nanoparticles in hemoglobin immobilization were investigated. It was found the hemoglobin Au-SBA-15 displayed good electrocatalytic reduction of hydrogen peroxide. Hemoglobin/Au-SBA-15 exhibited higher activity than biosensor with out gold nanoparticles.
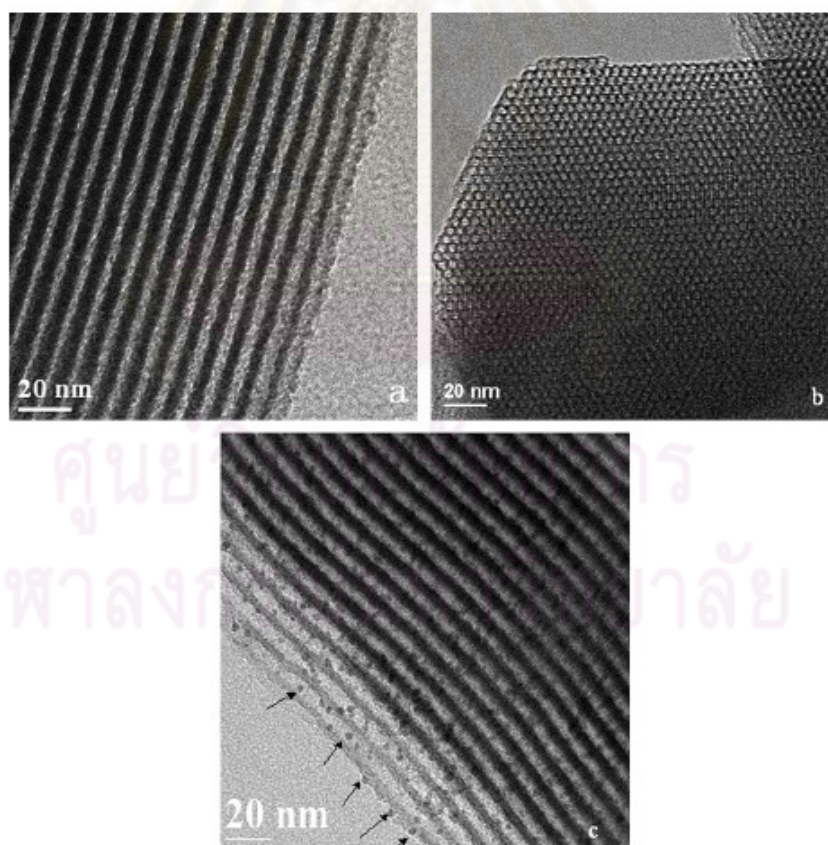
Figure 3.8 TEM images of mesoporous SBA-15: side view (a) top view

(b) and mesoporous Au-SBA-15(c) [20]

3. Platinum nanoparticles

Platinum nanoparticles can also facilitate the electron transfer and increase the surface area with enhanced mass transfer characteristics [76]. Platinum nanoparticles were doped in sol-gel solution to entrap glucose oxidase as biosensor [77]. Sol-gel solution containing amine group (by adding N-[3-(Trimethoxysilyl)propyl] ethylene diamine, EDAS) was utililized for increasing the affinity of $-NH_2$ groups toward metal nanoparticles for stabilization the nanoparticles in solution and prevented their aggregation. The nanoparticles in sol-gel solution were reduced with $NaBH_4$, and then glucose oxidase was immobilized. The size of nanoparticle was varied; the minimal size was around 2-3 nm and the largest ones was about 40 nm, with 60% of the particles were around the size of 20nm (Figure 3.9). Yang et al. [77] obtained glucose biosensor with high sensitivity, fast response, and low interferences. Moreover, the platinum nanoparticles were prepared by electrode deposition method to adsorb glucose oxidase [78-79], and covalent HRP by glutaric dialdehyde [76]. With the presence of Pt-nanoparticles on biosensor showed that electrode had good characteristics such as high sensitivity, short response time, and large current density than without Pt-nanoparticles. Even with Pt doping, this material still retained a biocompatible micro environmental for enzyme [79].
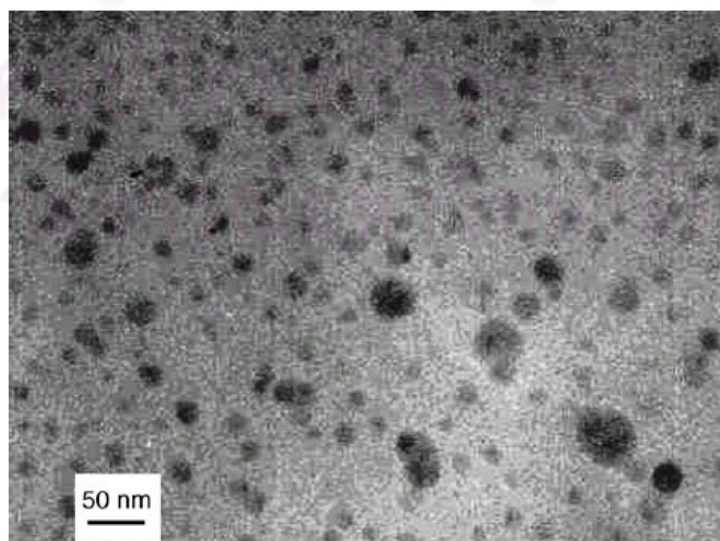
Figure 3.9 TEM micrograph of the Pt-silicated sol [77]

4. <u>Palladium nanoparticles</u>

Palladium nanoparticles (Pd) and glucose oxidase were deposited onto Nafion solubilized carbon nanotube (CNT) for making biosensor [80]. The co-deposited Pd – glucose oxidase biosensor retained its biocatalytic activity and offer an efficient oxidation and reduction of hydrogen peroxide, allowing for fast and sensitive glucose quantification. Comparing with Nafion-solubilized CNT, Pd-glucose biosensor storage time and performance was enhanced.

From above paragraphs, silver and gold have been wildly using to immobilize enzyme and also enhance electron transfer on the surface electrode of biosensor field. However, silver is much cheaper than gold, which is suitable and possible to be developed as a part of analytical device.

3.2.2 The synthesis of silver/mesoporous silica

There are many published techniques for the preparation of silver-silica nanocomposite or silver nanoparticles [21, 64, 71, 81-84]. In nanoparticle preparations, the control of particle size, shape, and particle size distribution is the critical factors to be considered [70, 85-86]. The different techniques may yield in the different properties of silver nano particles. The synthesis of silver nano particles are mainly different in the reduction techniques as given more detail in the paragraphs following.

1. <u>Co-condensation with silica precursor</u>

Co-condensation is one of the simplest ways to introduce metal to mesoporous silica. In this method, metal salts are added to the solution which contains surfactant and silica source molecules. This technique has been successfully applied for preparation of Al, Mn, V, Co or Cu containing materials. It has been shown that the structural properties and nature of metal oxide species are strongly relates to the

preparation condition, including pH of the solution, temperature and the ratio of silica and metal. The mechanism of formation of such systems is still under debate [87].

There are some researches which have been published above the synthesis of nanoparticles mesoporous silica composites with co-condensation approach. Gac et al. [87] compared the influence of the co-condensation (direct hydrothermal) and template ion exchange (TIE) method for preparation of Ag/MCM-41 composite. It was found that silver species obtained by the TIE technique were strongly dispersed on the silica support. On the other hand, direct hydrothermal provided more regular structure and higher surface area but obtained various sizes of silver species. AgBr species also were detected in the fresh support prepared by this method.

Moreover, silver nanoparticles were synthesized using SBA-15 as a template by Zhu et al. [70]. First, they synthesized mesoporous silver-SBA-15 composite then removed of template to obtain silver nanoparticles. The method in their study can be also used for silver nanoparticles mesoporous silica composite. They also recommended criteria to obtain silver nanoparticles mesoporous silica composite: (1) $AgNO_3$ forms the complex with a block copolymer surfactant (P123), (2) Ag is attached to the inner wall of the mesoporous silica and does not exist outside of the pore channels, (3) The Ag/SBA-15 materials prepared should maintain the original ordered mesoporous structure of the SBA-15 framework. They also proposed that silver nanoparticles are formed in mesoporous silica in steps described in Equation 3.1 - 3.3.

$$REO_m + HNO_3 \longrightarrow REO_m[(EO).H_3O^+]\ldots NO_3^- \qquad (3.1)$$

$$REO_m[(EO).H_3O^+]\ldots NO_3^- \xrightarrow{AgNO_3} REO_m[((EO).H_3O^+)\ldots NO_3^-.Ag^+]\ldots NO_3^- \qquad (3.2)$$

$$Si(OEt)_4 + nH_5O^+ \xrightarrow[pH<2]{Hydrolysis} Si(OEt)_{4-n}(OH_2^+) + nEtOH \qquad (3.3)$$
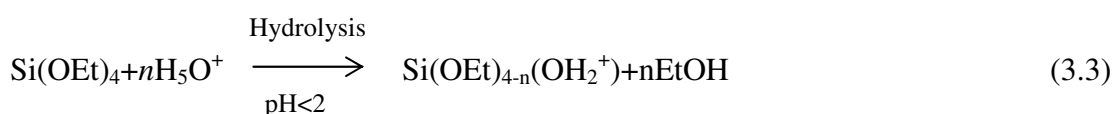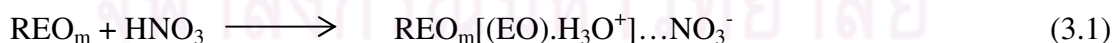
In Equation 3.1, P123 and nitric acid are dissolved; P123 forms micelles in aqueous solution with hydrophilic PEO groups on the external surface and hydrophobic PPO groups inside. At the same time, EO moieties of P123 can associate with hydronium ions in the strong acid media. In this condition, P123 can be assumed to has a net positive charge and participate in the electrostatic assembly of $AgNO_3$. PEO groups of P123 can form crown-ether-type metal –PEO complexes of form the metal-block copolymer hybrid with Ag^+ ions through weak coordination bonding. Therefore, it is believed that $AgNO_3$ is absorbed on the EO moiety surfaces to form a complex compound as shown in Equation 3.2. When TEOS are added to solution, it will hydrolyse under strong acid condition and forms compound shown in Equation 3.3. These charge- associated EO units and the cationic silica species are assembled together by a combination of electrostatic forces, hydrogen bonding, and van der waals force interaction to form $REO_m[((EO).H_3O^+)…NO_3^-.Ag^+]…NO_3^-$ $…(+H_2O)_2(EtO)_{4-n}Si$, which can be written as $(S^0Ag^+)(NO_3^-T^+)$. $(+H_2O)_2(EtO)_{4-n}Si$ attaches to the external surface of the complex to form the micellar rods. Silver existed into the pore of SBA-15 framework is shown in Figure 3.10.
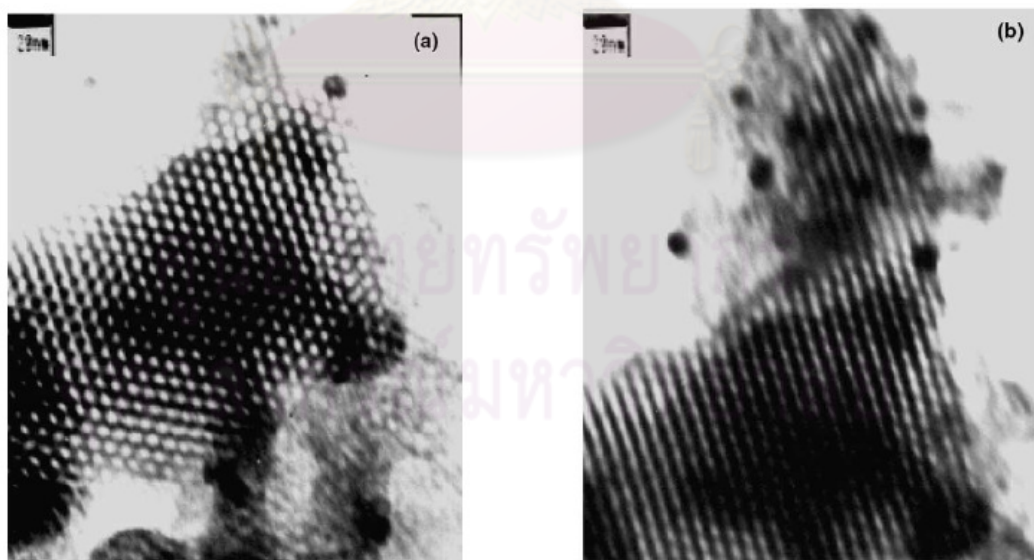
Figure 3.10 TEM images of the calcined hexagonal Ag/silica mesoporous materias along the (a) [110] and (b) [100] zone axis. The bright areas correspond to the silica walls and the dark areas to the Ag nanoparticles [70]

2. Thermal decomposition of silver nitrated method

The thermal is used to reduce $AgNO_3$ for this method. The porous silica were soaked in $AgNO_3$ solution for several days, then the dried samples were heated to let AgNO3 attached on the silica pore decomposed [88-89]. The important parameters to synthesize silver nanoparticles by this method, such as silver precursor concentration and reduction temperature were studied [88-89]. The amount of silver nanopartilces increased by the silver precursor concentration, and also resulted in red shift of the optical absorption edge [88]. The particle size of silver nanoparticles was increased by increasing of reduction temperature, the average size of particles increased from about 6 nm to 11 nm for the sample treated at 100°C to 700°C [89]. The Ag oligomers were found with the low reduction temperature (100°C), and they had the lifetime for 4 days in air [89]. The average size of silver nanoparticles obtained from this method is around 5-11 nm [88-89].

3. Chemical method

This method uses sodium hydrazine ($NaBH_4$) as a reductant to reduce silver ion deposited on silica surface. Normally, it was used with the template method to synthesize silver nanoparticles, silver nanowired or the Ag/SiO_2 nanocomposite [69, 71-72]. It is known that the template method (mesoporous silica material) is a good control over the size and the shape of silver nanoparticles or silver nanowire [69, 71-72]. The preparation of silver/mesoporous silica with thiol functionalized surface was achieved by reduction with $NaBH_4$ reducing agent [71]. The silver cations were absorbed on the thiol which substituted on the surface of mesoporous silica. Moreover, thiol functionalization assisted Ag particles to form inside the mesopore channel and also maintained the dispersed state and diameters (less than 6 nm) of silver nanoparticles as shown in Figure 3.11. On the other hand, without the help of thiol functionalized surface, Ag particles were formed on the outside of mesoporous silica channel and their sizes were in the range of 50-300 nm. The approach was used to load silver nonoparticles in pore channels of MCM-41 [72]. Functionalization of pore surface was done with APTES as shown the scheme in Figure 3.12.
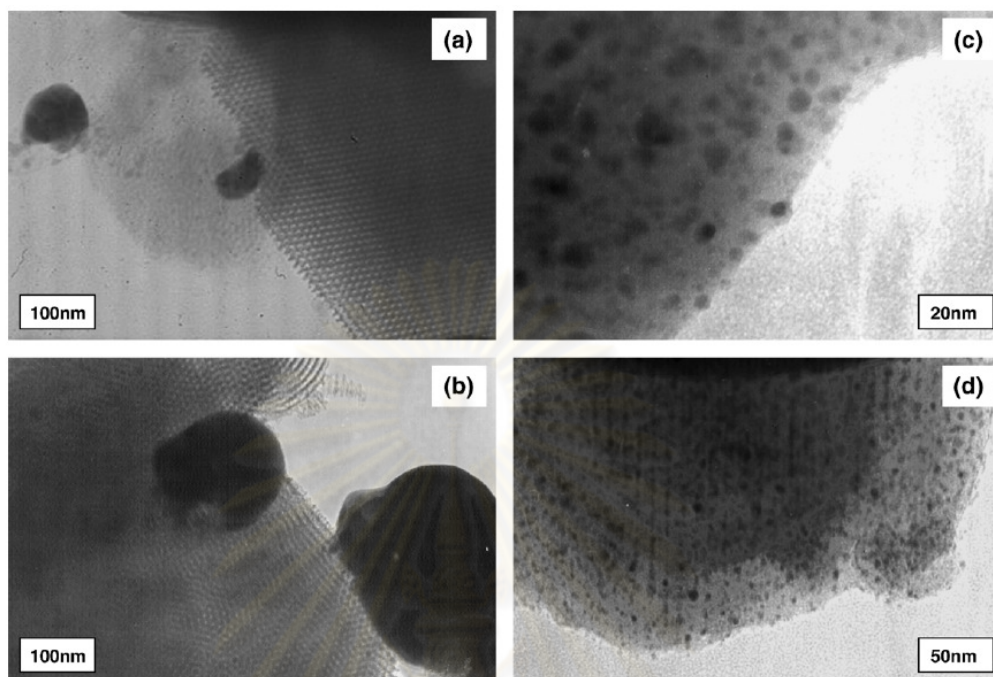
Figure 3.11 TEM image (a) silver mesorpous silica (x100k) (b) silver particle in silver mesoporous silica (x100k) (c) silver/thiol functionalized mesoporous silica (x500k) (d) silver/thiol functionalized mesoporous silica (x200k) [71]
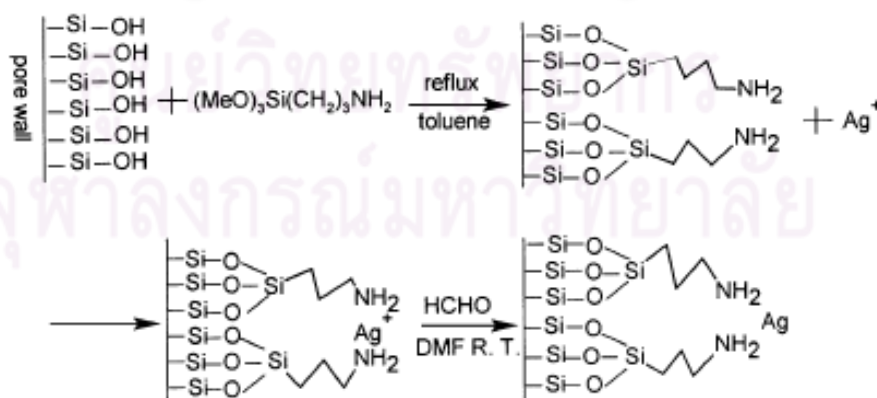
Figure 3.12 Schematic illustration of in situ formation of Ag nanoparticle inside the pore channels of MCM-41 [72]

Polyol process is the chemical reduction method using the polyol such as ethylene glycol and diethylene glycol. It was used to synthesize silver nanowire in SBA-15 [90], and silica-silver heterogeneous nanocomposite particles [91]. The advantage of this process is a convenient method to synthesize the silver particle by one step process [90-91], and to avoid the thermal treatments which can lead to phase segregation [90]. The silica particle was modified surface by thiol groups in order to immobilized silver ion [91]. In this process, the liquid polyol acts as the solvent of silver precursor, as a reducing agent, and a medium in which growth occurs in the same time [91]. Silver ions, which were bonded with thiol groups, were reduced to silver metal (Ag^0) by ethylene glycol and PVP [91]. Then silver nuclei are form and grown to become the silver nanoparticles on the modified surface of silica particle [91]. The size of silver nanopartilces immobilized on silica particles were controlled by the reaction temperature and time, the precursor concentration [91].

4. Ultrasonication and Sonochemical method

Ultrasonication and Sonochemical method has been used in material synthesis, including the metal nanoparticles and nanocomposites [21-23, 82]. Both methods work on the same technique, ultrasound which offers a very attractive method for the synthesis of metal nano particles [82].

Ultrasonication is the application of power ultrasound radiation into water to make the "cavitation" phenomenon. The "cavitation" is the formation, growth and implosive collapse of bubbles in a liquid by application of the high-intensity ultrasound [24, 92]. This collapse of the bubbles can break the chemical bond of water molecule to hydrogen radicals and hydroxyl radicals as equation 3.4 [21, 82]. Then, Hydrogen radicals formed during the sonolysis of water act as a reducing agent to reduce silver ion [equation 3.5] and then the silver nanoparticles are formed by the aggregation of the reduced silver atom as in the equation 3.6 [82, 85].

Sonochemical is the application the ultrasound to the chemical solution instance, such as alcohol [85].

Ultrasonication system

$$H_2O \longrightarrow H^\bullet + OH^\bullet \tag{3.4}$$

$$Ag^{(+)} + reducing\ radicals \longrightarrow Ag^{(0)} \tag{3.5}$$

$$nAg^{(0)} \longrightarrow Ag_n \tag{3.6}$$
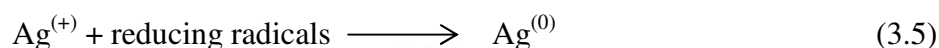
Additionally, this "cavitation" phenomenon generate the high temperature (>5000 K), pressure (>20Mpa), and very high cooling rate (>10^{10} Ks^{-1}) happened in the solution during cavitation collapses [94]. This high temperature and high cooling rate s can prevent the crystallization of the sonication products [95].

The ultrasonic irradiation was applied in the synthesis of silver nanopartilces by using amphiphilic block copolymer polyacrylonitrile-block-poly(ethylene glycol)-block-polyacrylonitrile [21]. It was revealed that size and size distribution of the resulting silver nanopartilces prepared basing on the copolymer were strongly dependent of the initial concentration of silver precursor and the irradiation condition. At the low concentration, silver precursor yielded the small size of silver nanoparticles. The size of silver nanoparticles increased with increasing silver ion concentration. Additionally, they found that ultrasonic temperatures between 20 and 40 °C only slight affect on the formation of silver nanoparticles. Furthermore, form these results, Lei and Fan [21] suggested that ultrasonic irradiation was proved to be an effective and simple way for the one-step preparation of silver nanoparticles at ambient temperature without using any reductant.

However, base on our knowledge, the other parameters such as, adsorption time of silver precursor, and the reduction time, and power of ultrasound which may affect the size and size distribution of silver nanoparticles on silica material does not reports elsewhere. On another hand, the effect of reduction was reported on the synthesis of polymer-gold nanoparticle nanocomposite by Park et al. [82]. They demonstrated that the size of gold nanoparticle increased with increasing of the

reduction time of ultrasonic irradiation. Park et al. [22] investigated the effect of concentration of stabilizer and ultrasonic irradiation power on the formation of gold in solution. They found that the shapes and size of gold nanoparticles were controlled by changing either the ratio of gold precursor/surfactant or the power of ultrasonic irradiation. The shape of gold nanoparticles was changed from multiple to spherical with increasing ultrasonic irradiation power. The size of the gold nanoparticles at high power ultrasound was smaller than that of obtained at the low power ultrasound. At the high power ultrasound, the high amounts of reactive radical species were generated, which rapidly promote the reduction of gold ion. On another hand, the lower amount of reactive radical was generated, as a consequence the reduction of gold ion was slower and coagulation occurred.

Therefore, the final shape and size of the gold nanoparticles also depend on nucleation, growth of particles [82], and ultrasonic irradiation power [22].

Sonochemical is the application the ultrasound to the chemical solution instance, such as alcohol [85]. The Ag/SiO$_2$ mesoporous nanocomposite was prepared by sonochemical method [85]. The silica mesoporous was immersed in the silver precursor solution for 3 weeks, then followed by ultrasonic irradiation at the frequency of 40 kHz in solution which presence of isopropanol. Therefore, the reducing radials were obtained from H atoms, (1-hydroxymethyl) ethyl radicals, pyrolysis radicals as shown in equation 3.7-3.9 [85]. Then the formation of silver nanoparticles (equation 3.10-3.11) were happened the same with ultrasonication method. They found that silver nanopartilces were uniform dispersion and controlled the size by the pore diameter of mesoporous silica. Additionally, they suggested that mesoporous silica host played three roles in the sonocation process, which are (1) it gave dispersion and allowed encapsulate ion of the metal nanoparticles (2) it controlled the particle size of metal with its pore dimension (3) it prevented the particles aggregation and provided a larger surface area for metal deposition.

Sonochemical system

$$H_2O \longrightarrow H^\bullet + OH^\bullet \tag{3.7}$$

$$(CH_3)_2CHOH + H^\bullet(OH^\bullet) \longrightarrow (CH_3)_2C^\bullet H + H_2O(H_2) \tag{3.8}$$

$$(CH_3)_2CHOH \longrightarrow \text{pyrolysis radicals} \tag{3.9}$$

$$Ag^{(+)} + \text{reducing radicals} \longrightarrow Ag^{(0)} \tag{3.10}$$

$$nAg^{(0)} \longrightarrow Ag_n \tag{3.11}$$
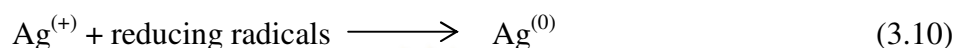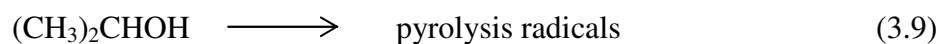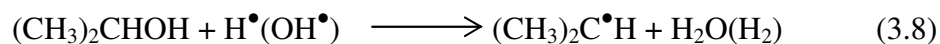
Among these methods for synthesizing metal silica nanocomposite, a sonochemical method offers several advantages over the others to synthesis metal nanoparticles [81-82], such as providing rapid reaction [92], resulting in dispersed nanoparticles, and being versatile and can be used with various materials [94]. However, this method may result in a broad size distribution due to the many parameters affecting the size of the metal nanopaticles during the synthesis, such as concentration of chemicals, stabilizer and ultrasonic power [22]. There also are several advantages to using ultrasonication method. It provides a pure phase because water is the only electron donor. The size and morphology of the nanoparticles were then easier to control [21]. Ultrasound radiation yielded smaller particles, higher specific surface [23-24], and more uniform distribution dispersion of the nanoparticles [25]. Additionally, it provided a narrower size distribution than the thermal method [21].

CHAPTER IV

EXPERIMENTAL DETAILS

4.1 Materials

Horseradish peroxidase (EC 1.11.1.7) was purchased from TOYOBO Co. Ltd. Hexadecytrimethyl-ammonium bromide (CTABr, 99%) was obtained from SIGMA. Pluronic P123 was procured from BASF. Ludox As-40 colloidal silica (40 wt %) and Tetraethoxysilane (TEOS, 98%) were purchased from Sigma-Aldrich. 1,3,5-Trimethylbenzene (TMB) was purchased from Suspelco. Ammonium solution (NH_3) was obtained from Carlo Erba. Acetic acid (CH_3COOH) and conc. Hydrochloric acid (HCl) were purchased from J.T. Baker. Pyrogallol was procured from POCH. Hydrogen peroxide (30%) was obtained from Polskie Opczynniki Chemiczne S.A.

4.2 Syntheses of mesoprous silica materials

Three types of silica supports were synthesized: MCM-41, SBA-15, and MCF. Brief description of the syntheses is given below. MCM-41 was synthesized according to the method reported by Cho and coworkers [95] which consisted of two solutions: A and B. Solution A was prepared by adding 12.15 g CTABr to 36.46 g deionized water, rigorous stirring was done to homogeneity. Next, 0.4 g of 25% NH_3 solution was added and the solution was again stirred for 30 minutes at room temperature (30±2 ^{o}C). Solution B which consisted of 2.66 g NaOH, 71.41 g deionized water, and 20.30 g Ludox was then added to solution A. After being mixed to homogeneity, the solution was poured into a Teflon bottle which was then closed tightly. The mixture was aged at 100 °C for five days, during this time its pH was adjusted daily to 10.2 with 30% CH_3COOH solution. After aging, the obtained particles were subsequently filtered and washed once with deionized water. The

synthesized particles were dried at 100 °C for 16 h. The surfactant template was then removed by calcination at 540 °C for 6 h.

SBA-15 was synthesized using the method proposed by Zhao and coworkers [96]. Pluronic P123 (4 g) was dissolved in 30 g of water and 120 g of 2 M HCl. Then, 8.50 g TEOS was added to the solution which was next stirred at room temperature for 20 h. The obtained mixture was poured into a Teflon bottle, and aged at 80 °C for 24 h. The particles achieved were filtrated and washed with deionized water until the filtrate pH was similar to that of deionized water. The synthesized material was subsequently dried at room temperature. Later, the template was removed by calcination at 500 °C for 6 h.

MCF preparation was initiated by dissolving 2 g Pluronic P123 in 75 mL of 1.6 M HCl at 35-40 °C [40]. Then, 1 g of TMB was added to the solution, and the mixture was stirred to homogeneity. Succeedingly, 4.25 g TEOS was added, and the mixture was continuously stirred at 35-40 °C for 24 h. It was next aged at 100-120 °C for 24 h. After that, MCF was achieved using the same procedures as those of SBA-15.

4.3 Characterization of mesoporous silica materials

Characterizations of mesoprous silicas were achieved by N_2-adsorption, XRD, TEM, FTIR, and Zeta potential measurement. The adsorption-desorption isotherms (Micromeritics ASAP 2020, USA) were obtained at 77 K. The surface area was determined by using Brunauer-Emmett-Teller (BET) method. The main pore diameter and pore volume of supports were obtained from the adsorption isotherm branch data and Barret-Joyner-Halenda (BJH) method. The structure of mesoporous silica supports was analyzed using X-Ray Diffraction (XRD; Bruker AXS Model D8 Discover), and Transmission Electron Microscopy (TEM; Jeol Jem 2010, Japan). Surface properties of supports were analyzed by Fourier Transform Infra Red (FTIR), spectrometer (Thermo scientific Nicollet 6700), by using the KBr technique. The Zeta

potential was measured by Zetasizer Nano (Malvern ZS 90, UK), 5 mg of supports were dispersed in 5 ml of buffer solutions of various pH.

4.4 Modification of silica nanopowder and MCF with aminopropyl groups

Aminopropyl groups were introduced on silica nanopowder (Aldrich) surface using the incipient-wetness impregnation method proposed by Luan and coworkers [60]. Briefly, 1 g of silica nanopowder or MCF was added to a vigorously stirred solution of 10 ml dry toluene solution (Lab Scan) containing 1% (3-aminopropyl) triethoxysilane (APTS, Fluka). The solution was then stirred at room temperature for 10 minutes. This mixture was next transferred into a Teflon bottle, heated to 100ºC, and held for 24 h prior to further processing. Following the sample holding time, the modified silica nanopowder (MSP) or modified MCF (MMCF) was collected by filtration, washed once with dry toluene, and twice with dichloromethane (Fisher Scientific), and dried at 120ºC for 12 h.

4.5 Synthesis of silver nanopartilces on modified silica nanopowder and on MCF

Ag/SiO$_2$ nanocomposite was synthesized by radical reduction of Ag$^+$ from AgNO$_3$ solution using ultrasonication. AgNO$_3$ (POCH S.A.) at 500, 1000, and 2000 ppm was dissolved in 50 g of distilled water and stirred in a closed container at room temperature (30±2°C). Then, 0.1 g of silica nanopowder or MSPs was added into AgNO$_3$ solution and left stirring for ion adsorption on the solid surfaces (silica nanopowder, and MSPs) for 3 to 12 h. The resulting suspension was filtered using Whatman filter paper, and the collected particles were added to 50 g of distilled water. Reduction of silver ions attached on solid surfaces was then achieved using ultrasonication (Crest ultrasonic, CP360, USA) at 40 kHz for 2-8 h. During ultrasonication, the suspension was purged with > 99.99 % argon, and the temperature was controlled at 20°C using a flowing cold water. The suspension was

again filtered, and collected particles were finally dried under vacuum (Blinder VD23, USA) at 50ºC for 10 h.

Ag/MCF nanocomposite was synthesized by radical reduction of Ag^+ from $AgNO_3$ solution using ultrasonication. $AgNO_3$ (POCH S.A.) at 2000 ppm was dissolved in 50 g of distillated water and stirred in a closed container at room temperature ($30\pm2^{o}C$). Then, 0.1 g of MMCF was added into $AgNO_3$ solution and left stirring for ion adsorption on the solid surfaces 12 h. The resulting Ag/MCF was achieved by follow the same conditions of the synthesis of Ag/SiO_2 nanocomposite, however the silver ions on MMCF were reduced for 2 and 8 h.

4.6 Characterization of MSPs, Ag/SiO₂ and Ag/MCF nanocomposite

The measurements of surface area, pore size, and pore volume of nanomaterials before and after modified surface, and with silver nanoparticles were carried out by adsorption and desorption of nitrogen (Micromeritics ASAP 2020, USA) according to Brunauer-Emmett-Teller (BET) method. Functional groups on support surfaces were indentified by Fourier Transform Infra Red (FTIR), spectrometer (Thermo scientific Nicollet 6700), by using the powder technique. Images of the resulting structure of Ag/SiO_2 and Ag/MCF nanocomposites were obtained by a transmission electron microscope (TEM, JEOL JEM 2010, Japan), operating at 200 kV. The absorption spectra of the colloidal suspensions were analyzed using a UV-Vis spectrophotometer (Shimadzu UV 2450, Japan). The type and structure of silver nanoparticles on silica nanopowder and MCF were analyzed using X-Ray Diffraction (XRD; Siemens D500, Germany). Finally, surface charges of Ag/SiO_2 and Ag/MCF nanocomposites were measured in the form of zeta potential using Zetasizer Nano (Malvern ZS 90, UK), 1 mg of supports were dispersed in 5 ml of buffer solutions of various pH.

4.7 Enzyme immobilization and enzyme leaching

To immobilize HRP on MPSs, an amount of 0.4 g MPS was added to 8 mL of 0.1 mgmL^{-1} enzyme solution of specified pH (pH = 6, 8, and 10). The mixture was subsequently gently stirred at 4°C for 24 h then the solid was filtered and washed with the same buffer to remove unattached enzyme. The solid was taken for an assay of immobilized enzyme activity.

The immobilization of HRP on the modified surface materials and the presence of SNP on mesoporous materials (Ag/SiO$_2$, Ag/MCF) were achieved in a solution buffer with a pH 8 and under the same conditions of the immobilization of HRP shown above.

Enzyme leaching was tested by adding 0.05 g of HRP containing MPSs (with/without silver nanoparticles) to 1 mL of a buffer solution of the same pH specified in the immobilization process. The mixture was next stirred at 300 rpm at room temperature (30±2 °C) for 2 h. Then the buffer solution was analyzed for free enzyme activity.

$$\text{enzyme loading}\,(\%) = \frac{\text{activity of IE in buffer solution} - \text{activity of FE remained in buffer solution}}{\text{activity of IE in buffer solution}} \times 100 \quad (4.1)$$

$$\text{enzyme leaching}\,(\%) = \frac{\text{activity of leached enzyme in buffer solution}}{\text{activity of initially loaded enzyme}} \times 100 \quad (4.2)$$

Where   IE is initial enzyme

FE is free enzyme

4.8 Storage stability test

The immobilized HRP on moesoporous silicas were kept in closed containers, and stored at room temperature (30±2°C) and 4°C for a specified period of time

without humidity control. Subsequently, 0.002 g of stored immobilized HRP was taken for activity assay.

The storage stability test of the immobilized HRP on the modified surface materials and the presence of silver nanopartilces on mesoporous silicas were kept at 4°C and performed under the same conditions as above.

$$residual\ activity\ (\%) = \frac{activity\ of\ immobilized\ enzyme\ at\ specified\ storage\ time}{activity\ of\ freshly\ immobilized\ enzyme} \times 100 \qquad (4.3)$$

4.9 Assay of free and immobilized enzyme

The analysis of free HRP was achieved using two substrates which were hydrogen peroxide and pyrogallol in a reaction according to Halpin and coworkers [97]. The reaction was initiated by an addition of 0.5 mL hydrogen peroxide (0.05 M) to a mixture of 2.4 mL phosphate buffer solution (pH 6.0) containing 0.013 M pyrogallol and 0.1 mL of a mixture solution of free HRP (0.02 mL) and a buffer solution in the same pH of the immobilization process. The reaction was carried out at 30 °C for 1 minute after which the absorbance of the product was measured at 420 nm using a spectrophotometer (spectronic® 20 Genesys TM). The extinction coefficient of pyrogallol was found to be 0.0126 $Lmol^{-1}cm^{-1}$ at 420 nm.

The assay of immobilized HRP was performed under similar conditions as those of free enzyme except that free HRP was replaced with 2 mg of HRP containing MPSs (with/without silver nanoparticles). All samples were analyzed in triplicate. One unit of HRP activity (EU) is equal to a change of 0.1 absorbance unit at 420 nm in 1 min of reaction time.

4.10 Amperometric phenol sensor

The method uses a reference electrode, working electrode, and counter electrode which in combination are sometimes referred to as a three-electrode setup.

The Ag/AgCl, glassy carbon, and platinum electrode were used as reference, working, and counter electrode respectively in this experiment. The potential is measured between the reference electrode and the working electrode and the current is measured between the working electrode and the counter electrode. The working electrodes were prepared by dropping 5 ml of 0.5% (w/v) chitosan containing 10 μg of MCF (Ag/MCF, silica nanopowder, and Ag/SiO$_2$) and 0.01 mg of HRP. The surface of working electrode was dried at the room temperature for 45 minutes. Then the amperometry was used for detecting the current of phenol by adding the 100 μl of 0.1 M phosphate buffer solution pH 7 (PBS pH 7) containing 0.1 mM hydrogen peroxide into 5 ml of 0.1 M PBS pH 7 containing 0.1 mM phenol in beaker 10 ml as substrate solution. The solution was stirred at a constant rate using a magnetic stirrer bar. The voltage of measuring the current by amperometry were fixed at -0.05 V followed the suggestion of Dai et al. [98].

CHAPTER V

RESULTS AND DISCUSSION

Since the ordered mesoporous materials (OMMs) offer good features carriers as for enzyme immobilization, the effects of pore structure, and pH of buffer solution under on HRP immobilization were firstly investigated. Since we aimed at applying immobilized HRP for biosensor applications. Silver nanoparticles were added hopefully to facilitate electron transfer. To understand the effect of mass transfer in enzyme immobilization and biosensor application, the silica nanopowder (SiO_2) was also used as another type of enzyme carrier. Since silica nanopowder is a commercial support, it is easily and conveniently using as a support for silver nanoparticles synthesis. Therefore, it was firstly used to investigate the synthesis conditions of silver nanoparticles by ultrasonication method. Ag/mesoporous silica was synthesized following the same condition with Ag/SiO_2. Consequently, these materials were used to immobilize HRP for investigating the effect of mass transfer and silver nanoparticles. Finally, Ag/SiO_2 and Ag/mesoporous silica were tested on biosensor to demonstrate the effect of silver particles addition.

5.1 Selection of suitable OMMs for HRP immobilization

In this part of the thesis, we aimed at investigating effects of OMMs pore characters and immobilization pH on HRP immobilization. OMMs with different pore characters and surface charges namely; MCM-41, SBA-15, and MCF were selected for the study. It is revealed in this part that both immobilization pH and OMMS pore characters play significant and interactive roles on enzyme loading, leaching, activity, and storage stability.

5.1.1 Support characterization

1. Pore structures

Characteristics of OMMs as enzyme supports are important information for understanding enzyme immobilization and their activities. XRD patterns of the calcined MCM-41, SBA-15, and MCF are shown in Figure 5.1. MCM-41 and SBA-15 exhibited highly distinct patterns at low 2θ angles reflecting the ordered hexagonal mesoporous structures [35]. On the other hand, the primary XRD characteristic peak of MCF was not resolved from others suggesting different mesoporous structure. TEM micrographs of all the supports as shown in Figure 5.2 confirmed the hexagonal structures and long cylindrical pores of MCM-41 and SBA-15 whereas the spherical cells and frame structure were observed for MCF.
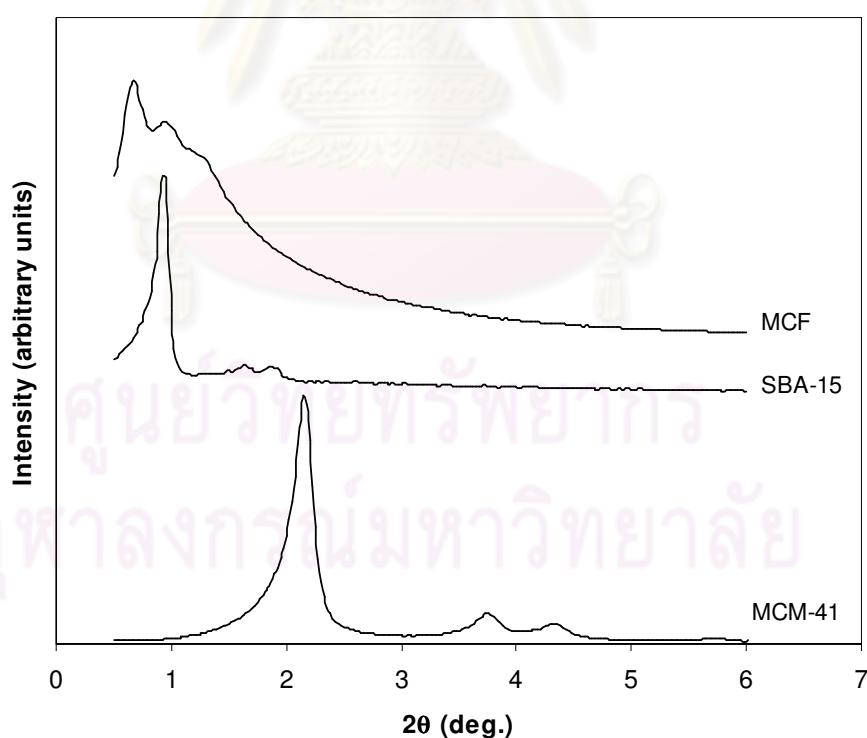
Figure 5.1 Powder XRD patterns of mesoporous silicas : MCM-41, SBA-15, and MCF
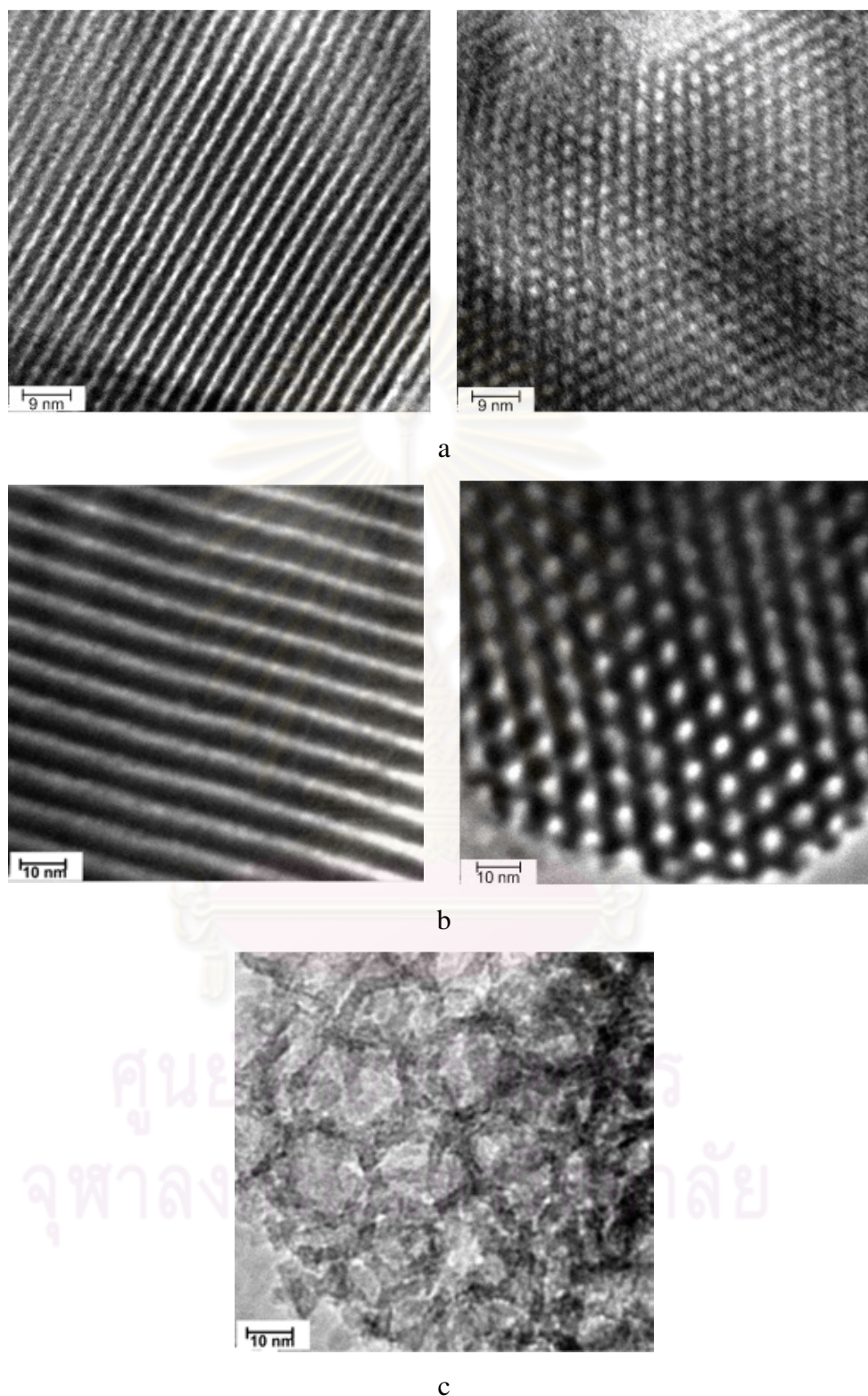
Figure 5.2 TEM images of mesoporous silicas : (a) MCM-41 observed perpendicular
(left) and parallel (right) to the pores, (b) SBA-15 observed
perpendicular (left) and parallel (right) to the pores, and (c) MCF

Structure parameters of OMMs such as pore diameter, surface area, and pore volume were evaluated through the nitrogen adsorption isotherms using the BET, and BJH methods. Table 5.1 shows main pore diameters and pore volumes as well as BET surface areas of the three supports. MCM-41, SBA-15, and MCF have the main pore diameters of 32, 54, and 148 Å, respectively. As expected, MCM-41 with the smallest pore diameter possessed the highest the surface area, and followed by BSA-15 and MCF. On the other hand, MCF with the biggest pore possessed the highest pore volume. Pore size distributions of the synthesized supports are shown in Figure 5.3. As expected, MCM-41 and SBA-15 possessed very narrow main pore size distributions which were dissimilar to MCF. In this study, MCF was the only OMM synthesized using TMB as an agent to enlarge pore sizes, therefore, the average pore size obtained was undoubtedly larger than that of MCM-41 and SBA-15. In addition, the wider pore size distribution achieved in the case of MCF was postulated to be due to the difficult to control pore size with an existence of TMB.

Table 5.1 Pore characteristics of MCM-41, SBA-15, and MCF

Supports	Pore diameter (Å)	BET surface (m^2g^{-1})	Pore volume (cm^3g^{-1})
MCM-41	32	888	0.84
SBA-15	54	798	1.06
MCF	148	618	1.60
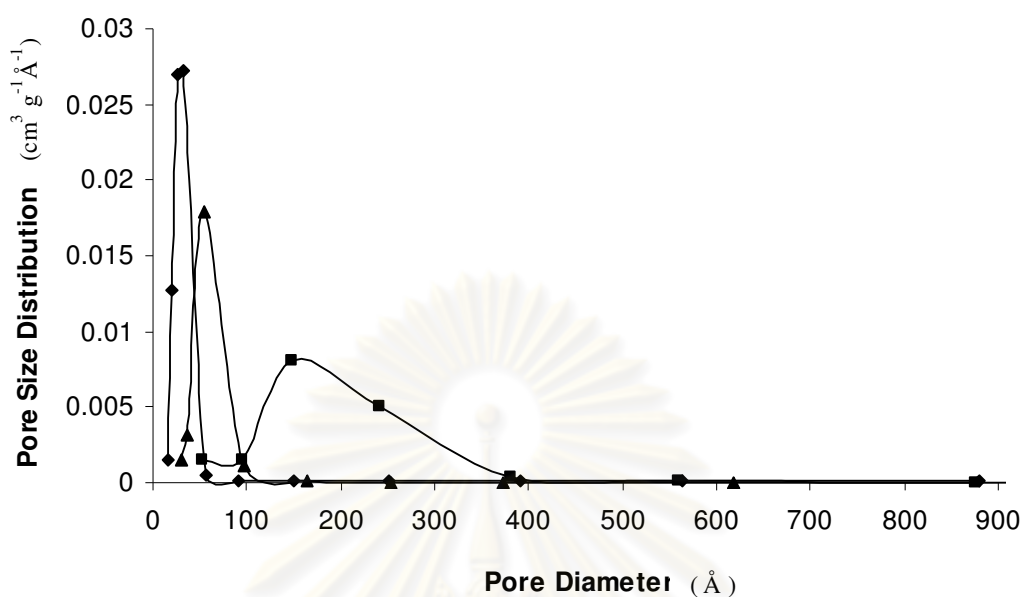
Figure 5.3 Pore size distribution of mesoporous silicas: (♦)MCM-41, (▲) SBA-15,

and (■) MCF

2. Surface properties

Figure 5.4 shows FTIR spectra of MCM-41, SBA-15, and MCF. The band between 3700-3200 cm^{-1} is attributed to Si-OH stretching (silanol group), while between 1200-1000 cm^{-1} and at 1630 cm^{-1} are shown respectively for siloxane, $-(Si-O)_n$ -, and water molecules. The similar trends of FTIR spectra observed for the three OMMs indicated identical surface functional groups. Moreover, the Si-OH/Si-O area ratios (area ratios of Si-OH/Si-O were 0.8477, 0.8229, and 0.8320 for MCM-41, SBA-15, and MCF, respectively) were comparable suggesting similar contents of free silanol groups among these supports [99]. Hence, resemble interactions between immobilized HRP and surfaces of different OMMs are expected.
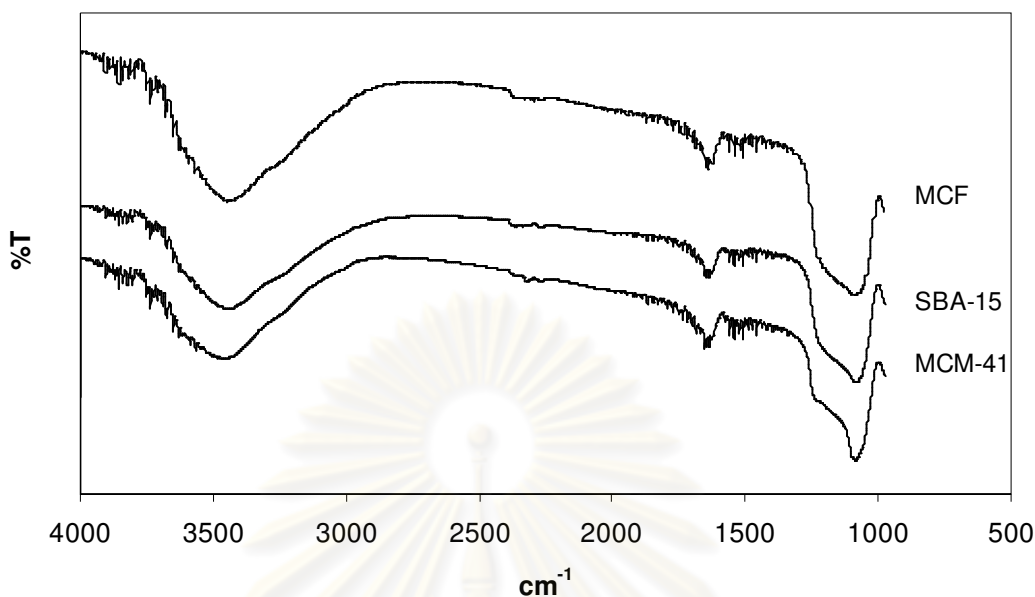
Figure 5.4 FTIR spectrum of calcined OMMs : MCM-41, SBA-15, and MCF

3. The effect of pore character on the mechanism of HRP immobilization

Table 5.2 compares main pore diameters and pore volumes as well as BET surface areas of the three supports after HRP immobilization. As already mentioned that MCM-41, SBA-15, and MCF have the main pore diameters of 32, 54, and 148 Å, respectively, while the elongated shape HRP molecule has the approximated respective long and short axes of 64, and 37Å [27]. The reduction in surface area, and pore volume after HRP immobilization for all the OMMs was most likely attributed to the adsorption of HRP inside the mesopores. The fact that HRP molecules were able to diffuse into the channels of MCM-41 even of their slightly bigger sizes than the main pore diameter was also evidenced by Yiu et al. [35] for trypsin immobilization in MCM-41.   The slight decreases in main pore diameters of MCM-41, and SBA-15 after HRP immobilization suggested that some HRP were immobilized on the pore mouths of the supports [99]. The schematic diagrams representing HRP allocation in/on mesoporous silica supports are proposed in Figure 5.5. For MCM-41, only a small amount of HRP could occupy the mesoporous space due to the relatively small main entrance sizes of the pores in comparison to HRP molecular size. Therefore, most of the enzyme molecules were expected to be adsorbed on the external surface.

This assumption was evidently confirmed by slight decreases of BET surface area and pore volume of MCM-41 after HRP immobilization (decreased by 18.0% and 14.6%, respectively). Since the main pore diameter of SBA-15 was comparable to the dimensions of enzyme molecules, HRP was easier adsorbed in the pores. Large decreases in BET surface area and pore volume of SBA-15 (42.4% and 36.6%, respectively) were therefore observed after HRP immobilization. MCF which contained the largest main pore diameter and pore volume among the three supports undoubtedly allowed comfortable entrapment of HRP in the pores. The BET surface area and pore volume of MCF decreased by 34% and 10%, respectively after HRP immobilization. A slight decrease of MCF pore volumes was probably due to its initially larger pore volume compared to MCM-41 and SBA-15.

Table 5.2 Pore characteristics of MCM-41, SBA-15, and MCF before and after immobilization processes

Supports	Pore diameter (Å)		BET surface (m^2g^{-1})		Pore volume (cm^3g^{-1})	
	Before	After	Before	After	Before	After
MCM-41	32	27	888	724	0.84	0.71
SBA-15	54	52	798	460	1.06	0.67
MCF	148	148	618	408	1.60	1.44

Calculated from adsorption branch of the N_2 isotherm
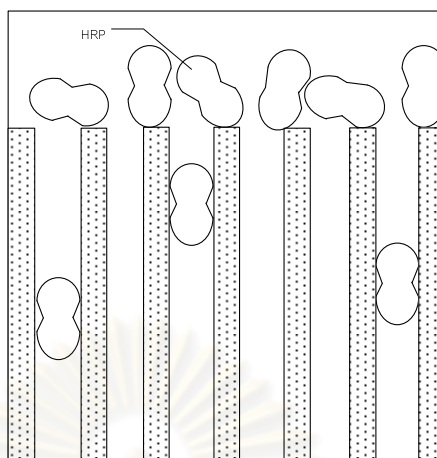
(a)
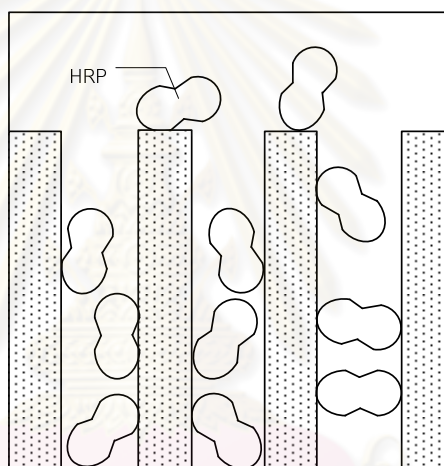
(b)
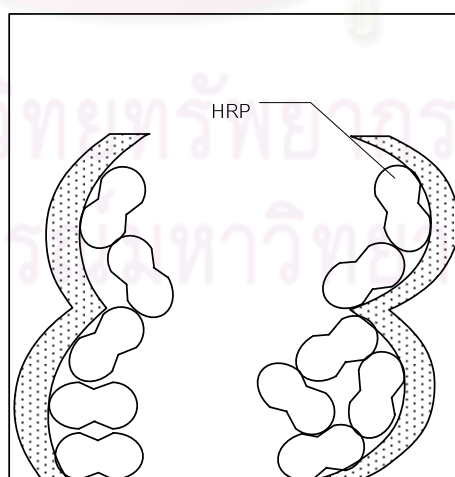
(c)

Figure 5.5 Schematic diagram of immobilized HRP in (a) MCM-41, (b) SBA-15, and
(c) MCF

5.1.2 HRP loading and leaching

In this work, two parameters influencing HRP immobilization namely; immobilization pH (pH of the buffer solution used in the immobilization step) and support pore characters were simultaneously investigated. The effect of immobilization pH on HRP loading is shown in Figure 5.6. At immobilization pH equaled to or lesser than 8, the net charge of the enzyme was positive (pI~ 8.9) while that of the support surface was negative (pI of silica ~ 2). Thus, high electrostatic attractions were obtained which led to almost 100% of enzyme loading at pH 6 and 8 for all types of supports investigated. This is in accordance to Rezwan et al. [100] who studied the influence of surface charge on the adsorbed amount of lysozyme and bovine serum albumin on silica particles. They concluded that the amount of adsorbed protein strongly corresponds to the sign of the net charge of the protein and of the particle surface. The reason that MCM-41 was able to exhibit comparable enzyme loading capacity even of its small main pore diameter might be due to its notably higher surface area, and improved anionic potential of the silanol group on the pore surface owing to the use of cationic surfactant as a template [2]. This is confirmed by the zeta-potential data reported in Table 5.3. It is demonstrated that MCM-41 held higher negative charges than other supports (synthesized using nonionic surfactant as templates) at every pH. At pH 10, both the enzyme and support surfaces possessed net negative charges, therefore only between 60- 84% HRP loading were attained. At this pH, it is obvious that the effect of support main pore size was more pronounced than electrostatic interactions. Significant amount of HRP molecules could still be loaded into pores of MCF even under electrostatic repulsions. The results in this study, however, emphasized that adjustment of enzyme immobilization pH can significantly enhance amounts of enzyme adsorbed on the supports, regardless of the types of surfactant template used.
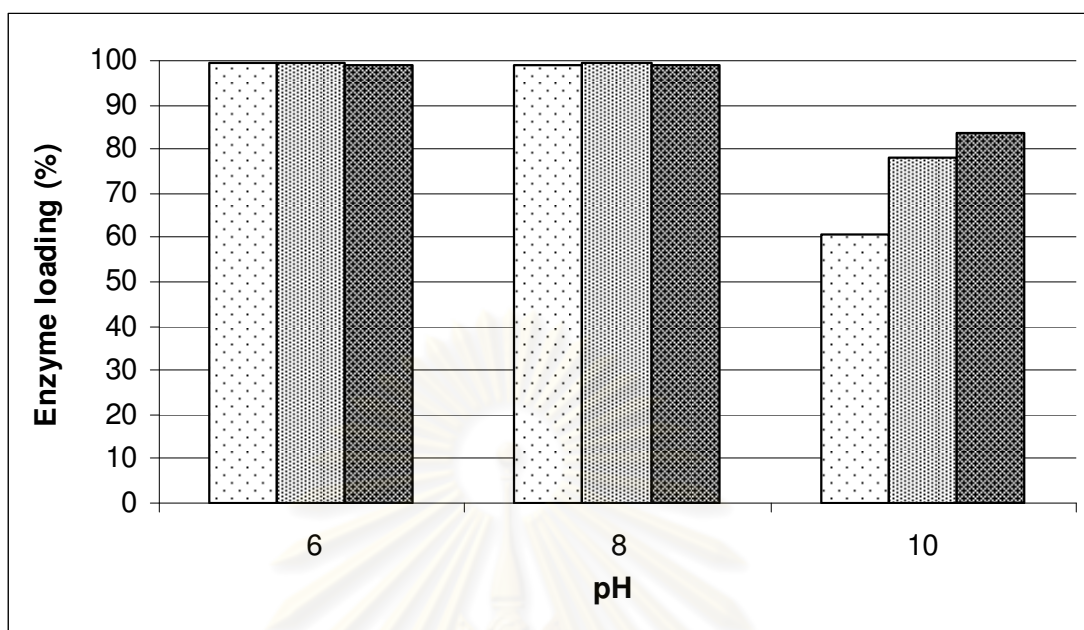
Figure 5.6 Effect of immobilization pH on HRP loading in mesoporous silicas : (☐)
MCM-41,(▨)SBA-15, and (▩) MCF

Table 5.3 Zeta potentials (mV) of silica support surface in different pH solutions

pH/support	MCM-41	SBA-15	MCF
6	-8.17	-5.54	-7.738
8	-17.46	-11.53	-14.90
10	-27.17	-21.27	-25.32

The amount of enzyme leaching also depends on pore characters of support
and interactions between enzyme and support surfaces. It is clearly seen in Figure 5.7
that immobilized HRP was leached out from MCF, with a large main pore diameter
and of spherical cells and frame structure, in a greater extent than smaller and long
cylindrical pores of SBA-15 and MCM-41, especially at relatively high pH (pH 8 and
10). This is in accordance to Lin et al. [67] who found that HRP leaching from silica
materials increased with increasing pore size. This demonstrates significant effects of
support pore characters on enzyme leaching. At pH 6, leaching of enzyme from all
supports was negligible. This supports our assumption that charges of HRP molecule
and support surface have strong influence on their attachment. At this pH, their

attractive interactions were very strong therefore less leaching was observed. The interactions became weaker as pH increased. However, for a given support type, the amounts of leached enzyme were not significantly different comparing between pH 8 and 10.
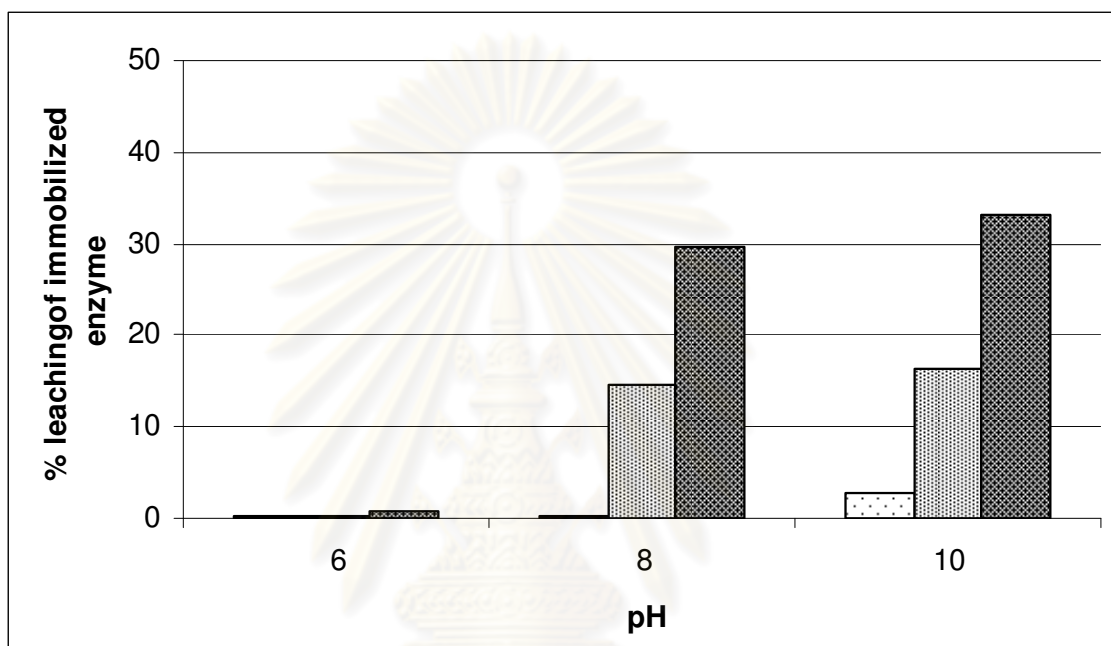
Figure 5.7 Leaching of immobilized HRP at different immobilization pH tested with various mesoporous silicas. (☐) MCM-41,(▨)SBA-15, and (▨) MCF

5.1.3 HRP activity and storage stability

Effects of immobilization pH and support pore characters on immobilized HRP activity are demonstrated in Figure 5.8. Under the same reaction pH 6, immobilization pH appeared to be a pivotal parameter governing immobilized enzyme reaction. Maximum and minimum specific activities were obtained from immobilization pH of 8 and 6, respectively, for all support types. This is surprising since free HRP was reported to be most active at pH 6. We postulated that strong electrostatic attractions between high negatively charged silica and high positively charged enzyme at pH 6 caused inflexible HRP molecules or hindered enzyme active

sites thus hampered their activities. Caramori and Fernandes [102] also reported that immobilized HRP onto polymer composite material was less active at pH 6 than other pH. The activity of immobilized enzyme on different silica supports was in the order: MCF > SBA-15 > MCM-41. The obtained results are in accordance to the literature that wider pore diameters facilitate substance mass-transfer to and from enzyme active sites. In addition, MCF structure of spherical cells and frame was anticipated to be more suitable for mass-transfer than long cylindrical structures of SBA-15 and MCM-41. The maximum specific activity obtained from immobilized HRP on MCF was ca. 30% of free enzyme. This suggests that a part of HRP was denatured during immobilization or was inaccessible to the substrate. Moreover, Carrado et al. [103] postulated that the chemical nature of the material's surface could modify the enzyme conformation to a less active one. The results obtained in this report indicated the significance of electrostatic interaction effect over the effects of support pore characters on immobilized enzyme activity.
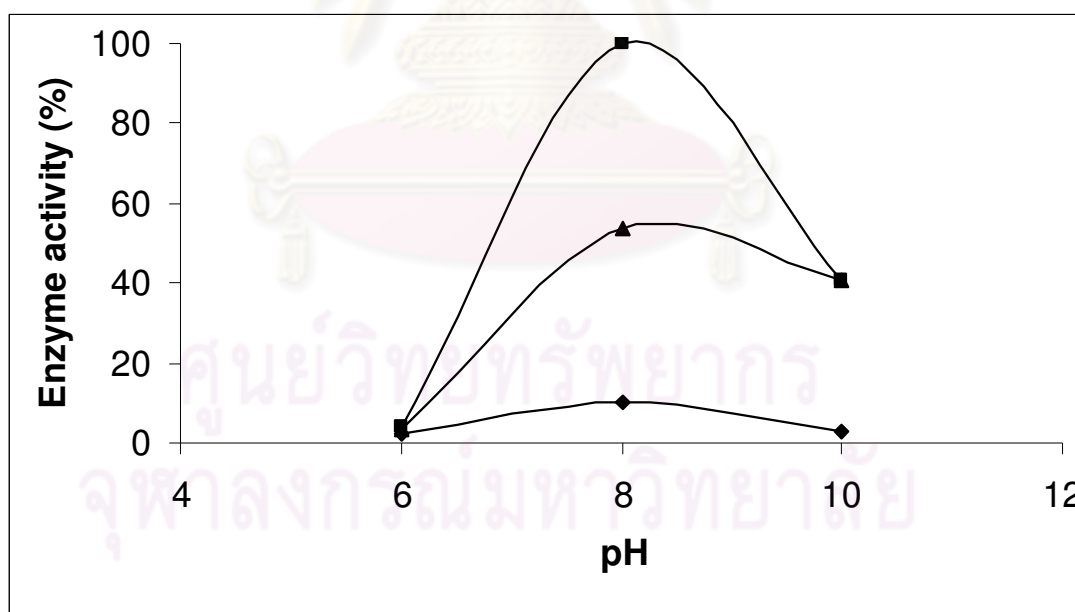
Figure 5.8 The Relative activity of immobilized HRP at different immobilization pH

tested with various mesoporous silicas : (♦)MCM-41, (▲) SBA-15, and (

■) MCF

Storage stability of immobilized HRP was evaluated every 2 weeks after the enzyme was kept in dried form at 4°C and room temperature (see Figure 5. 9). It is evident that HRP immobilized at pH 8 had the highest storage stability, in contrast to pH 6 which gave the lowest stability. Lower electrostatic interactions between enzyme and support occurred to be better for enzyme storage. These phenomena were true for both storage temperatures and for all types of supports. This indicates that electrostatic interaction was one of the key parameters influencing storage stability of the enzyme. Equally important were the support pore characters, since it was found that storage stability of immobilized HRP in MCF was much greater than in MCM-41. Supports with bigger main pore diameters appeared to be better for enzyme storage stability than those with smaller pores. The conclusions may be drawn here that HRP is likely to be denatured under conditions that rigidly control its three dimensional structure and the denaturation increases with storage time.

Therefore, the experimental results from this part indicates that the electrostatic interactions and pore characters of OMMs play the important role on enzyme loading, leaching, activity, and storage stability. It was found that activities of immobilized HRP increased with support pore diameters in the order: MCM-41 < SBA-15 < MCF. The maximum and minimum activity of immobilized HRP was obtained from pH 8 and pH 6, respectively. HRP immobilized at pH 8 had the highest storage stability (both at 4°C and room temperature), and in opposition to pH 6. In addition, HRP immobilized in MCF was the most stable under storage. Based on the highest of loading, activity and storage stability of immobilized HRP, MCF and pH 8 were choose to develop and further studied in followed parts. Using enzyme loading, activity, and storage stability as criteria for selection of a carrier type and immobilization pH, MCF and pH 8 were preferably selected and used for further studies.
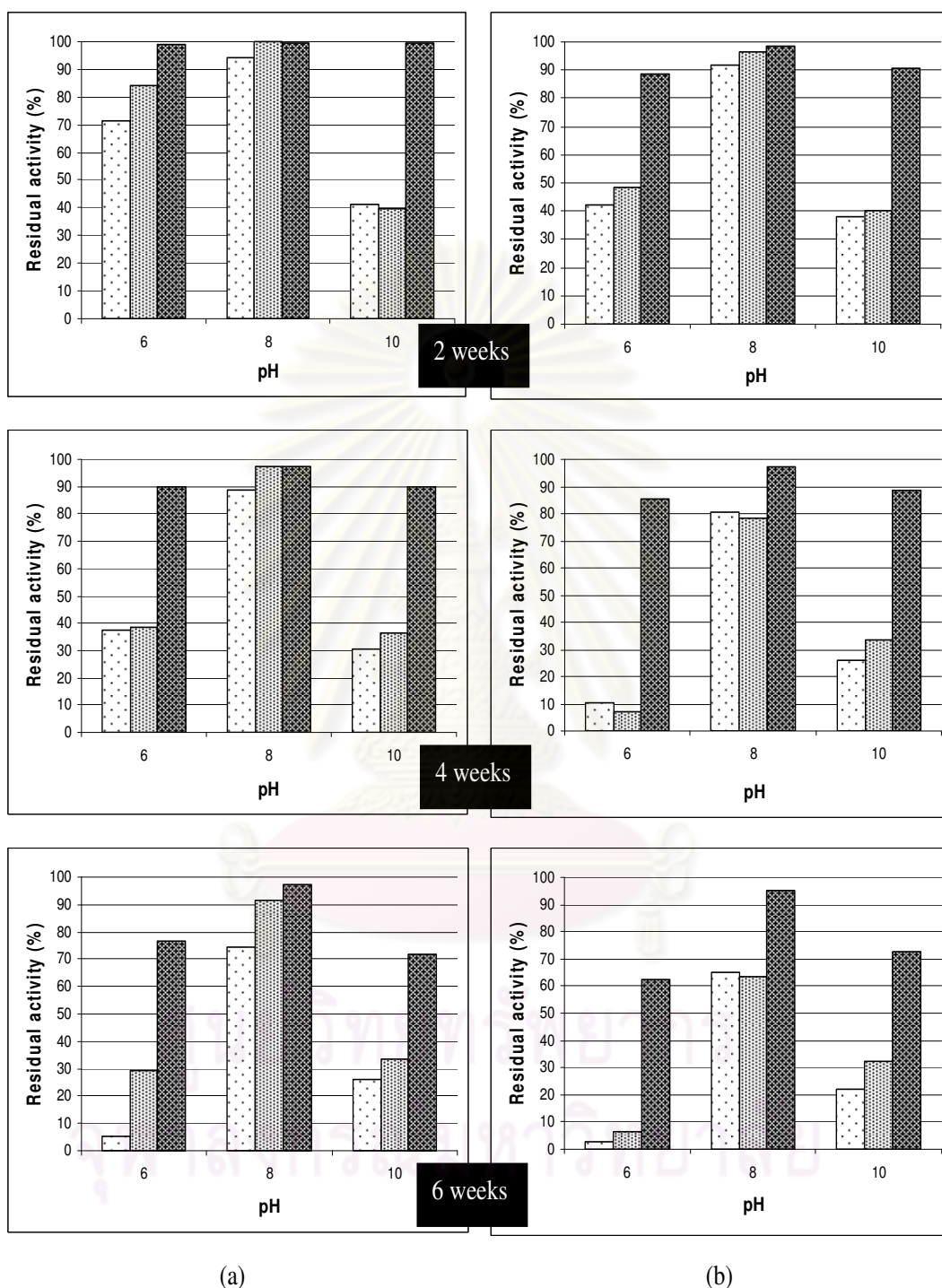
Figure 5.9 Activities of immobilized HRP were kept at 4°C (a) and room temperature

(b) in 6 weeks, (▢) MCM-41,(▨)SBA-15, and (▩) MCF

5.2 The synthesis of Ag/SiO$_2$ nanocomposite by ultrasonication

Since the ultimate aim of this thesis was utilize immobilized HRP in mesoporous silica for biosensor applications, MCF which was found in section 5.1 to be the best support for HRP immobilization in terms of enzyme loading, activity, and stability was further modified to Ag/MCF nanocomposite. This nanocomposite was postulated to enhance electron transfer between enzymes and electrode due to the specific property of silver nanoparticles. To obtain more in depth knowledge on mass transfer mechanism, Ag/SiO$_2$ synthesized using silica nanopowder was also utilized as enzyme support in comparison of those of Ag/MCF. This is became silica nanopowder almost non-porous, while MCF was mesoporous. Therefore, less substrate mass transfer resistance was expected for the case of SiO$_2$ in comparison to that of MCF as shown the schematic in Figure 5.10.
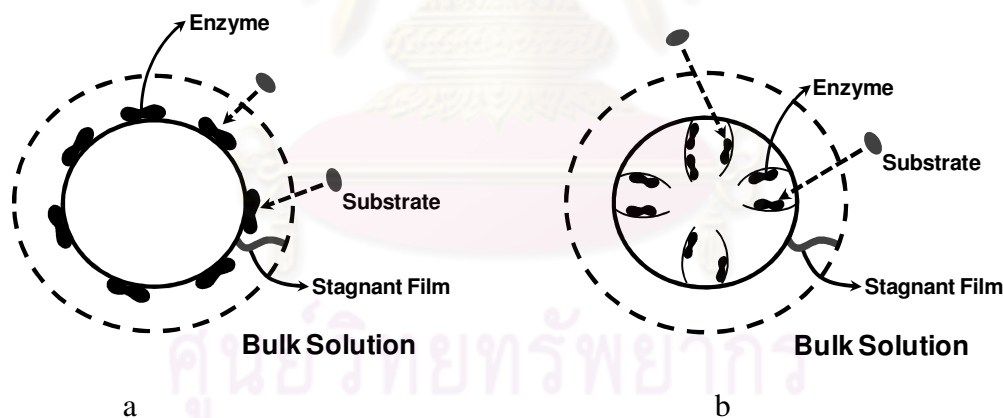
Figure 5.10 Schematic diagram of the enzyme immobilization: (a) on non porous support and (b) on porous support.

Since, synthesis conditions for Ag/MCF and Ag/SiO$_2$ have not been documented elsewhere, we, therefore, firstly needed to determine these suitable conditions (adsorption time, ultrasonication time, silver nitrate concentration), and SiO$_2$ was used as a model support.

In order to synthesize Ag/SiO$_2$ nanocomposite, silica nanopowders were used as support for attachment of silver nanoparticles. Silica surface modification was primarily carried out by grafting aminopropyl groups via a one-step reaction between surface silanol and ethoxy groups of APTES, the synthesized process is shown in Figure 5.11. Adsorption of solution silver ions on the modified surface was then followed, and accomplished via coordination of amine nitrogen with Ag$^+$ ion and form a "metal-ion core" of the precursor [103]. Subsequently, radical reduction of silver ion precursors was attained by ultrasonic irradiation as will be described in the section 5.2.1. The sections that follow will discuss effects of synthesizing conditions namely; silica surface modification, silver precursor concentration, ion adsorption, and radical reduction times on nanocomposite production.
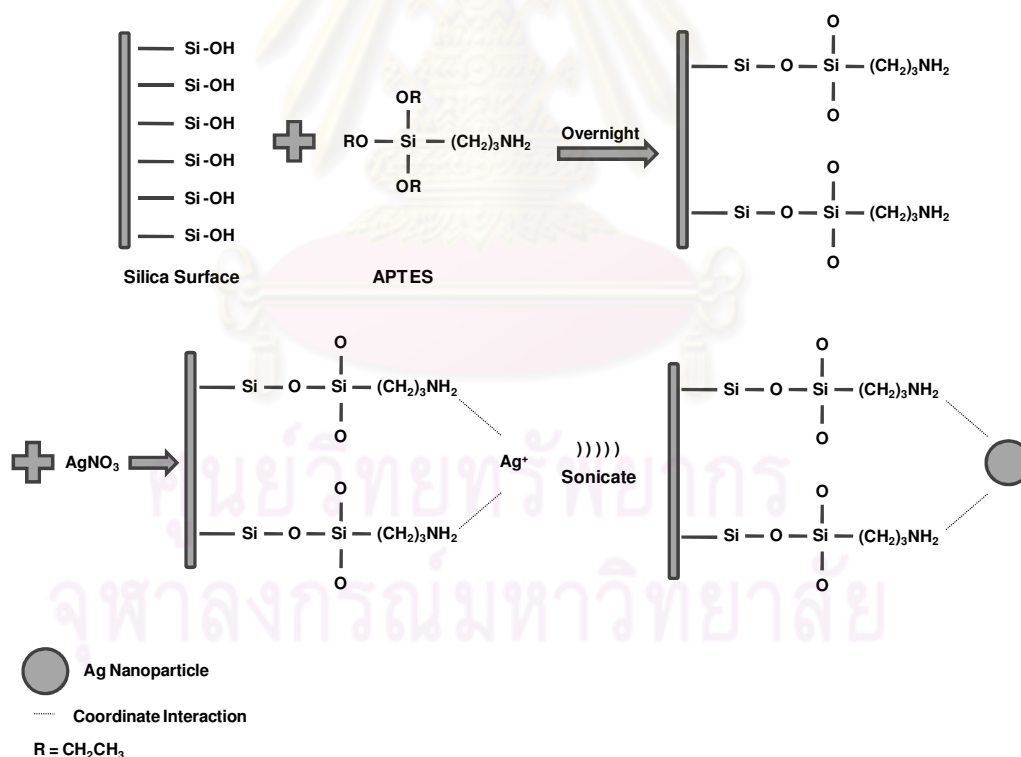
Figure 5.11 The synthesized process of Ag/SiO$_2$ by ultrasonication method

5.2.1 Synthesis of silver nanoparticles

The silver nanoparticles could be synthesized by ultrasonication in an aqueous solution of silver nitrate. The mechanism of the reduction of silver ions by ultrasonication method was described before as in section 3.5.4, as in equations 3.4-3.6. Briefly, hydrogen and hydroxyl radicals were generated from water molecules by cavitation obtained under ultrasonic irradiation. The achieved hydrogen radicals then act as electron reducers of silver ions which were attached on the surface of silica nanopowders. Subsequently, silver nanoparticles are formed by aggregation of the reduced silver atom.

$$H_2O \longrightarrow H^{\bullet} + OH^{\bullet} \tag{3.4}$$

$$Ag^{(+)} + \text{reducing radicals} \longrightarrow Ag^{(0)} \tag{3.5}$$

$$nAg^{(0)} \longrightarrow Ag_n \tag{3.6}$$
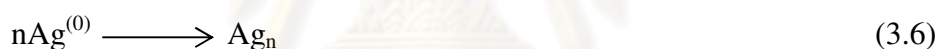
Formation mechanism

The formation mechanism of silver nanoparticles deposited on silica nanopowder in this thesis is suggested based on the above results combined with ultrasonication as explained in the following discussion. MSPs were added into the silver precursor solution. In this stage, silver ions were bound with aminoproply group by coordination with amine nitrogen. At the second staged, silver ions are reduced to silver atom (Ag^0) by obtaining electrons from amine nitrogen (more discussion in section 5.2.2). Then, silver nuclei are formed on the surface of MPS. The longer adsorption period allows the silver nuclei to grow and form silver nanoparticles. At the third stage, the remained silver ions and nuclei are reduced and grow during the ultrasonication according to equation 3.4-3.6. Finally, once silver nanoparticles are formed, the process continues to formation of clusters of nanoparticles.

5.2.2 Effects of surface modification

The grafting or post-synthesis method was used for modifying the surface of MCF and silica nanopowder by attachment of functional group via terminal hydroxyl or silanol groups (Si-OH). Although, the distribution of functional groups is sometimes non-uniform but it is known that this method preserved the framework structure of the mesoporous material [104]. The surface modification of silica nanopowder was carried out following the post-synthesis method by Luan et al. [60]. The free SiOH on silica surface was replaced by functional groups with adsorption and condensation method as already demonstrated in the first part of Figure 5.11.

Modification of the silica surface was found to be essential for synthesizing Ag/SiO$_2$ nanocomposite as revealed in Figure 5.12. Figure 5.12(a) demonstrates predominantly bound silver nanoparticles on the modified surface of silica nanopowder. The average particle diameters were determined using equation 5.1 [106].

$$\bar{d} = \frac{1}{N} \sum_{i=1}^{n0} d_i n_i$$

5.1

The particles obtained were well dispersed and of small sizes with average diameters of 15.2 nm. In contrast, without surface modification only a few silver nanoparticles with average diameters of 12.8 were found attached (Figure 5.12 (b)). These results indicate that aminopropyl functional groups on modified silica nanopowders (MSPs) acted as anchorage points for coordination of amine nitrogen with silver ions and helped facilitating silver ion adsorption [71, 72, 103, 106], while also prevents silver nanoparticles from agglomeration [103]. The coordinate interaction between amine nitrogen and silver ions is occurred by amine nitrogen that donates lone-pair electrons to silver ion. The metal ion can be bound by one or more neutral molecules or anions [107]. Therefore, in this study, silver ion can bind to amine nitrogen more than 1 molecule.

More interestingly, silver nanoparticles (with average diameters 3.9 nm) were observed on MSPs even without ultrasonication (Figure5.12(c)). Under this condition, no cavitation occurred, hence, H and OH radicals from water decomposition could not be formed. Therefore, reduction of silver ions was essentially due to APTES molecules. We postulated that the reduction occurred through the withdrawal of electrons from amine nitrogen to metal ions after the coordination between the lone pair electrons in precursor solution at pH 5.4, as similarly explained by Moresseanu et al. [108]. Moreover, Chong et al. [3] found that APTES can be easily protonated under acidic condition, this result also explained our postulation that silver ions were reduced by amine nitrogen.

Hence, it was demonstrated here that surface modification is an essential step in synthesizing Ag/SiO_2 nanocomposite. In addition, aminopropyl groups obtained from surface modification could also help reduction of silver ions although to a much lesser extent than radical reduction under ultrasonication.

a b

c
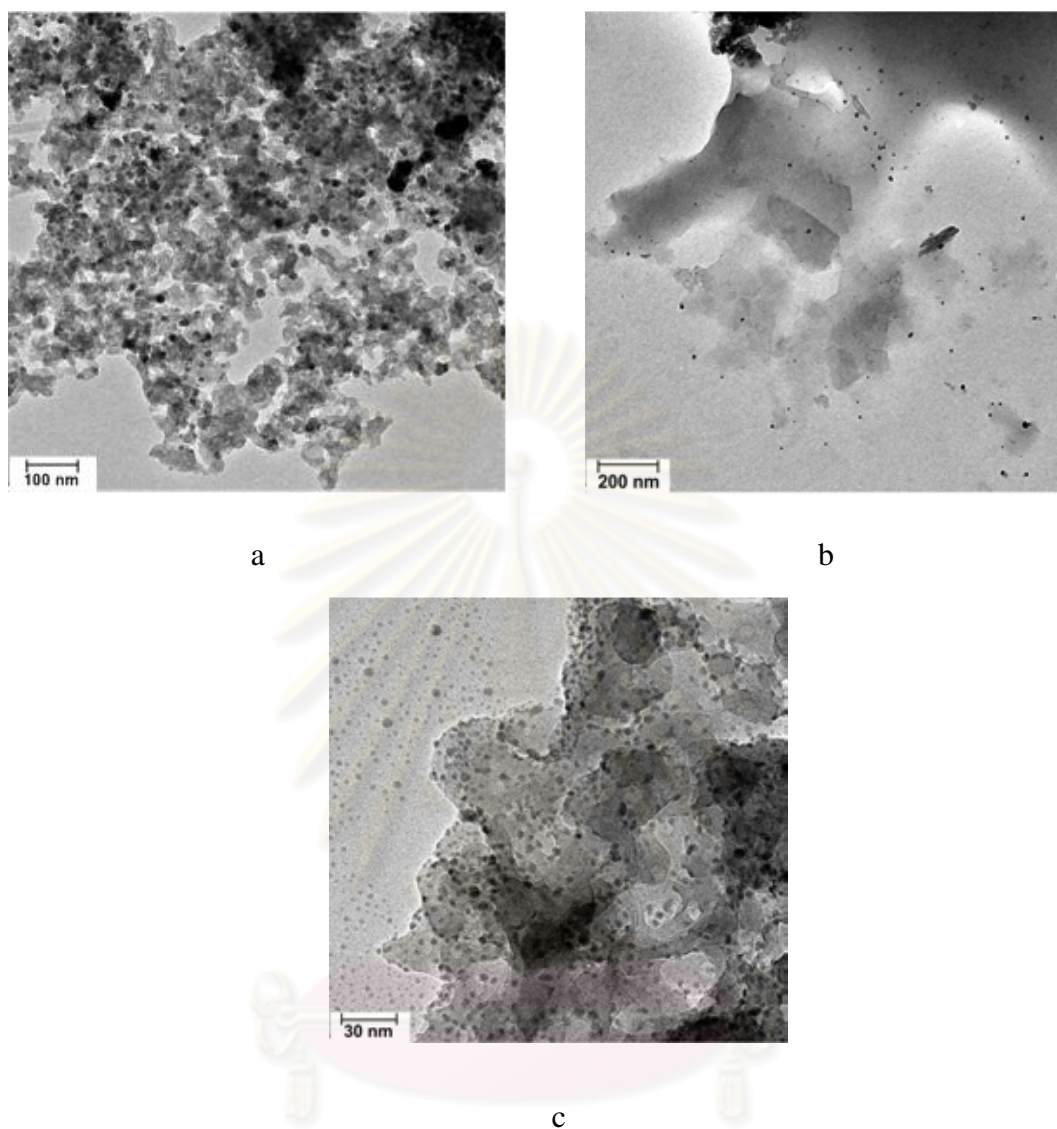
Figure 5.12 TEM micrographs of silver nanoparticles on (a) MSPs, (b) silica
nanopowder and (c) MSPs without reduction.

5.2.3 Effects of adsorption time

Effects of silver ion adsorption time on the synthesis of Ag/SiO$_2$
nanocomposite were studied at a fixed silver precursor concentration (AgNO$_3$) of 500
ppm, and ultrasonic irradiation time of 4 h. UV-Vis absorption spectra of MSPs and
Ag/SiO$_2$ nanocomposite synthesized are shown in Figure 5.13. MSPs sample did not

show any absorption peak, while maximum absorption peaks of Ag/SiO_2 samples were observed at wavelengths between 420-425 nm. These peaks, therefore, undoubtedly ascribe the surface plasmon resonances of spherical and nearly spherical-shaped silver nanoparticles as widely evidenced [21, 72].
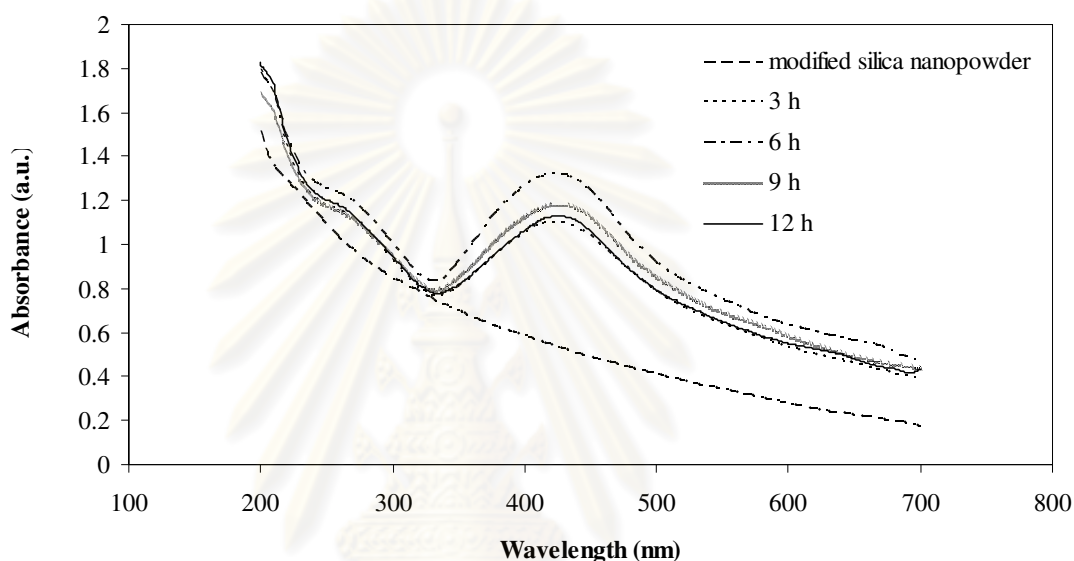
Figure 5.13 UV-Vis adsorption spectra of Ag/SiO_2 nanocomposite at various adsorption time of 500 ppm of silver precursor and 4 h of reduction.

As has been reported, there are two notable parameters of adsorption spectra to be considered; (1) the intensity which indicates a change in the number of particles [109], and (2) the maximum peak position which relates to the change in the particle size of silver nanoparticles [64]. The affect of adsorption time related the change of number and size of silver nanoparticles will be discussed as follows.

The change in number of particles, from Figure 5.13, maximum peak intensity was found to increase with adsorption time up to 6 h, while further allowable time resulted in lower peak intensity. As already mentioned, silver ions could also be reduced using electrons from amine nitrogen in aminopropyl groups. Therefore, both nucleation of silver ions and growth of these nuclei into nanoparticles could occur during this stage of adsorption. Hence, longer adsorption time arise higher numbers of silver nuclei and larger nanoparticles. The decreased numbers and larger in sizes of silver nanoparticles witnessed using 12 h adsorption time was probably due to agglomeration of small nearby particles, as also revealed by TEM images in Figure 5.14.

On the other hand, all of the positions of maximum absorption peak at different adsorption time are similar. The range of maximum absorption peaks of absorption time at 3 and 6 h were respectively 416-429 and 419-428, as well as 9 and 12 h of adsorption time that were in the same range of 421-430. From this results indicated that size of silver nanoparticles were not significant different enough to result in the position change of absorption peak. Additionally, the positions of absorption peaks are also affected by shape of the metal nanoparticles [44]. Therefore, the similar absorption peaks clearly indicated that the uniform nanosize silver was generated.

Figure 5.14 TEM micrographs of silver nanoparticles on MSPs, prepared from 500
ppm of silver precursor, 4 h of reduction, and various of adsorption time
at; (a) 3 h, (b) 6 h, (c) 9 h , and (d) 12 h.

5.2.4 Effects of silver precursor concentration

In order to investigate effects of silver precursor concentration on the
synthesized Ag/SiO$_2$ nanocomposite, silver ion adsorption and ultrasonic irradiation
times were fixed respectively at 12 and 4 h, while silver precursor concentration was
varied from 500 to 2,000 ppm. Figure 5.15 demonstrates an increase in absorption
peak intensity with silver precursor concentration. The higher silver precursor

concentration resulted in an increase number of silver nuclei during the early stage of nucleation, which led to increasing numbers of silver nanoparticles [103]. However, with sufficiently long adsorption time (12 h), the high precursor concentration resulted in the aggregation of the smaller number of nuclei, the larger particles were finally formed. Furthermore, Figure 5.16 supports this reasoning and shows the larger average sizes of silver nanoparticles with higher precursor concentration. Broader size distributions of silver nanoparticles were also obtained by increasing silver ion concentration. The possible reason behind this phenomenon is the slow nucleation rate of the silver nanoparticles that occurred during synthesis of the particles at lower concentration which causes narrower size distributions [21, 110].
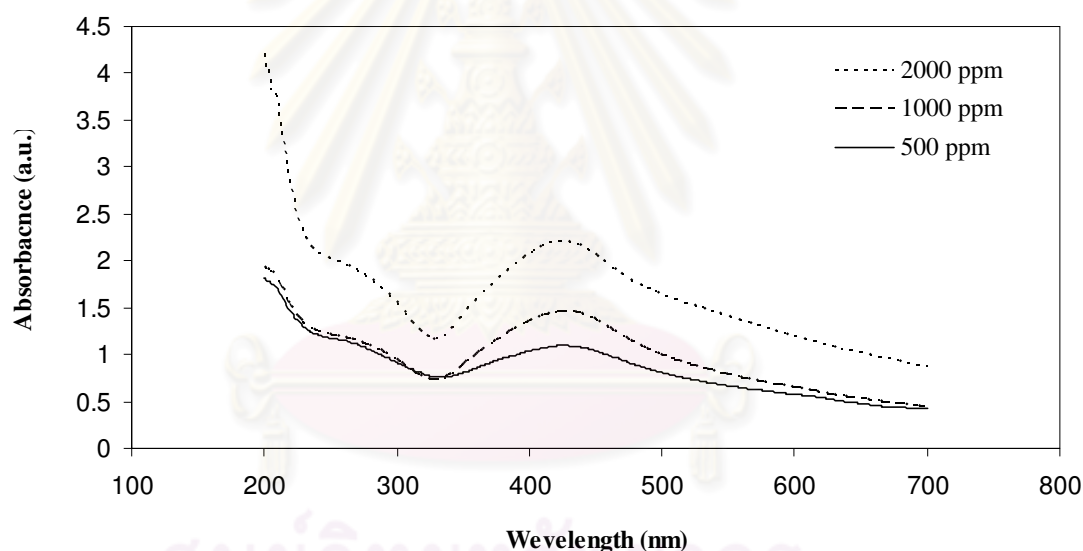
Figure 5.15 UV-Vis adsorption spectra of Ag/SiO$_2$ nanocomposite at various concentration of silver precursor, 12 h of adsorption, and 4 h of reduction.

a

b

c
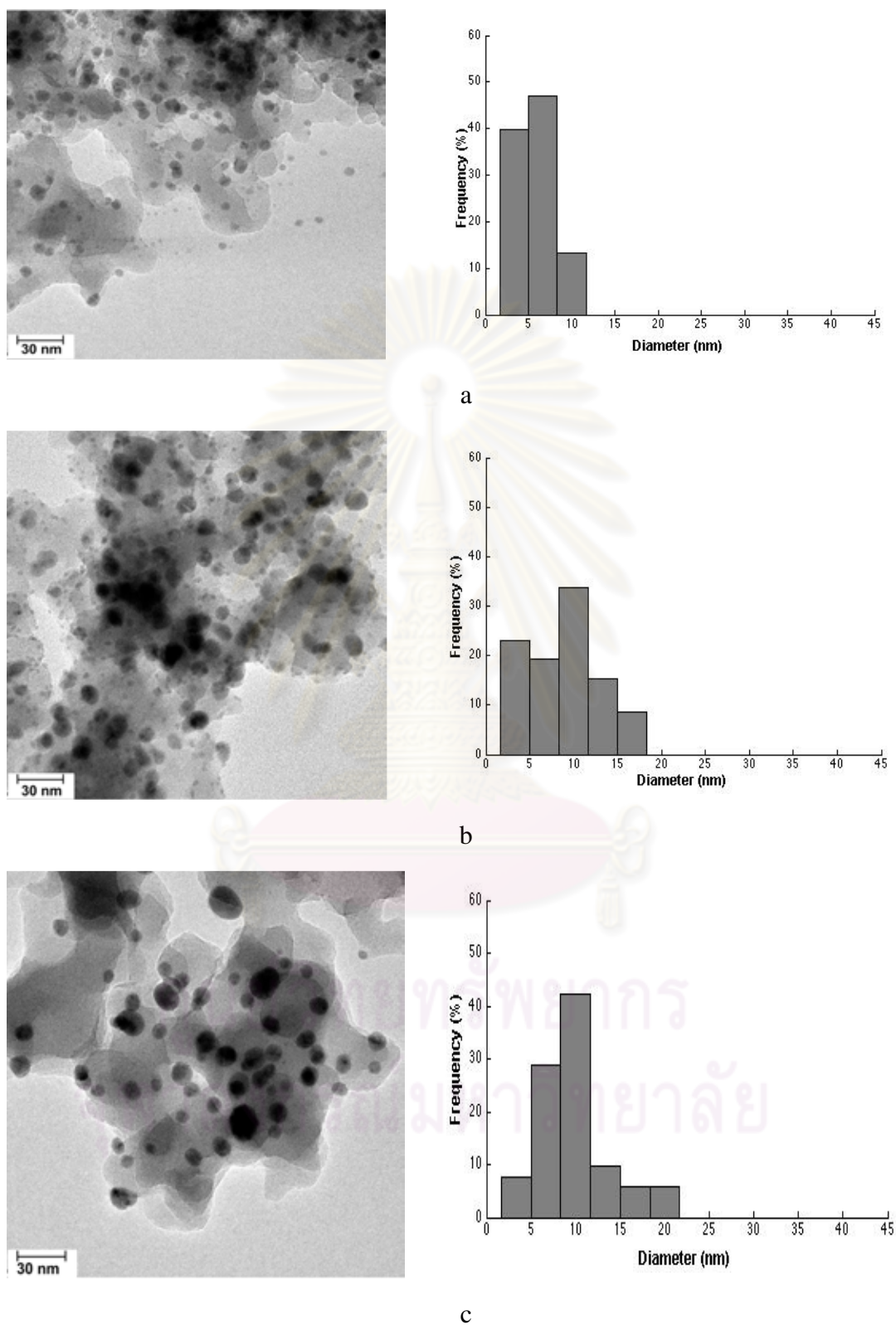
Figure 5.16 TEM micrographs of silver nanoparticles on MSPs, prepared from

various concentrations of silver precursor, 12 h of adsorption, and 4 h

of ; (a) 500 ppm, (b) 1000 ppm, and (c) 2000 ppm.

5.2.5 Effects of radical reduction time

Effects of radical reduction time on the synthesized Ag/SiO$_2$ nanocomposites were explored by varying ultrasonic irradiation times from 2 to 8 h at a fixed silver precursor concentration of 2000 ppm, and adsorption time of 12 h. The average sizes of silver nanoparticles were found to increase with radical reduction time (see Figure 5.17). This is because the longer ultrasonic irradiation time resulted in longer time for radical formation, hence longer time for silver precursor reduction and agglomeration. Bimodal distribution was also observed for the case of 8 h irradiation time. This was probably the consequence of aggregation.
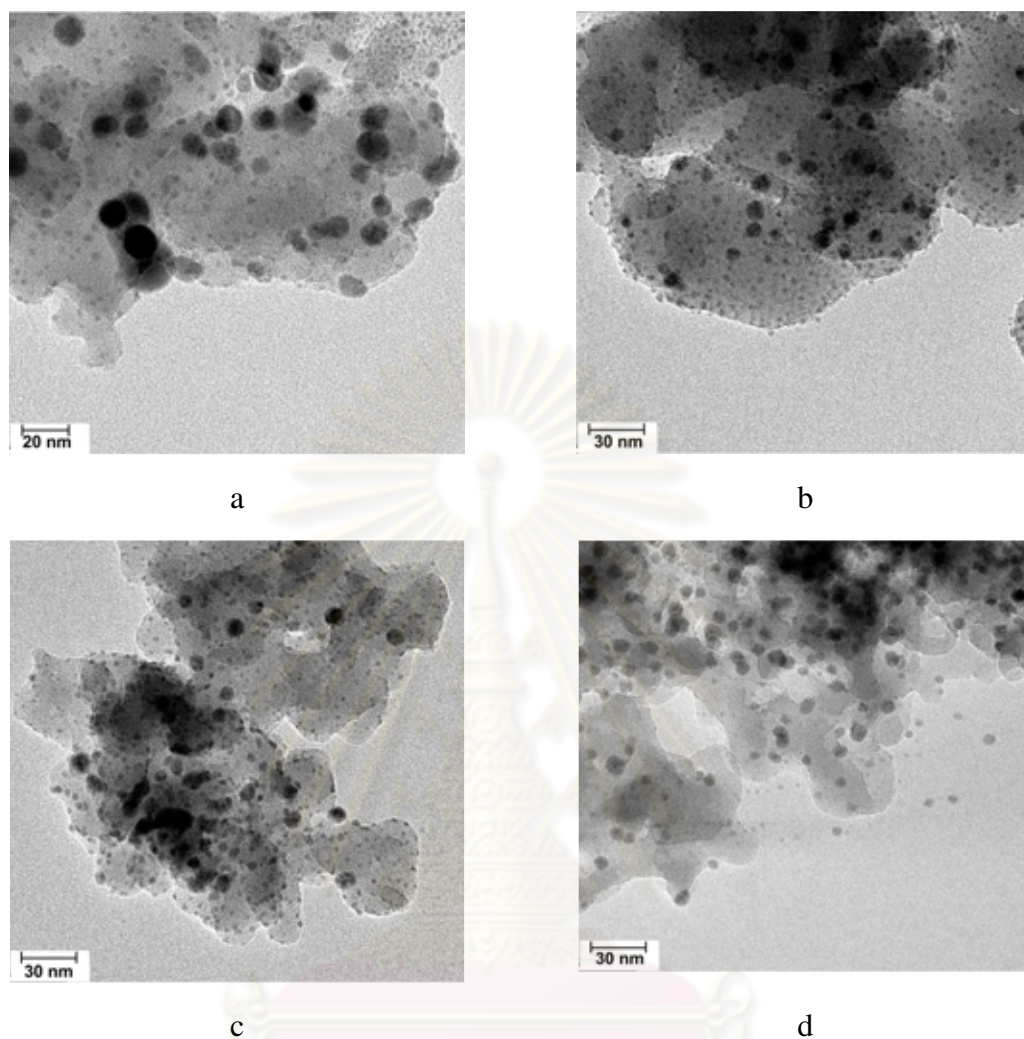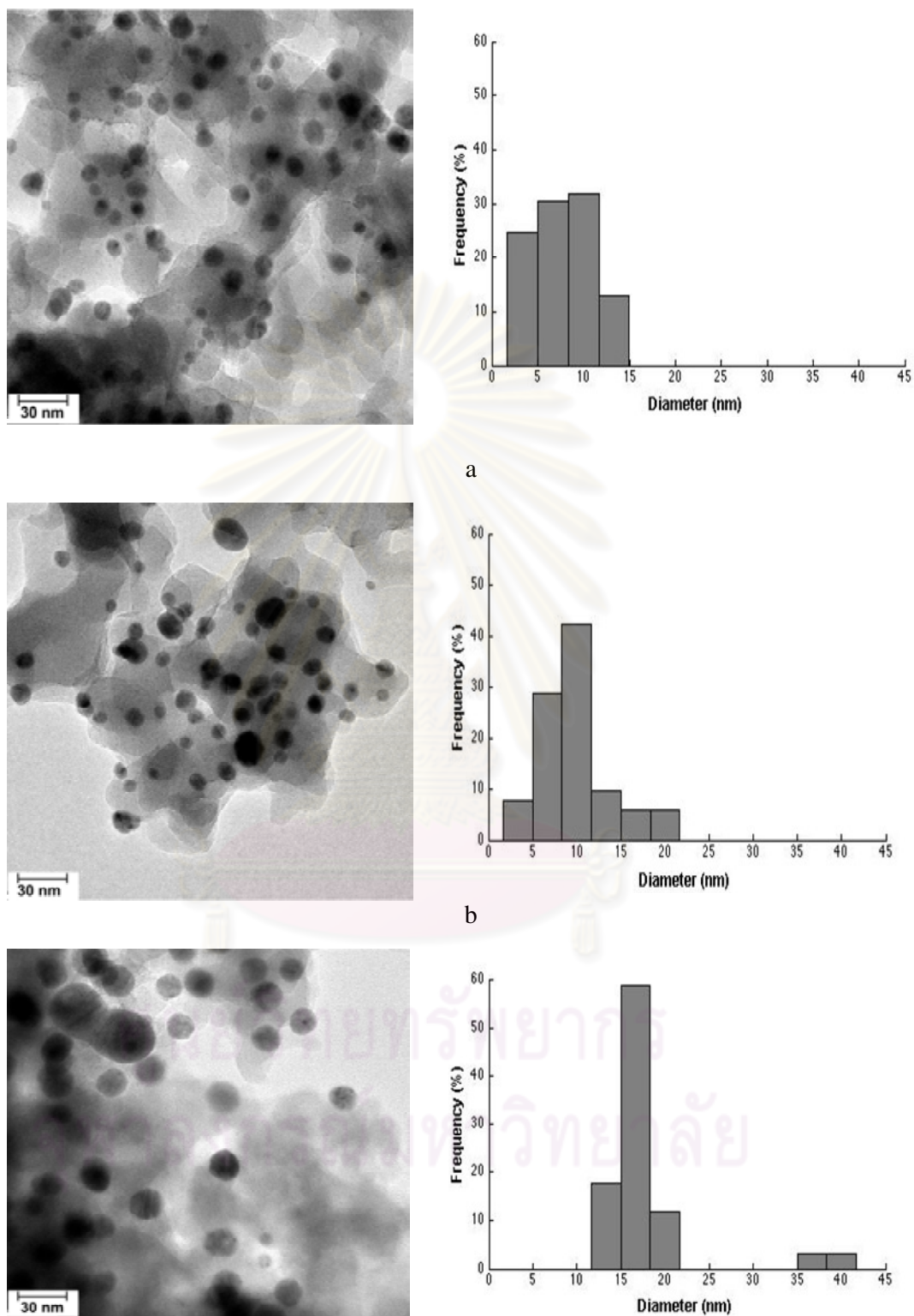
Figure 5.17 TEM micrographs of silver nanoparticles on MSPs, prepared from 2000
ppm of silver precursor, 12 h of adsorption, and the reduction time at ;
(a) 2 h, (b) 4 h, and (c) 8 h

5.2.6 The physical structure of Ag/SiO₂ nanocomposite

Table 5.4 shows pore volumes, and BET surface areas of silica nanopowder, MSPs, and Ag/SiO₂. This shows that the different supports of silica nanopowder possess the low surface area and low pore volume. The surface area of silica nanopowder itself is considerably smaller in comparison to that of mesoporous silica which has a high specific surface area, around 1000 m^2/g, [33]. However, the area was found to be decreased by 28% after surface modification with APTES. The APTES, which covered the surface of silica nanopowder, also made the particles more agglomerated and resulted in a reduced surface area as show in SEM image in Figure 5.18. After the reduction step, the BET surface area of Ag/SiO₂ nanocomposite was slightly increased. The additional surface area comes from the silver nanoparticles. This result agreed with Pérez-Rodríguez et al. [23] and Gedanken [24] that smaller metal nanomaterial can increase the specific surface of metal nanocomposite. This is shown in the schematic of silver nanoparticles deposited on MSPs in Figure 5.19. Additionally, volume of the pores was not significantly changed by functionalized chemical and silver nanoparticles. The similar of their pore volume was probably due to its initially smaller pore volume.

a   b
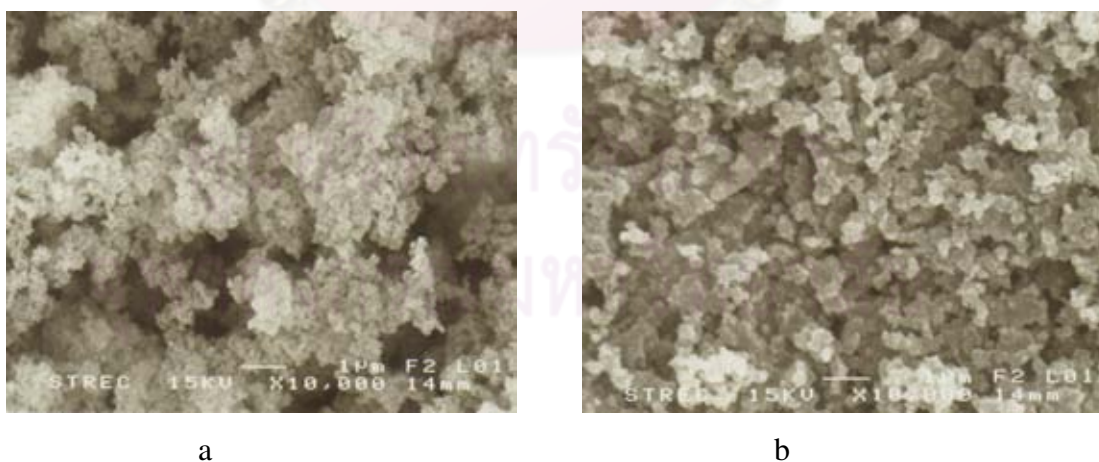
Figure 5.18 SEM image of silica nanopowder (a) before modification (b) after modification (MSPs)

Table 5.4 Physical properties of silica nanopowder, modified silica nanopowder, and
Ag/SiO$_2$ nanocomposite.

Supports	BET surface area (m^2.g^{-1})	Pore diameter (nm)	Pore volume (cm^3.g^{-1})
Silica nanopowder	60	na	0.16
MSPs	43	na	0.13
Ag/SiO$_2$	51	na	0.15

[na] the supports did not contain the mesoporous pores
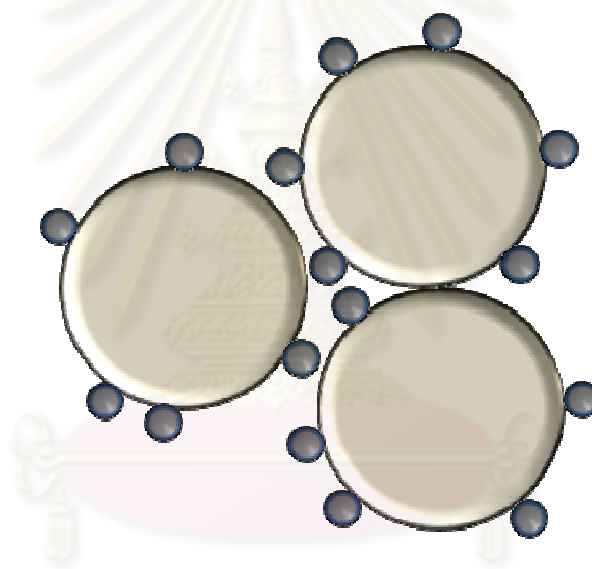
Figure 5.19 The schematic of silver nanoparticles deposited on the modified silica
nanopowder (not to scale)

The XRD pattern of the Ag/SiO$_2$ nanocomposite is shown in Figure 5.20(a).
The four diffraction peaks are at 38.18, 44.42, 64.66, and 77.26. This pattern is in
agreement with the database pattern, PDF number 04-0783, which represents the face
centered cubic lattice structure of silver nanoparticles [21, 91, 103]. However, there is
another XRD pattern with peaks at 27.88, 32.32, 46.23, 55.45, and 57.6. The pattern
relates to the pattern of AgCl (PDF number 06-0480). This AgCl was a contaminant
from the precursor, silver nitrate as shown in XRD pattern in Figure 5.20(b).
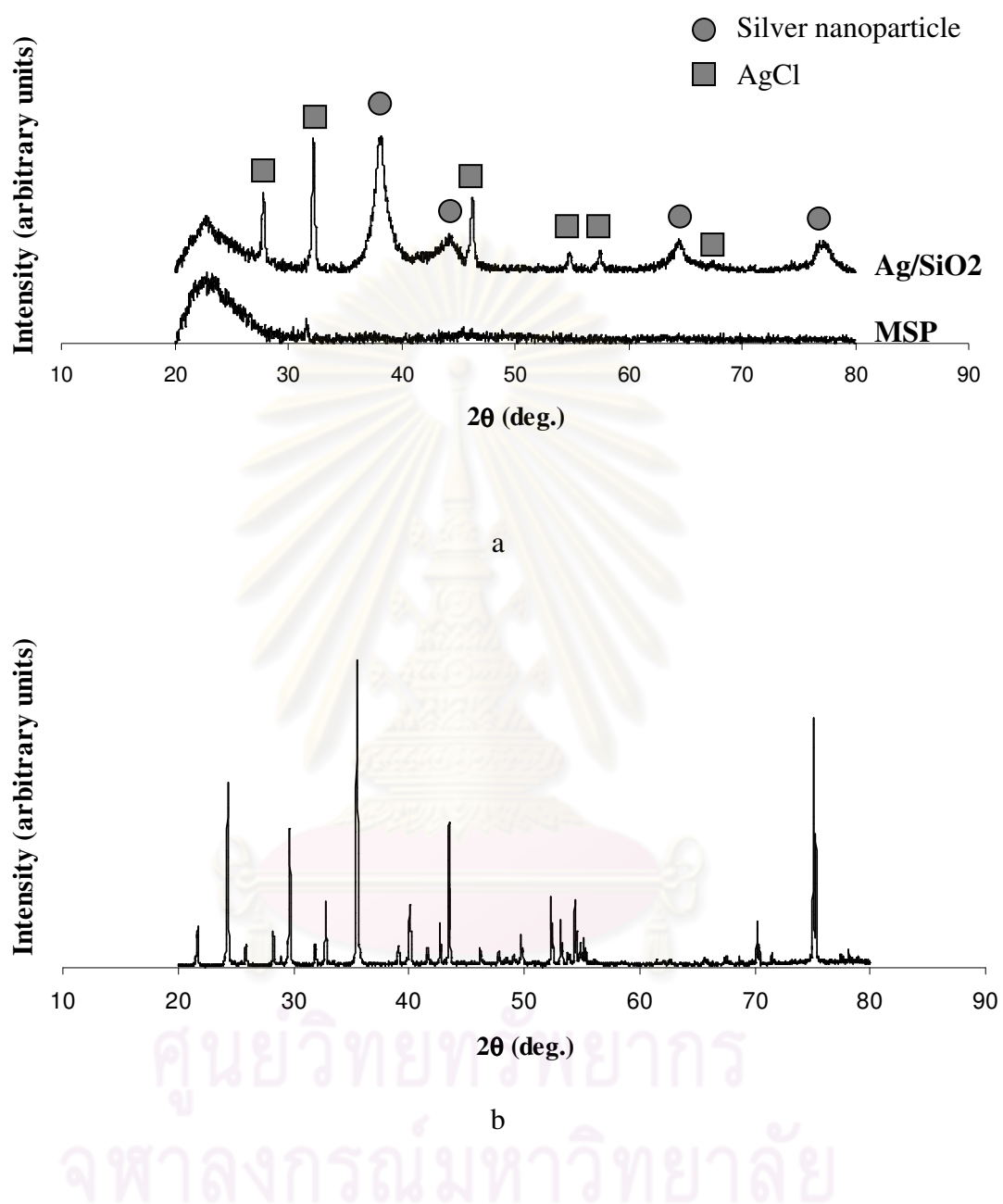
Figure 5.20 XRD Patterns of (a) MSPs and Ag/SiO$_2$ nanocomposite prepared with
2000 ppm of silver precursor, 12 h of adsorption, and 8 h of reduction,
(b) Silver nitrate

5.2.7 Charge on surface of Ag/SiO₂ nanocomposite

It is known that zeta potential relates to the charge of the support surface and enzyme molecule. This data is greatly useful for choosing the pH of immobilization by surface interaction, or adsorption method, as well as understanding the enzyme immobilization. The type of interaction between the enzyme and support could be identified by this data. Therefore, for enzyme immobilization application, the zeta potential at pH of immobilization needs to known, and the trend of this data could be known by doing zeta potential measurement at various pH.

The zeta potential of silica nanopowders, MSPs, and Ag/SiO₂ nanocomposite were measured under different pH solution, as shown in Figure 5.21. All materials had the zeta potential which was more negative with increasing pH following the theory as explained in the section 2.3.5 that zeta potential of particles depends on solution pH. At high pH the zeta potential has a higher negative than at low pH. After surface modification, the surface of silica nanopowder was more positive. This was probably due to the aminopropyl groups which led the surface to be more positive [111]. After silver nanoparticles were synthesized, it was found that the surface of Ag/SiO₂ nanocomposite was more negative than modified silica nanopowder surface. The negative surface charge of Ag/SiO₂ nanocomposite originated from the hydroxide ions, which were strongly adsorbed on various silver surfaces [112]. This result agreed with Alvarez-Pucbla et al. [113] who reported that the zeta potential of silver nanoparticles was negative by the adsorption of citrated ions. For this reason, we suggested that the negative charges in the system perhaps affected the surface charge property of silver nanoparticles. However, at the same pH, the zeta potential of Ag/SiO₂ nanocomposite was less negative than the silver nanoparticles that were synthesized by other methods, which were in the range of -40 to -50 mV [112-113], due to the aminopropyl groups that cause the silver nanoparticles deposition on the MSPs to be more positive [112]. Therefore, it can be concluded that the zeta potential of the silver nanoparticles also depends on type of attached support.

Additionally, the zeta potential also indicated the stability of the particles or colloids. According to table 2.4, the results in Figure 5.21 clearly shown that silica nanopowder were of incipient instability, while MSPs, and Ag/SiO$_2$ were of rapid coagulation.
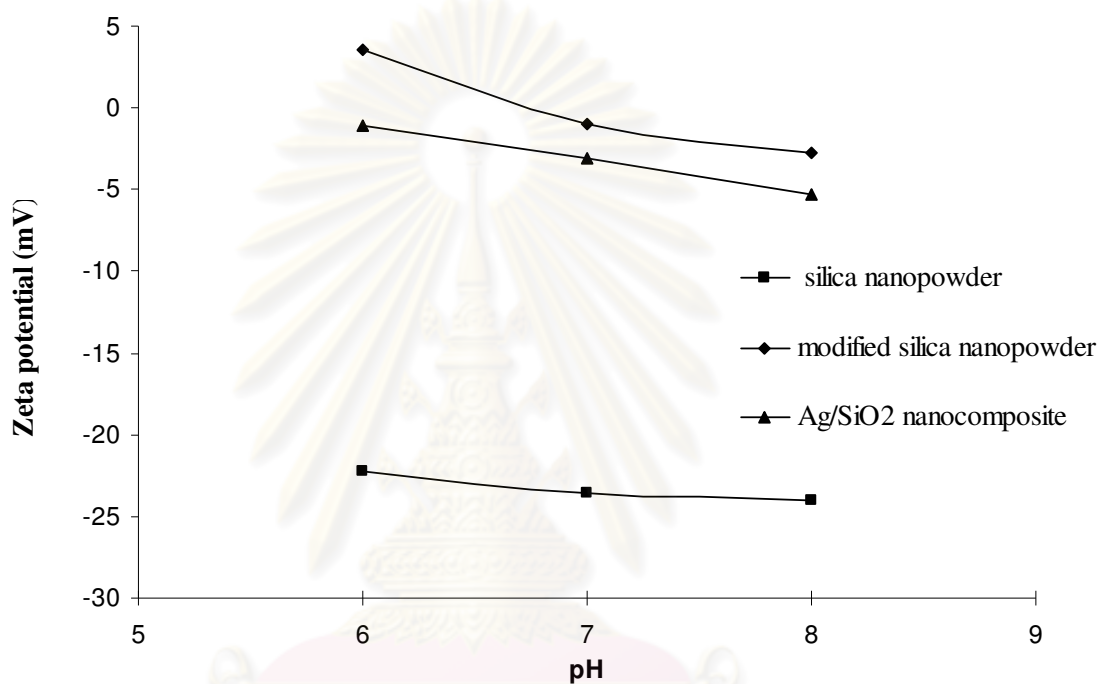
Figure 5.21 Effect of pH on zeta potentials of silica nanopowder, MSPs, and Ag/SiO$_2$

On the basis of the experimental results of the section 5.2 of this thesis, silver nanoparticles were successfully deposited onto the surface of silica nanopowder by ultrasonication. The aminopropyl groups play an important role as a chemical anchor to bind the silver ions and also act as a reductant. The adsorption time and the precursor concentration significantly influence the numbers of nuclei of silver atoms because the reduction occurs at the first stage (adsorption stage). While, the reduction time strongly affect the size control. Since it was postulated that the size of silver nanoparticles should markedly affect substrate and product mass transfer as well as enzyme immobilization, we chose two reduction times (2 and 8 h) to test this

conditions were carrier out at fixed silver nitrate concentration of 2000 ppm and adsorption time of 12 h in order to ensure considerable number of silver nanoparticles.

5.3 The immobilization of HRP on Ag/MCF and Ag/SiO$_2$ nanocomposite

The experiments in this part were related to 2 subsections; the synthesis of the silver nanoparticles on the surface of silica supports of different structures (MCF and silica nanopowder) and the HRP immobilization as shown in Figure 5.22. The aim of this part is study and compares the influence of support character on HRP immobilization, and biosensor application. Then silver nanoparticles deposited into MCF (Ag/MCF) were synthesized following the same synthesizing condition and procedure as of Ag/SiO$_2$. The surface of MCF containing with silanol groups were partly covered by an aminopropyl groups after overnight treatment with APTES. The obtained terminal aminopropyl groups acted as attachment points for silver ions through coordinate interactions. According to the results in section 5.2, this was found that the size of silver nanopartilces was controlled by reduction time. Therefore, silver particles on modified surface of MCF were finally achieved by radical reduction using ultrasonication at reduction time 2 and 8 h under controlled temperature at 20ºC. Finally, HRP was further immobilized on silver nanoparticles and on aminopropyl group by different interaction. The interactions between HRP and support surface will be discussed more in section 5.3.3.
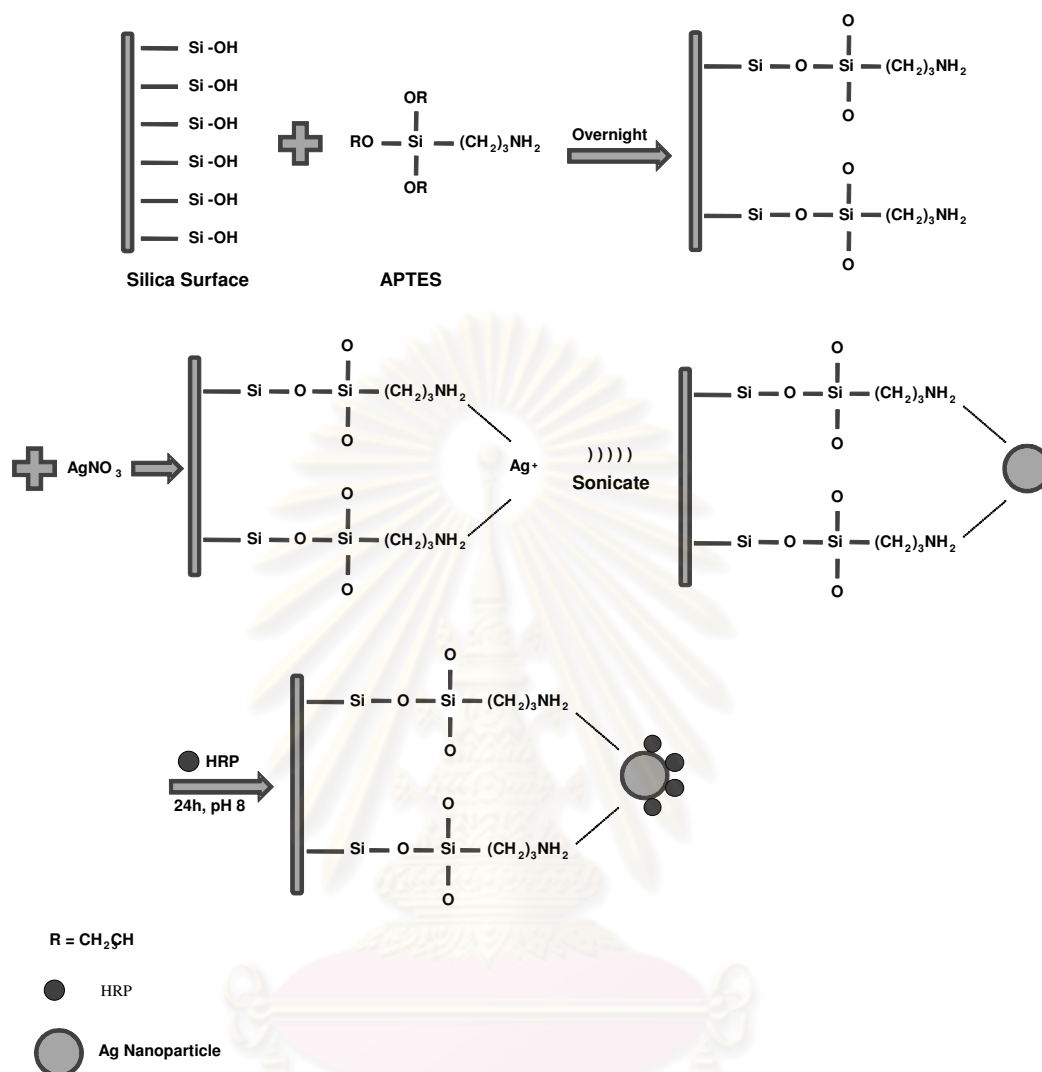
Figure 5.22 The process of HRP immobilized on Ag/MCF and Ag/SiO₂ nanocomposite.

5.3.1 Characteristics of modified surfaces
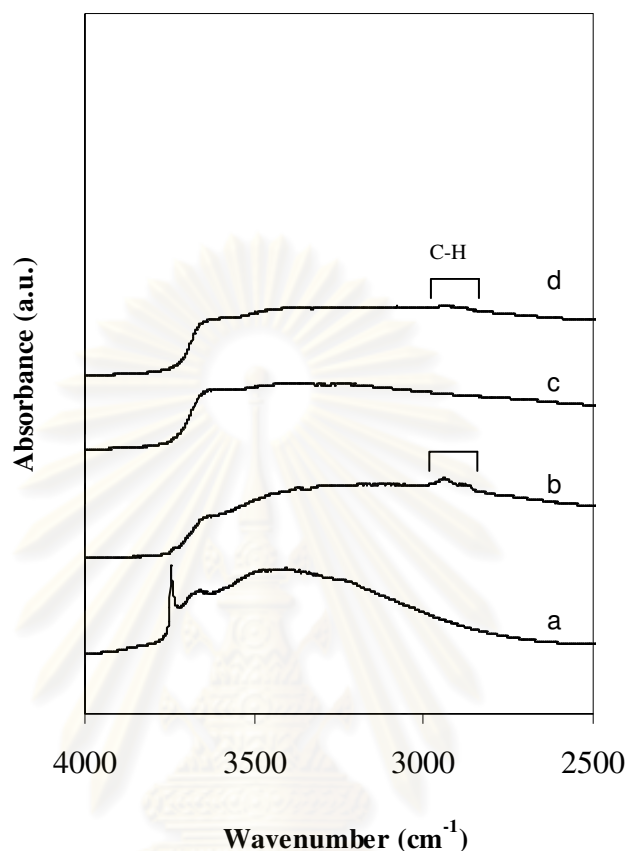
Figure 5.23 FTIR spectra of (a) MCF (b) MMCF (c) silica nanopowder (d) MSP

As discussed in section 5.2.2, the surface functionalization with organosilane was found necessary for attaching metal ions and forming metal nuclei on silica surface. The functional group acts like an anchor which binds the precursor on silica nanomaterial [71-72, 106], and also prevents the agglomeration of silver nanoparticles [103]. Figure 5.23 shows the FTIR spectra of MCF and silica nanopowder with and without surface modification. The silanol group on MCF surface which is represented by spectrum (a) is markedly observed at 3745 and 3400 cm^{-1}. On the other hand, the peaks of silanol groups of silica nanopowder (c) are not clearly observed probably due to the low surface area which causes low density of OH functional groups (see table 5.5). After surface modification, free silanol groups were mostly replaced by organic moieties using adsorption and condensation method [60]. The appended aminopropyl

groups which are represented on the spectra (b, d) are shown by the presence of C-H stretching band at 2929 cm^{-1} and 2871 cm^{-1} [60]. Since the surface area of MCF was much higher than that of silica (see Table 5.5), the C-H stretching band is much more pronounced. Furthermore, the decreases in BET surface area and pore volume of both supports in Table 5.5 after surface modification confirmed that aminoproply groups were also functionalized in the pores of the supports. The pore diameters of both supports were not significantly changed by surface modification, which indicated that the APTES did not distinctly block the pore opening.

Table 5.5 Pore characteristics of MCF and silica nanopowder, before and after modified with APTES.

Supports	Pore diameter (Å)	BET surface area (m^2/g)	Pore volume (cm^3/g)
MCF	148	618	1.60
MMCF	144	383	1.22
Silica nanopowder	na	60	0.16
MSP	na	43	0.13

[na] the supports did not contain the mesoporous pores

Figure 5.24 displays the TEM images of MCF with and without surface modification, it shows that the structure of MCF did not change after surface modification. Additionally, the structures of modified and unmodified MCF were evaluated through the nitrogen adsorption isotherms. The lower volume of nitrogen adsorbed onto modified MCF surface as shown in Figure 5.25 confirmed that APTES was attached into the pores of MCF, and the mesopore structure was still obtained.

a   b
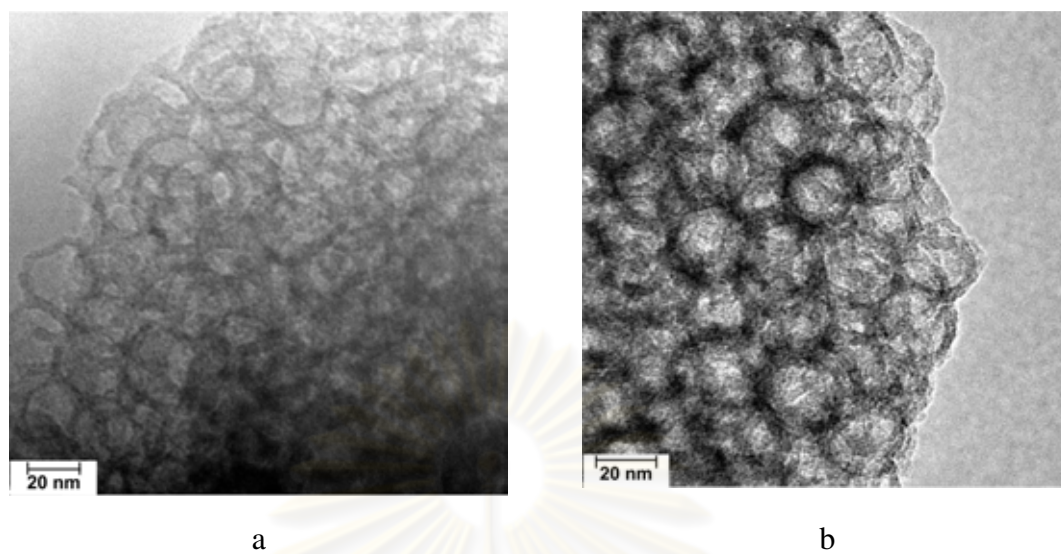
Figure 5.24 TEM images of MCF; (a) before and (b) after modified surface
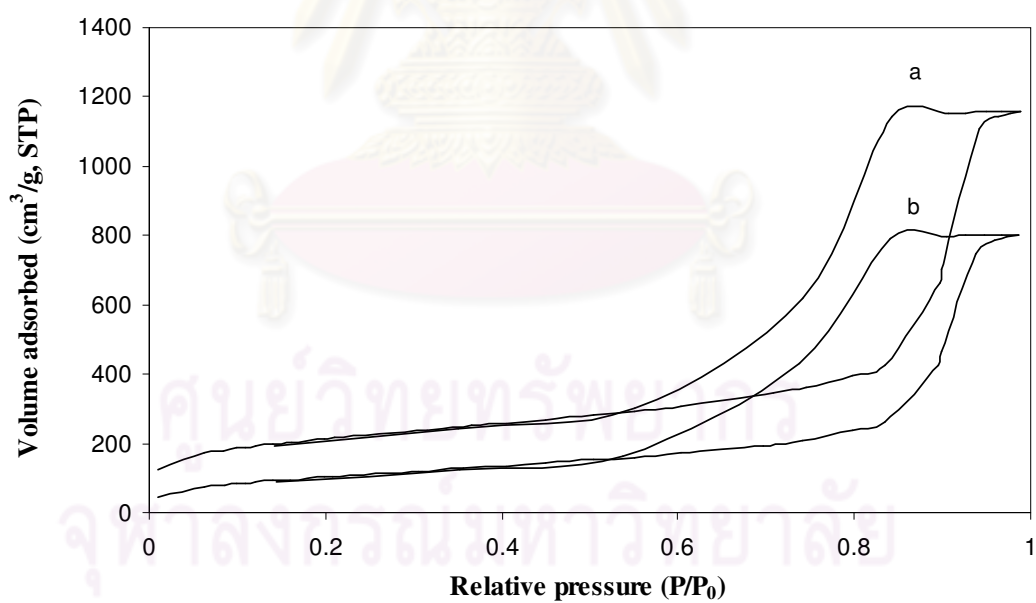
Figure 5.25 nitrogen adsorption-desorption isotherms of MCF (a) before, and (b) after surface modification

5.3.2 The synthesis of Ag/MCF

The synthesis of Ag/MCF was achieved by ultrasonication method following the same conditions used for Ag/SiO$_2$ nanocomposite synthesis as was already discussed in section 5.2. Briefly, the silver ions attached on the aminopropyl groups modified on silica surface were reduced by electrons from 2 stages during the synthesis. The first reduction stage was during silver ion adsorption period, where amine nitrogen was an electron donor. The second stage was during the hydrogen radical reduction under ultrasonication. The influence parameters on the reduction and formation mechanism of Ag/SiO$_2$ was clearly explained in the second 5.2

Since we previously found that reduction time was the governing parameter for synthesizing different sizes of Ag/SiO$_2$. The synthesis of Ag/MCF was, therefore, tested under two different reduction times (2 and 8 h).

The UV-Vis absorption spectra of Ag/MCF and Ag/SiO$_2$ nanocomposite with different reduction times are shown in Figure 5.26. The UV-Vis absorption spectra of bare MMCF and MSP show no distinct peaks. After silver nanoparticles were synthesized on/into MMCF and MSP, the maximum absorbance peaks of silver nanoparticles on/into all supports (Figure 5.26(a), Figure 5.26(b)) appear at the similar wavelength of 420-425 nm. This was also in accordance to some previous researches which reported the band between 410-430 nm for silver nanoparticles [72, 83, 85, 114]. Figure 5.26(a) clearly shows an increase in the amount of synthesized silver nanoparticles following the reduction time, while silver nanoparticles on MSPs in Figure 5.26(b) are not distinctly different in terms of intensity. According to the different structures, silver ions attached into the pore of MCF must take longer time to be reduced. However, the analogous plots of the surface Plasmon absorption of Ag/SiO$_2$ nanocomposite were distinctly different from Ag/MCF. Their band width are different, from the suggestion of Weiping and Lide [105], that interface interaction between pore wall of silica (with high specific area) and silver nanoparticles plays important role on the broadening and lowering surface plasmon resonance as shown in Figure 5.26(a). This interaction is large when the size of silver nanoparticles is

small, so it might act to suppress surface plasmon resonance. On the other hand, this interaction between silica nanopowder and silver nanoparticles is much smaller, due to the silver nanoparticles were attached at outer surface, no wall interaction. (from TEM image, Figure 5.27), resulting in the narrower in width and higher in peak height as shown in Figure 5.26(b).

a

b
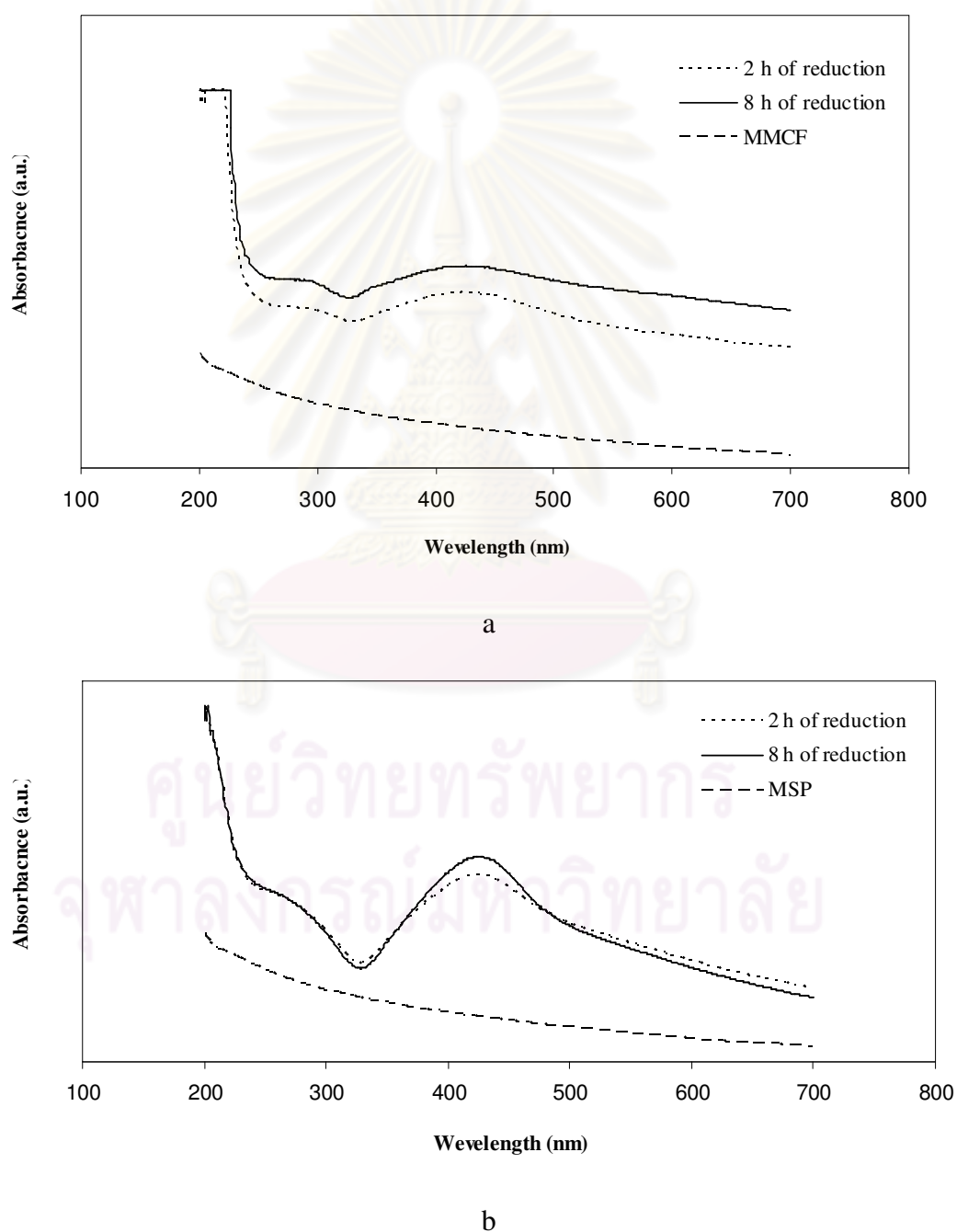
Figure 5.26 UV-Vis adsorption spectra; (a) Ag/MCF (b) Ag/SiO$_2$

1. The size and shape of silver nanoparticles

As shown in section 5.2.5 that the reduction time affected the size of silver nanoparticles on silica nanopowder. The size of silver nanoparticles are increased by increasing reduction time, the average size of silver nanoparticles of Ag/SiO$_2$-2 and Ag/SiO$_2$-8 were respectively determined at 10 and 16 nm as shown in Figure 5.27 (c, d). However, it was found that the reduction time did not significantly affect the size of synthesized silver nanoparticles. The average size of silver nanoparticles of Ag/MCF-2 and Ag/MCF-8 are around 5 nm. This result can be explained by high surface area of MMCF may smoothly distribute the silver nanoparticles with the proper distance between particles. For that reason, the longer reduction did not cause the small nanoparticles to form the larger particles. On the other hand, in the case of Ag/SiO$_2$, silver precursors were deposited at the outer surface of MSPs, therefore the reduction between precursors and the generated hydration electrons were not blocked by the pore wall. Then, hydration electrons were easily approached to silver ions. Moreover, the silver nanoparticles were not limited by the space then they can grow easily.

However, the TEM image in Figure 5.27 (a, b) shows that the synthesis of Ag/MCF was achieved and that the silver nanoparticles attached inside of the pores could be observed. They are attached near the inner pore wall, so they might be attached to aminopropyl groups which act as the anchor to the pore surface.

a

b

c

d
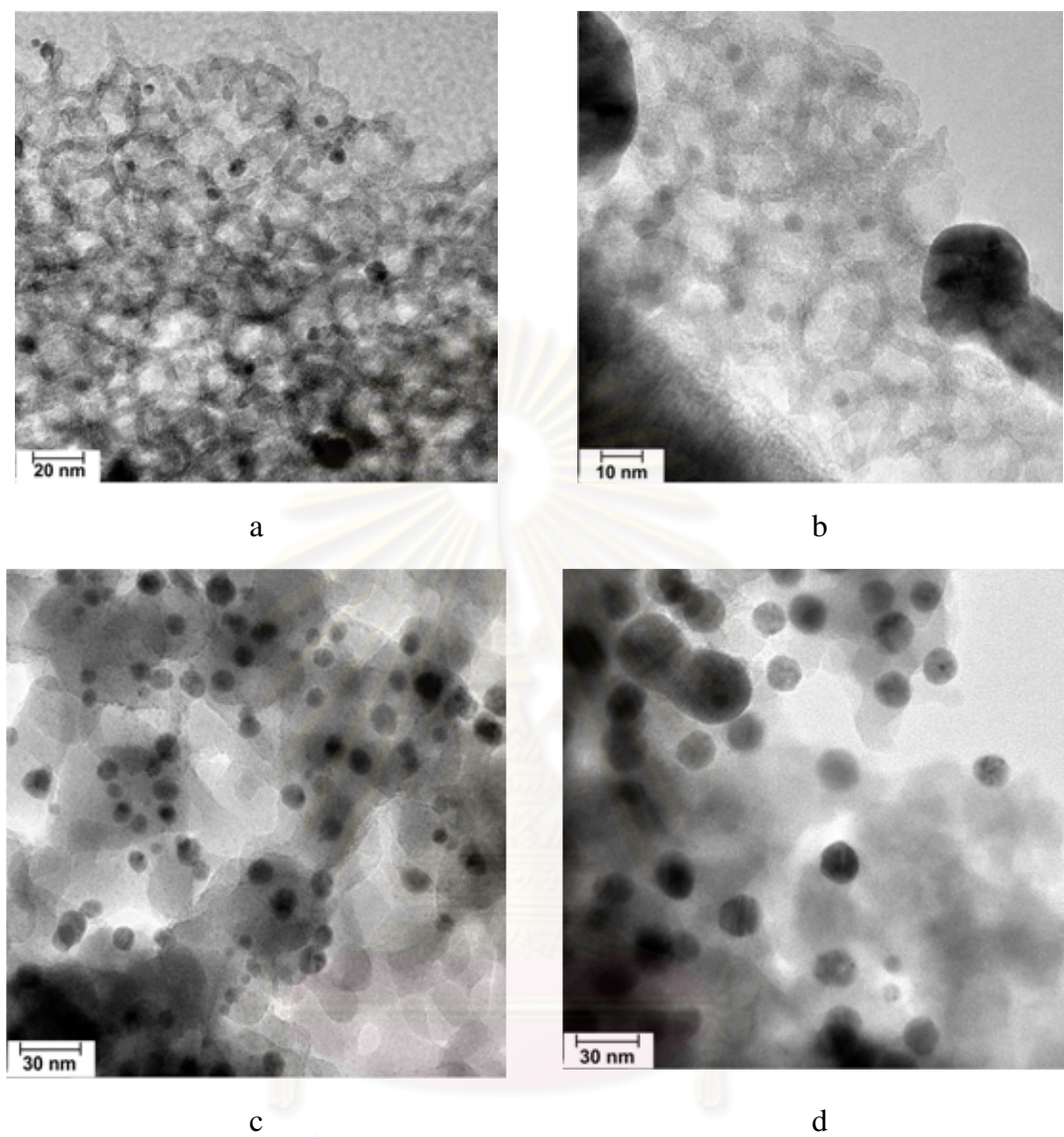
Figure 5.27 TEM images of Ag/MCF and Ag/SiO$_2$ of 2 and 8 h of reduction time ;
(a) Ag/MCF-2, (b) Ag/MCF-8, (c) Ag/SiO$_2$-2, and (d) Ag/SiO$_2$-8
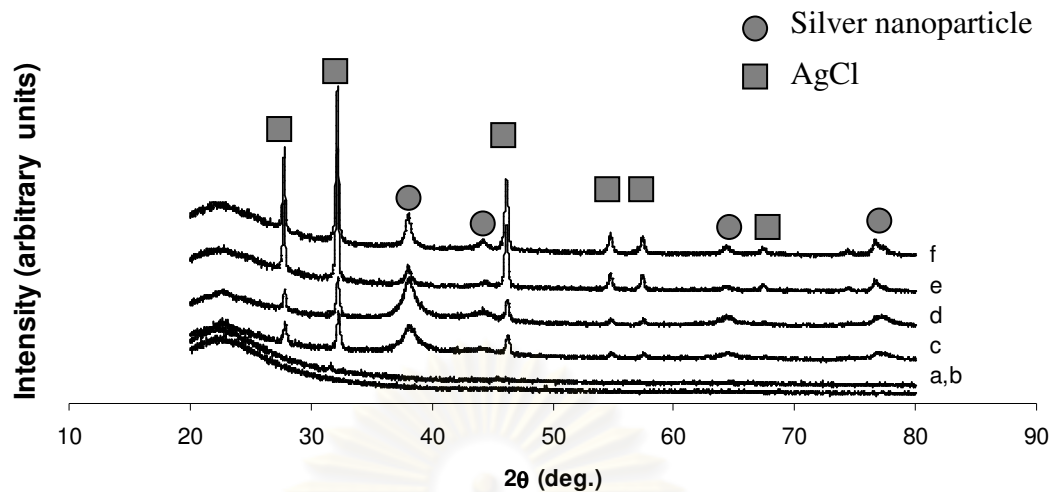
Figure 5.28 XRD patterns of (a) silica nanopowder and (b) MCF, (c) Ag/SiO_2-2, (d) Ag/SiO_2-8, (e) Ag/MCF-2, and (f) Ag/MCF -8

The XRD patterns of the Ag/MCF and Ag/SiO_2 nanocomposite are shown in Figure 5.28. All of them show the similar patterns, which indicated the same type of silver nanoparticles produced. As has already been discussed in section 5.2.6, silver nanoparticles with face centered cubic lattice structure were synthesized. The silver nanoparticles are represented by the four diffraction peaks at 2θ values of 38.18, 44.42, 64.66, and 77.26 respectively. However, AgCl were also observed on modified supports. It was found that AgCl was contaminated in the silver nitrate precursor reagent. Moreover, the intensities of Ag/SiO_2 of both samples are higher than Ag/MCF. This is because the silver nanoparticles on MSPs possess the bigger size than on of MMCF as confirmed by TEM image in Figure 5.27, and relates with the equation 5.2 [115].

$$\beta_{hkl} = \frac{K\lambda}{L_{hkl}\cos\theta_{hkl}}$$ (5.2)

Where:

β is the width of the peak at half maximum intensity of a specific phase (hkl) in radians

K is a constant that varies with the method of taking the breadth (0.89<K<1)

λ is the wavelength of incident x-rays

θ is the center angle of the peak

L is the crystallite length

2. The pore character of Ag/MCF and Ag/SiO₂

The pore characters of MCF and silica nanopowder after the surface modification and silver nanoparticle addition, as well as the location of silver nanoparticle, were discussed in this section. This data is necessary for indicating that enzyme could diffuse though the pore or be immobilized at outer pore surface of supports. Furthermore, the changing of pore surface and pore volume is useful in explaining the enzyme immobilization.

Ag/MCF and Ag/SiO₂ were synthesized by varying the reduction times. For Ag/MCF, the bigger pore diameter of Ag/MCF-2 and Ag/MCF-8 in Table 5.6 indicates that the pores of MMCF were collapsed, as consequence of the lager pore volume and reduced surface area were obtained. Even though this speculation of the pore collapsing could not be observed by TEM image in Figure 5.27 (a, b), but it could be confirmed by the pore size distribution of Ag/MCF-2 and Ag/MCF-8 in Figure 5.29(a). This shows that the pore diameter of around 15 nm disappears, while the bigger pore diameters are formed. The large pore may be formed by the collapse of the small pore which was broken by the ultrasound power. It shows that the pore diameters of MMCF and are bigger with the longer reduction time (8 h). However, the TEM image from Figure 5.27 (a, b) still shows frame network structure of MMCF. Additionally, the mesoporous structure was still obtained as confirmed by the nitrogen adsorption isotherms as shown in Figure 5.30.

Furthermore, as discussed in section 5.2.6, the surface area of Ag/SiO₂ was increased by the synthesized silver nanoparticles. Table 5.6 shows that the surface

areas of Ag/SiO$_2$ were slightly increased by increasing the reduction time. This also suggests that most of silver nanoparticles were attached on the outer surface. However, as shown by the pore size distribution of Figure 5.29(b) that the bigger pores at around 15-20 nm were observed from Ag/SiO$_2$-8. This also indicated that the pores of MSPs were collapsed by ultrasonic power, which was increased by increasing the reduction time.

Table 5.6 Pore characteristics of MCF and silica nanopowder, after modification with APTES, and after compositing with silver nanoparticles using 2 and 8 h of reduction time

Supports	Pore diameter (A)	Surface area m^2/g	Pore volume cm^3/g
MMCF	144	383	1.22
Ag/MCF-2	246	291	1.35
Ag/MCF-8	255	287	1.35
MSP	na	43	0.13
Ag/SiO$_2$-2	na	50	0.14
Ag/SiO$_2$-8	na	51	0.15

[2] reduction for 2 h

[8] reduction for 8 h

[na] the support did not contain the mesoporous pores

a

b
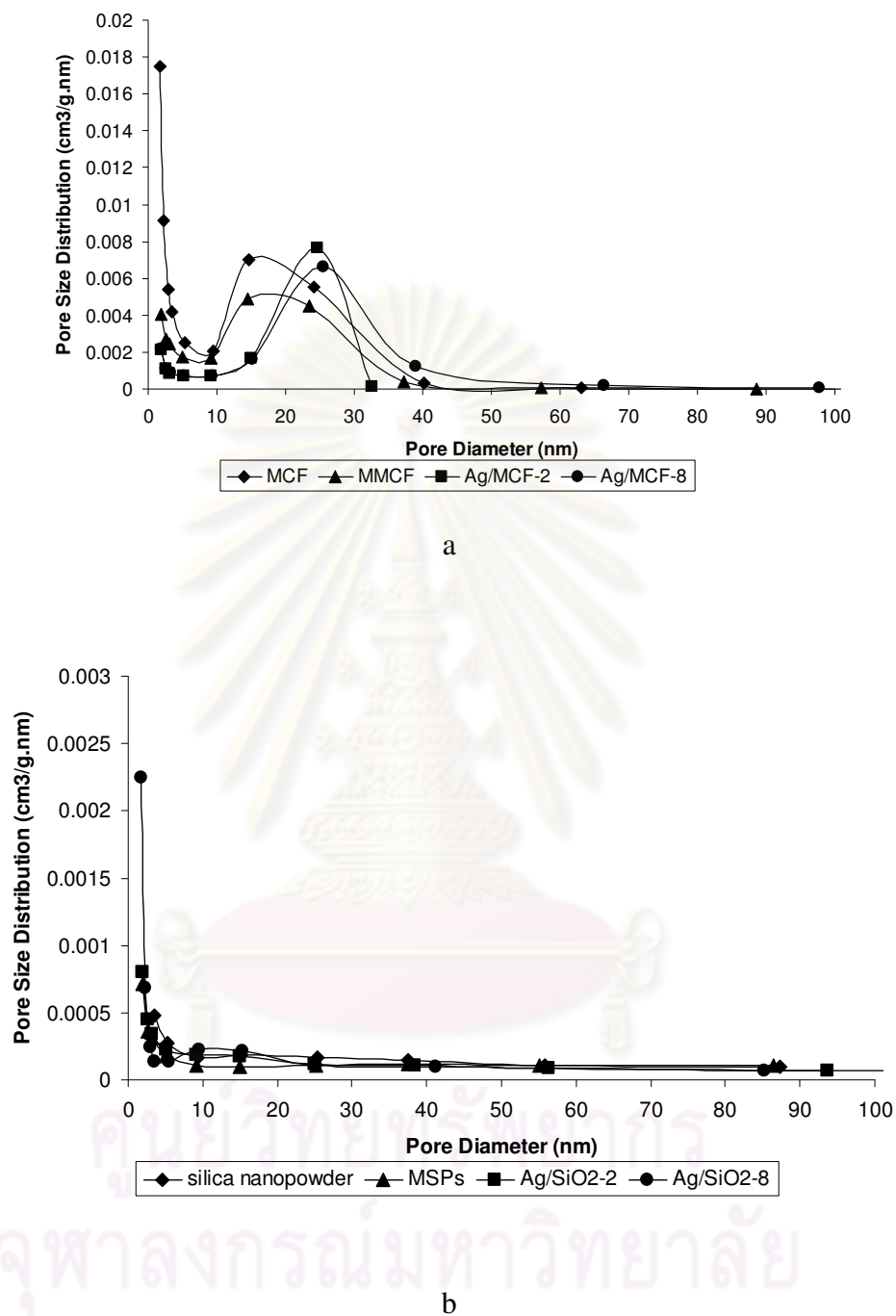
Figure 5.29 Pore size distribution of supports : (a) various type of MCF and (b)
various type of silica nanopowder
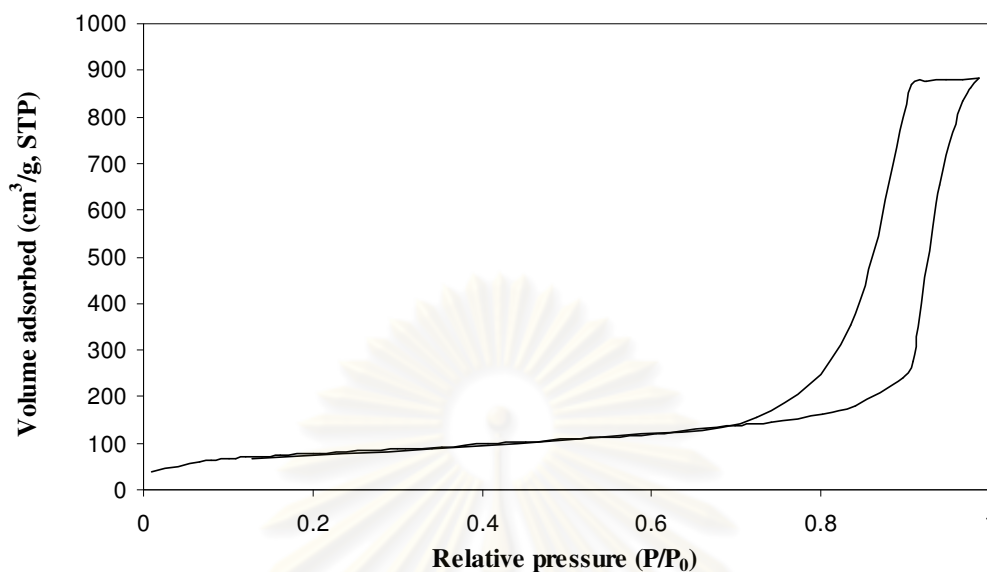
Figure 5.30 nitrogen adsorption-desorption isotherms of Ag/MCF-8

3. The surface charge properties Ag/MCF and Ag/SiO$_2$

Table 5.7 The zeta potential of MCF and silica nanopowder with/without
modification and with silver nanoparticles

Support	Zeta potential	Support	Zeta potential
MCF	-23.55	Silica nanopowder	-22.40
MMCF	-4.87	MSP	-2.80
Ag/MCF-2	-5.22	Ag/SiO$_2$-2	-5.27
Ag/MCF-8	-6.92	Ag/SiO$_2$-8	-5.46

Table 5.7 shows zeta potential values of all supports in buffer solution with pH
8. It was found in section 5.1 that pH 8 of enzyme immobilization, provided the
highest specific activity and storage stability of immobilized HRP. The unmodified
supports, MCF and silica nanopowder surface are mostly covered with a large amount

of silanol (Si-OH) group, pI of silica around 2, so that the zeta potential of these materials at pH 8 were highly negative value. On the other hand, after surface modification the zeta potential of MMCF and MSPs were apparently less negative. This caused by the protonation of aminopropyl groups on the functionalized material. The protonation will lead to the formation of a positively charged shell on the surface of support [111]. According to Chong and Zhao [9], the negative zeta potential of MMCF and MPS may suggest that silanol groups on support surface were not completely covered.

After silver nanoparticles were composited with silica, the zeta potential slightly decreased. The surface potentials became more negative by the adsorption of hydroxide anion from the water [112], it has been published that hydroxide ions strongly adsorbed on various silver surface [112]. However, the zeta potential of Ag/SiO_2-2 and Ag/MCF-2 were less negative than Ag/SiO_2-8 and Ag/MCF-8. It may indicate that unreduced silver ions remained on the surface of silver nanoparticles on both supports at the reduction time of 2 h. This speculation is supported by the report of Ma et al. [116]. They found that the fresh silver particles may still contain the silver ions. They suggest that silver nanoparticles should be aged before being used in biomolecular field. Additionally, it was found that HRP immobilization on Ag/MCF-2 was less active than on Ag/MCF-8, this related to this assumption, which will be further discussed in section 5.3.3. However, Ag/SiO_2-2 and Ag/SiO_2-8 show only small difference in zeta potential. This could be explained by the following. At 2 h of reduction time, silver ions which were attached on the outer surface of MSP was easier to be reduced than on MMCF, resulting in more silver nanoparticles formed, therefore less silver ions were left.

Therefore, the knowledge of the pore characters and surface properties of supports are useful for enzyme immobilization. The changing of pore characters and surface properties, before and after surface modification with functional groups and silver nanoparticles of those supports, were clearly known. This data will be used for understanding and discussion of the enzyme immobilization in following paragraph.

5.3.3 The immobilization of HRP on Ag/MCF and Ag/SiO₂ nanocomposite

From the first part of this chapter, section 5.1, pH and pore structure play important role on HRP immobilized on mesoporous silica. HRP was probably mainly immobilized on silica surface by electrostatic interaction. HRP molecule is positive charge at pH below 8.9 (pI), the maximum specific activity and stability of immobilized HRP was obtained at pH 8 and on MCF. Nevertheless, the leaching of immobilized HRP still be a problem. Therefore, in this part of our work, we investigated other parameters influencing HRP immobilization and biosensor application. The improvement of surface properties by adding the silver nanoparticle was considered for improving the properties of immobilized HRP. Therefore, the surface modification by aminopropyl groups and presence of silver nanoparticles on MCF were used to study HRP immobilization. However, the enzyme immobilization into the pore of supports, the mass transfer resistance must be considered. To clearly understand the influence of surface properties and mass transfer on HRP immobilized on Ag/MCF, silica nanopowder (Ag/SiO₂) with almost non pore structure was used to immobilize HRP. Finally, the comparing of the properties of immobilized HRP namely; enzyme leaching, enzyme loading, enzyme activity, storage stability and electrochemistry on Ag/MCF and Ag/SiO₂ nanocomposite were discussed.

1. interaction between enzyme and surface supports

It is known that interaction between enzyme and support surface, enzyme immobilization by adsorption method, depends on the functional groups and charge on the surface of support. Since MCF and silica nanopowder were surface functionalized by aminoproply groups and silver nanoparticles. Resulting in there were various functional groups on one support surface. Therefore, the interaction between HRP and support surface, which was carried out in solution pH 8 that could occur on different supports are proposed in the following paragraphs.

The hydrogen bond of the support surface and the enzyme could be taking place with aminoproply groups on the modified surface and amino or carboxylic

groups of the enzyme. The hydrogen atom, which is covalently bonded to the nitrogen atom at the support surface, may interact to nitrogen or oxygen atom of enzyme molecules as shown in Figure 5.31(a).

At the same time, since APTES is a nonpolar molecule, it consists of hydrocarbon chains. It was possible that R groups (CH_2CH_3) of APTES molecules were remained on the surface. According to the suggestion of Veliky and McLean [49], the enzyme could be rearranged so their molecules adsorb on the modified agent through the hydrophobic interaction, as shown in Figure 5.31(b).

The electrostatic interaction plays an important role in the HRP immobilization on OMMs as discussed in section 5.1. It is the interaction between the different charge of the enzyme molecule and support surface. Electrostatic interaction depends on their isoelectric point; the pH of the enzyme is 8.9, silica is 2, and aminopropyl is 8.7 [117]. At pH 8 (pH for enzyme immobilization), HRP possesses the positive charge similar to that electrostatic repulsion of aminopropyl groups, therefore it could not interact with aminoproply groups by attractive electrostatic interaction. However, since the zeta potential (see table 5.7) of the support surface, with the presence of silver nanoparticle, are negative potential. For that reason, enzyme may interact with silver nanoparticles by the attractive electrostatic interaction, as show in Figure 5.31(c). Additionally, silanol groups of silica surface might not be homogeneously covered by the grafting method. Therefore, the electrostatic interaction between enzyme and silanol groups also might be occurring.
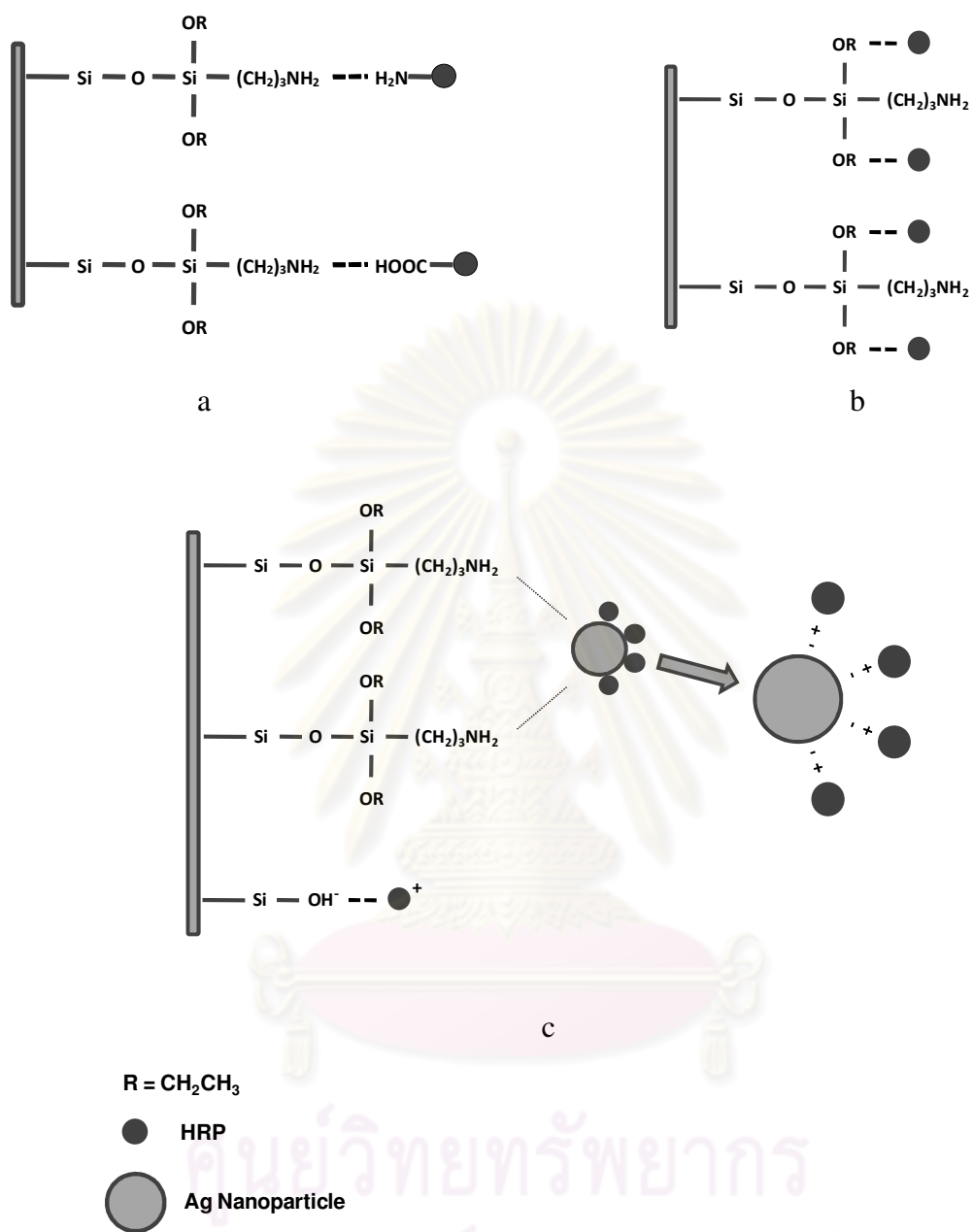
Figure 5.31 Interactions between enzyme molecules with different support surfaces
(a) hydrogen bonding, (b) hydrophobic interaction, and (c) electrostatic
interaction

2. The effects of support characters and surface properties on HRP immobilization

The HRP immobilization on different MCF and different silica nanoparticles supports in buffer solution pH 8 for 24 h at 4ºC, are shown in Figure 5.32(a) and Figure 5.32(b), respectively. The considered parameters of immobilized HRP; enzyme loading, leaching, and activity are discussed based on the character of supports as follows. From Figure 5.32, support characters strongly affect the loading, leaching, and activity of HRP. In terms of enzyme loading, the different MCF supports possessed the higher surface area and larger pore volume than the silica nanopowder type (see data in Table 5.6), resulting in the higher amount of HRP absorbed as shown in Figure 5.32. MMCF provided the lowest of enzyme loading of 95%, while MCF, Ag/MCF-2, and Ag/MCF-8 provided the similar enzyme loading up to 99 %. From Table 5.5 and Table 5.6, they show that surface area and pore volume of MCF were moderately reduced by surface modification, while the pore opening was not blocked. The synthesis of Ag/MCF-2 and Ag/MCF-8 caused the reduction of surface area, while there was a little change on the pore volume. However, the bigger pore diameters were formed, which were discussed in the section 5.3.2. Therefore, these data indicated that HRP could diffuse through the pore and was immobilized in the pore of MMCF, Ag/MCF-2 and Ag/MCF-8, similar to that of MCF. On the other hand, there were only a little of HRP immobilized on different silica nanopowder supports which posses a low surface area. The lowest of enzyme loading was ~2 % of initial enzyme, obtained from MSPs. The other of different silica nanopowder supports provided the similar enzyme loading of ~ 3%.

In terms of enzyme leaching, the predictable results were obtained in this work as shown in Figure 5.32. Immobilized HRP leached from MCF less than from silica nanopowder. It has been proven in our previous section 5.1.2 that because of the spherical cell and frame network structure of MCF, so it was difficult for enzyme to leach from MCF. The enzyme leaching was not obtained from Ag/MCF-2, while the highest of enzyme leaching was obtained from MMCF of ~32% of immobilized HRP. This indicated that enzyme was interacted with the support surface by a weaker

interaction than that with the other MCF supports. On the other hand, silica nanopowder has the wide and shallow pore, HRP may also be immobilized in the pore and on outer surface. Therefore, immobilized HRP leached out easily from its pore, and from the outer surface. The enzyme leaching had the similar results of MCP supports; the lowest leaching was obtained from Ag/SiO_2-2, of ~2%, while the highest enzyme leaching up to 82% from MSPs.

In terms of enzyme activity, it is known that the immobilization method and mass transfer resistance strongly influence on the specific activity of immobilized enzyme. In this case, only the mass transfer was considered, because the same immobilization method was used for both supports under comparison. The HRP immobilization on silica nanopowder was aimed to investigate the effect of mass transfer on immobilized HRP. The specific activity of immobilized HRP on different MCF supports and different silica nanopowder supports are distinctly shown in Figure 5.32. The specific activity of HRP immobilized onto silica nanopowder was around 3 times higher than the one immobilized into MCF. This could be explained by the effect of mass transfer resistance as follows.

For HRP immobilization in silica nanopowder which was of very low porosity (almost non porous), external mass transfer should be more significant than internal mass transfer. As introduced in section 2.5.2 that the mass transfers of substrate and product depend on the driving force of their different concentration between bulk and support surface, and as well as the mass transfer coefficient as shown in question 2.3. The mass transfer coefficient relates to the stagnant film; the mass transfer increases when the stagnant film is thinner.

$$N_s \qquad = \qquad k_s(S_0 - S) \qquad\qquad (2.3)$$

In the case of enzyme is immobilized into the porous material. The internal mass transfer resistance is considered since it has been generally found that internal mass transfer resistances are much higher than external mass transfer resistance.
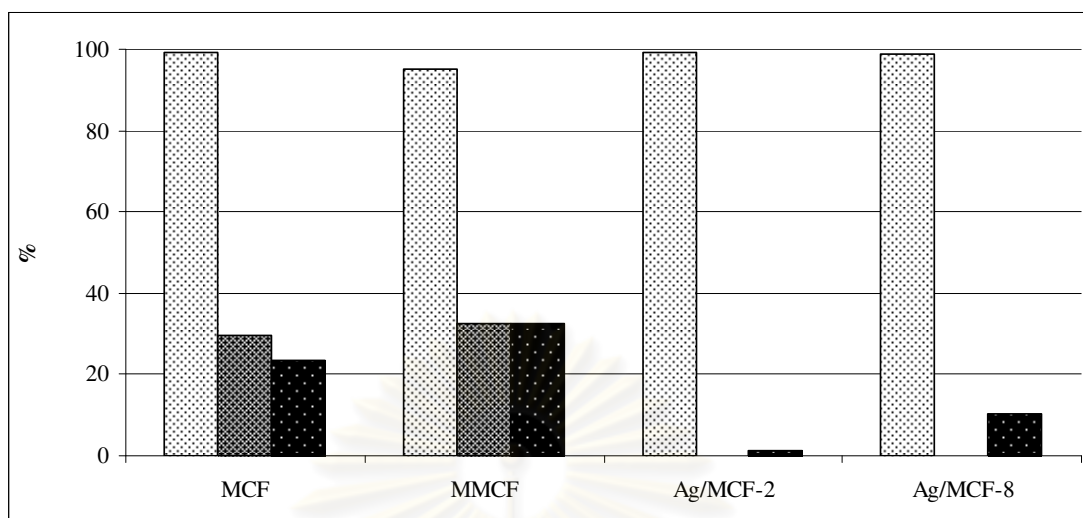
a
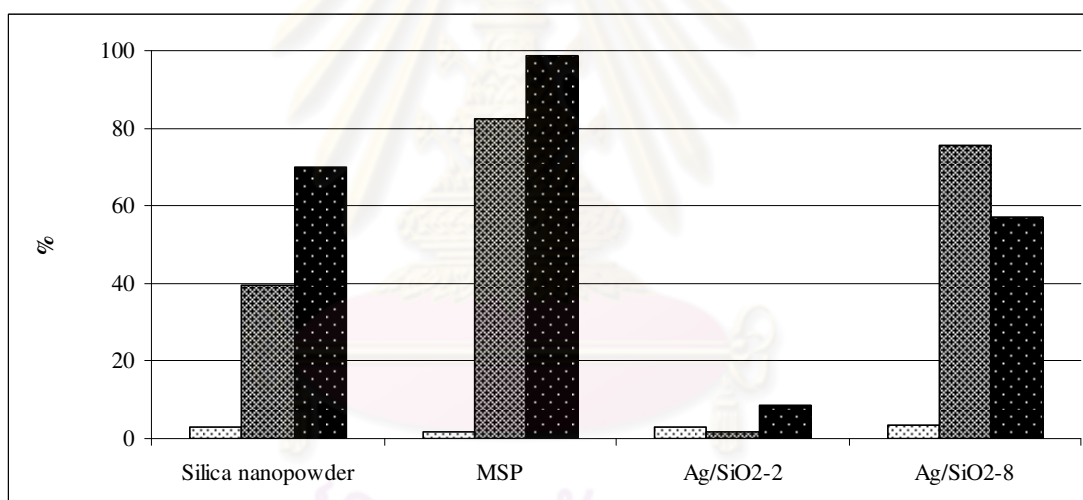
b

Figure 5.32 Effects of support structure and surface properties on HRP immobilization; (a) MCF with/without surface modification and present of silver nanoparticles (b) silica nanopowder with/without surface modification and present of silver nanopartilce, (▦) % HRP loading compared to initial enzyme, (▦) % HRP leaching compared to immobilized HRP, (■) % HRP specific activity compared to free enzyme.

.

From Figure 5.32(a) represents of the HRP immobilization into porous materials; various MCF supports, while Figure 5.32(b) represents the HRP immobilization on the almost nonporous supports. Comparing the specific activity of immobilized HRP on both type supports, it is clearly shown that the internal mass-transfer is the limitation of the reaction. The specific activity of immobilized HRP, which expected to immobilize at outer surface of silica nanopowder, are much higher than the one that immobilized into the pore of MCF.

While comparing the specific activity of immobilized HRP between the different MCF supports, it shows that specific activity of immobilized HRP on MMCF was the highest, although its surface area and pore volume were moderately reduced from the surface modification (see data in Table 5.5). The specific activity of immobilized HRP on MCF was higher than Ag/MCF-2 and Ag/MCF-8, respectively. Compared to the free enzyme, the highest specific activity was obtained from MMCF of ~32%. The specific activities of immobilized HRP on different silica nanopowder supports have the same analogous with of different MCF supports. The highest specific activity of immobilized HRP was 98%, obtained from MSPs. This could be explained by 2 reasons; the enzyme was immobilized on outer surface of support, which facilitated the substrate to approach the immobilized HRP; and the aminopropyl groups provided a weaker interaction between enzyme and support surface, resulting in the more active immobilized enzyme. The effect of aminopropyl groups on HRP immobilization will be discussed more in the next section.

2.1 The effects of aminopropyl groups on HRP immobilization

The aminopropyl groups functionalized on support surface also influenced properties of enzyme immobilization and provided the essential interactions between the surface of support and enzyme [3-4, 9]. From Figure 5.29, the amount of HRP adsorbed on both modified silica surface supports was slightly less than unmodified surface supports. These results may be caused by 2 parameters, surface area and surface properties. The surface area of supports was considerably reduced after modification, which caused the surface area of MCF and silica nanopowder reduced

38 and 28 %, respectively. The surface property of silica supports was changed by addition of aminopropyl group, which increased the hydrophobic property of support surface. This addition also improved the hydrogen and hydrophobic interactions between enzyme and support surface [9]. On the other hand, the attractive electrostatic interaction between HRP and support surface was reduced because aminopropyl groups are positively charged at this pH [3], its isoelectric point is 8.7. The attractive electrostatic interaction can be proven by zeta potential at pH 8, which was strongly lowered because of the presence of aminopropyl groups. Thus, the difference in charge between support surface and HRP was also reduced. Some researchers commented that hydrophobic and hydrophilic properties of support surface have more influence on adsorption of some proteins on mesopous silica than electrostatic interaction [9, 55-56].

On the contrary, the aminopropyl group did not improve the leaching of HRP immobilized on both supports in this study probably due to the weak interaction between HRP and modified support surface. As a consequence, immobilized HRP was slightly leached from the MMCF and considerably leached from MSPs. Moreover, the HRP was in more flexible form because of the weak interaction, so that the specific activity of the enzyme immobilized on modified surface was much higher than on the unmodified surface. This specific activity was 38% and 47 % higher than MCF and silica nanopowder, respectively. In addition, aminopropyl groups which have the similar functional groups with enzyme molecules, may provide a biocompatible environment for enzyme to be active. Therefore, based on the results of this study, the electrostatic interaction which is stronger than hydrogen and hydrophobic interactions, is strongly influential on the less specific activity of immobilized HRP.

3. The effects of silver nanoparticles on HRP immobilization

The synthesis of silver nanoparticles onto both modified supports affected 2 parameters of HRP immobilization. First is the charge surface property. The silver nanoparticles slightly reduced the zeta potential, consequently increasing the

attractive electrostatic interaction between the surface of the support and enzyme. Therefore, the silver nanoparticles with negative charge could attach HRP molecule through the electrostatic interaction between the cysteine or NH_4^+-lysine residues of HRP and silver surface [61]. Second is the support structure, due to the 3 dimension property, one silver nanoparticle (main size $\approx$ 17 nm) was able to adsorb several HRP molecules (approximate diameter $\approx$ 48 nm) [2], resulting in an increase in the amount of enzyme adsorbed on support. The attractive electrostatic interaction between the enzyme and support surface was increased by silver nanoparticles, consequently leading to a reduction in leaching of adsorbed enzyme.

The silver nanoparticles strongly affected the specific activity of HRP, also depending on the surface charge and pore structure. It was observed that the specific activity of HRP immobilized on Ag/SiO_2-2 and Ag/MCF-2 was considerably lower than that Ag/SiO_2-8 and Ag/MCF-8. This is due to the silver ion that remained on the support surface inhibiting the specific activity of the enzyme [116, 118]. This result confirmed the data from zeta potential, which indicated some silver ion remained on the silver nanoparticles surface. However, Ma et al. [116] suggested that the remaining silver ions on the surface of silver nanoparticles could be eliminated by aging after synthesis. But, results from this work at the high concentration of silver precursor that were synthesized did not support this conclusion. Comparing the specific activity on the different structural supports having similar chemical surface characteristics, the specific activity of HRP absorbed on Ag/SiO_2-8 was several times higher than from Ag/MCF-8. This showed that under the similar interaction between the enzyme and surface, the substrate was easily approached to HRP immobilized on Ag/SiO_2 nanocomposite materials. On the other hand, silver nanoparticles attached on MCF create a steric hindrance that prevents substrates to approach the immobilized HRP. However, the specific activity of HRP immobilized on Ag/SiO_2-8 was considerably lower than the one attached on silica nanopowder and MSPs. This result suggests that even without the mass transfer problem, silver nanopaticles also did not improve the specific activity of HRP. This result does not agree with the previous published research that suggested that silver nanoparticles induced the activity of Papain immobilized on silica spheres by covalent bonding [119]. Therefore, we can

conclude that the electrostatic interaction between silver nanoparticles and HRP makes enzyme in a more inflexible form than another interactions.

5.3.4 The storage stability of immobilized HRP
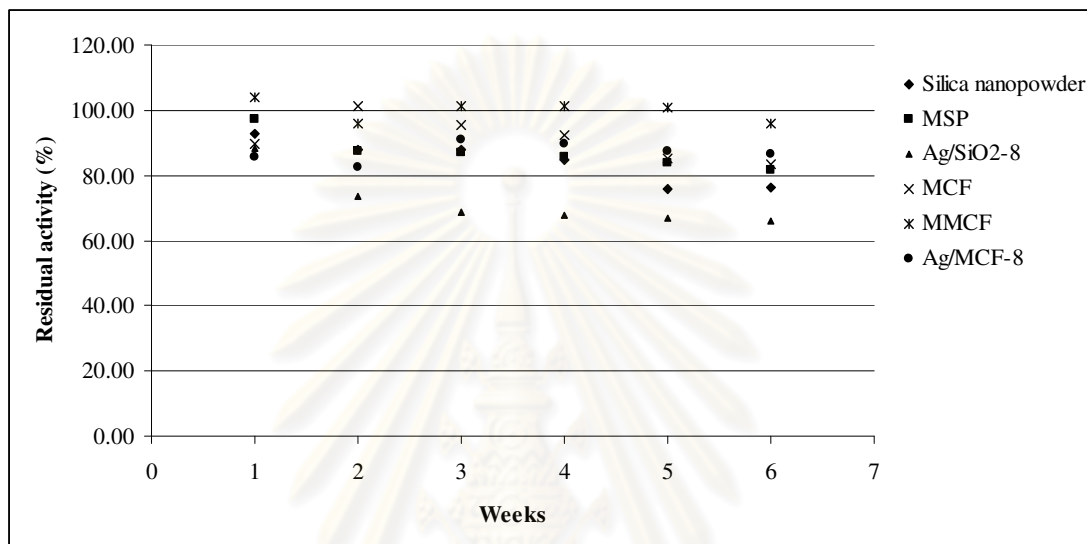
Figure 5.33 Storage stability of immobilized HRP on various supports at 4ºC

The storage stability of immobilized HRP was indicated by the residual specific activity of enzyme at 4ºC at specific storage time. The residual activities of immobilized HRP on different supports at pH 8 are shown in Figure 5.33. The maximum residual activities of immobilized HRP were obtained from the modified surface support. This is because the NH_2 functional group on the modified surface support resulted in a low negatively charged surface combined with the low positively charged enzyme at pH 8, provided the hydrogen, hydrophobic and weakly electrostatic interaction between modified surface and HRP. These weak interactions caused the HRP molecules to be more flexible. This result supported our previous work showing that the lower electrostatic interaction between support and HRP provided the better storage stability. However, the immobilized HRP on Ag/SiO$_2$-8 and Ag/MCF-8 still presents good stability at 4ºC. The residual activities of HRP immobilized on the support type MCF were higher than the one immobilized on silica

nanopowder type. Due to the enzyme being immobilized inside the pore of supports, it was consequently protected leading to more storage stability. Therefore, it can be concluded that silver nanoparticle is biocompatible and provides a good environment for the enzyme to be active.

5.3.5 Biosensor application using modified electrodes for phenol detection

In this part, biosensor applications of Ag/MCF and Ag/SiO$_2$ for phenol detection are discussed. The electrodes modified with different supports with/without HRP were tested. The electrochemical reactions were tested by observing respond current at a fixed -0.05 V [98] in 0.1 M phosphate buffer (pH 7.0) containing 0.1 mM H$_2$O$_2$ and 0.1 mM phenol, which acted as substances.

The possible catalytic mechanism of HRP reactions with H$_2$O$_2$ and phenol on electrode surface was explained by Ruzgas et al. [118].

$$HRP\ (Fe^{3+}) + H_2O_2 \longrightarrow HRP\ (Fe^{5+}) + H_2O \qquad (5.4)$$

$$HRP\ (Fe^{5+}) + phenol \longrightarrow HRP\ (Fe^{4+}) + Product \qquad (5.5)$$

$$HRP\ (Fe^{4+}) + phenol \longrightarrow HRP(Fe^{3+}) + Product + H_2O \qquad (5.6)$$
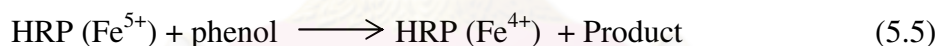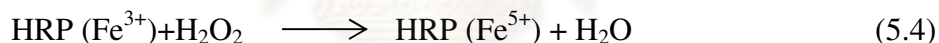
The HRP immobilized on the biosensor surface was oxidized by H$_2$O$_2$ to form the first intermediate (HRP (Fe^{5+}) in equation 5.4). And Compound I was reduced by phenol to form the second intermediate (HRP (Fe^{4+}) in equation 5.5). HRP (Fe^{5+}) and HRP (Fe^{4+}) expressed the two- and one- electron oxidation state of the native ferriperoxidase respectively. Compound II is subsequently reduced back to the native HRP by accepting one more electron from phenol (in equation 5.6).

The electrochemical reaction of MCF and Ag/MCF nanocomposites with and without HRP were investigated on glassy carbon electrode (GCE) using amperometry as shown in Figure 5.34(a). It was found that the electrode with modified MCF containing HRP produced high current up to -3.14 µA. In the presence of silver nanoparticles on MCF, the response current was -3.49 µA, higher than of MCF 11%.

While the response current of MCF and Ag/MCF without HRP is not significantly observed. This demonstrated that silver nanoparticles can enhance the rate of electron transfer as expected. However, in section 5.3.3, silver nanoparticles were found to inhibit the reaction of immobilized HRP. Compared to unmodified surface support, MCF and silica nanopowder, the specific activity of immobilized HRP of Ag/MCF-8 and Ag/SiO$_2$ were reduced 55 and 18 %, respectively. In similar conditions, the enzyme immobilization on GCE modified with Ag/MCF may be inhibited by silver nanoparticles. In fact, therefore the response current was produced by silver nanoparticles supposed to be higher than that of 17%.

Figure 5.34(b) shows the currents of GCE modified silica nanopowder and Ag/SiO2 with and without HRP. The results are analogous to the currents of MCF and Ag/MCF in Figure 5.34(a). The response current of HRP on silica nanopower was -2.8 μA, while the response current of Ag/SiO$_2$ was -3.53 μA, higher than of silica nanopowder 26%. This confirms that silver nanoparticles on MPSs highly enhance the electron transfer.

It is interesting that the current from amperometry, which produces by HRP immobilization on MCF was higher than that of silica nanopowder. As a result from the fact that MCF possesses higher surface area than silica nanopowder, it could adsorb more HRP (see enzyme loading in Figure 5.32). This resulted in higher response current from MCF electrode. However, the response currents which were obtained from electrode modified with Ag/MCF and Ag/SiO$_2$ were similar. The different in enhancement of the electron transfer rate on both supports may be caused by the character of silver nanoparticles. First, the different sizes of silver nanoparticles; the main sizes of silver nanopartilces were 5 and 17 nm on Ag/MCF and Ag/SiO$_2$ respectively. Second, the different location of silver nanoparticles, they were attached inside the pore of Ag/MCF while they were attached outer surface of Ag/SiO$_2$. Third, the different number of silver nanoparticles as well affected the electron transfer rate.
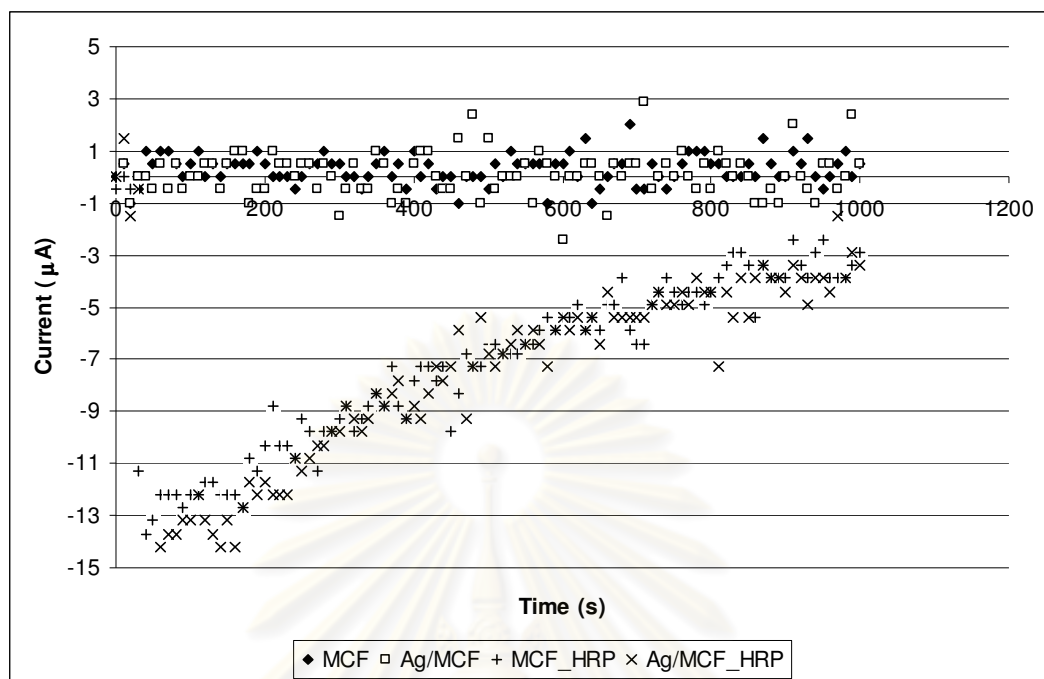
a
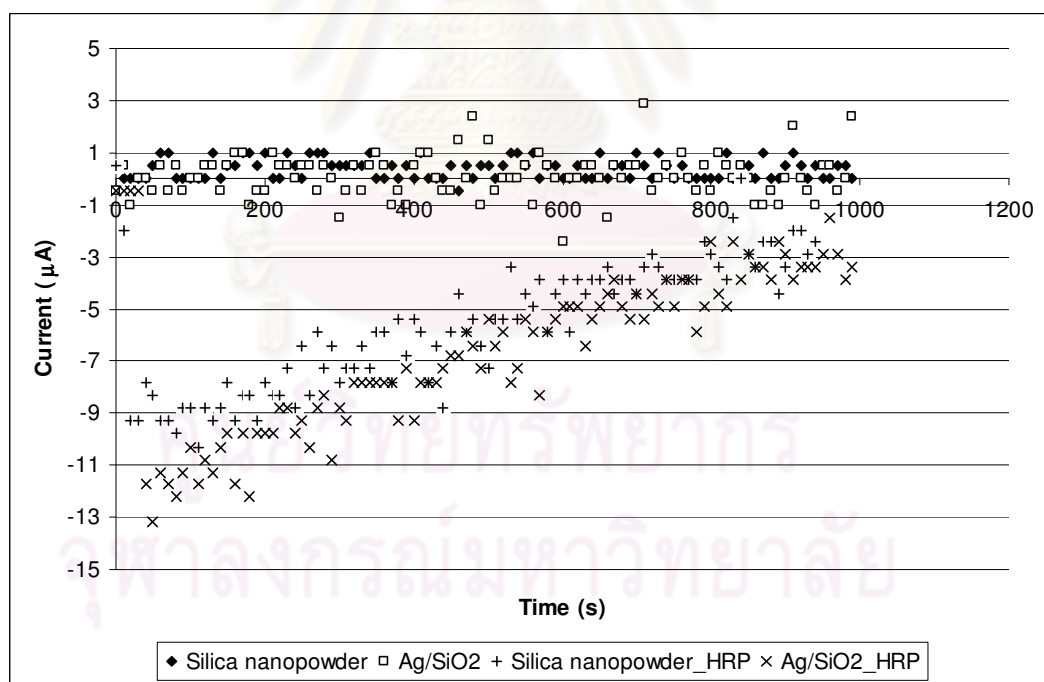
b

Figure 5.34 The currents amperometry obtained from Glassy carbon electrode on (a)
MCF and Ag/MCF (b) silica nanopowder and Ag/SiO$_2$ with and without
HRP in 0.1 M phosphate buffer (pH 7) containing 0.1 mM H$_2$O$_2$ and 0.1
mM phenol at -0.05 V.

To conclude, results in section 5.3 for MCF supports and silica nanopowder supports that were synthesized under the similar conditions are applicable for HRP immobilization and biosensor. For enzyme immobilization, after surface modification by aminopropyl groups as well as silver nanoparticles, surfaces of MCF supports still are large enough to play an important role in enzyme loading. Almost 100% of the initial enzyme was immobilized as well as that of the unmodified support. On the other hand, the almost nonporous supports of silica nanopowder and aminopropyl groups which provided the weak interaction between enzyme and support surface plays the important role in terms of activity of immobilized enzyme. The specific activity of immobilized HRP was up to 98% on MSPs. However, it was found that the addition of silver nanoparticles on support inactivated the immobilized HRP. Compared to MSPs, the specific activity of immobilized HRP was reduced from 98 to 57%. The reduce of specific activity of immobilized HRP could be explained by interaction between enzyme and support surface. Enzyme was immobilized on Ag/SiO2 by electrostatic interaction which restricts immobilized HRP, resulting in inactivation of enzyme. However, the modification of supports by functional groups and silver nanoparticles did not improve the enzyme leaching as was expected. For biosensor application, Ag/MCF and Ag/SiO$_2$ was used for phenol detection. It was found that silver nanoparticle plays more important role than the large surface property to greatly enhance the current at the electrode surface.

CHAPTER VI

CONCLUSIONS

6.1 Selection of suitable OMMs for HRP immobilization

The experimental results obtained in the present work revealed significant roles of electrostatic interactions and MPSs pore characters on enzyme loading, leaching, activity, and storage stability. MCM-41 and SBA-15 were rod-like with respective main pore diameters of 32, and 54 Å, while that of MCF with spherical cell and frame structure was 148 Å. Under attractive interactions (at immobilization pH 6 and 8) almost 100% HRP loadings were obtained for all types of supports. However, effects of pore characters were more pronounced under repulsive interactions at immobilization pH 10. In this case, MCF which was of the biggest pore diameters gave both the highest enzyme loading and leaching. Insignificant HRP leaching was observed at immobilization pH 6 for all types of supports.

Maximum and minimum HRP activities were obtained at respectively immobilization pH 8, and 6. Inflexibility of HRP molecules at pH 6 or hindered enzyme active sites were postulated to be reasons for the low enzyme activity. It was found that activities of immobilized HRP increased with support pore diameters in the order: MCM-41 < SBA-15 < MCF. HRP immobilized at pH 8 had the highest storage stability (both at 4°C and room temperature), and in opposition to pH 6. In addition, HRP immobilized in MCF was the most stable under storage. It was therefore hypothesized that HRP was likely to be denatured under conditions that rigidly control its three dimensional structure. The conclusions drawn in this work may be significant for the understanding of enzyme immobilization in mesoporous silicas and undoubtedly useful for their applications in the fields of biocatalysis or biosensors

6.2 The synthesis of Ag/SiO$_2$ nanocomposite by ultrasonication

The Ag/SiO$_2$ nanocomposite was successfully synthesized by ultrasonic method. In this method, the silver nanoparticles were adsorbed on aminopropyl functionalized silica nanopowder. It was found that the functionalization agent, APTES, also acted as a reducing agent during the synthesis. The synthesis conditions strongly affected the number and size and size distribution of silver nanoparticles. The adsorption time and silver nitrate concentration influenced on the number of silver nanoparticles, while they only slightly affected the size of silver nanoparticles. On the other hand, size of silver nanoparicles could be strongly controlled by the reduction time. With increasing reduction time from 2 to 8 h, the size of main silver nanoparticles were changed from 10 to 17 respectively. Since the reduction strongly affect the size of silver nanopartilces which was expected that the size of silver nanoparticles should affect on enzyme immobilization as well as biosensor application. Therefore, the two reduction time (2 and 8 h) were chosen to test this condition on MCF support. In order to ensure considerable number of silver nanoparticles, silver nitrate concentration and adsorption time were fixed at 2000 ppm and 12 h respectively.

6.3 The immobilization of HRP on Ag/MCF and Ag/SiO$_2$ nanocomposite

The Ag/MCF nanocomposite was synthesized under the same conditions as that of Ag/SiO$_2$ nanocomposite. The small silver nanoparticles (main size 5 nm) were successfully synthesized inside the pores of MCF. It was found that the reduction time of the synthesis did not affect the size of silver nanoparticles on MCF.

For enzyme immobilization, there were many factors affecting the HRP immobilization such as, surface area and structure of supports, functional group and charge properties on the supports surface, and the remaining silver ion and silver nanoparticles. The support characters strongly influenced the loading, leaching, and

activity of HRP. The different MCF supports; MCF, MMCF, and Ag/MCF possess the large surface area, resulting in higher amounts of HRP adsorbed than those of silica nanopowder based supports. The structure of support strongly affected the activities of immobilized enzyme. HRP immobilized on silica nanopowder provided almost as high activity as than of free enzyme activities due to the almost non porous structure of silica nanopowder, which also provided substrate easily approached to immobilized enzyme. Additionally, aminopropyl groups functionalized on the surface of silica nanopowder also provided the weaker interaction between enzyme and support surface than that of unmodified support. As a consequence, immobilized HRP was in a more flexible form because of the weak interaction. The activity of the enzyme immobilized on modified surface was much higher than on the unmodified surface. However the drawback of MSPs is the high amount of enzyme leaching.

Silver nanoparticles on MCF or silica nanopowder inhibited the activities of immobilized HRP. The activities of HRP on Ag/MCF-2 and Ag/SiO$_2$-2 were inhibited by the remaining silver ion on silver nanoparticles. The activity of HRP on Ag/MCF-8 was lower than of MCF. This indicated that silver nanoparticles may block the mass transfer inside the pore of MCF. The presence of silver nanoparticles on the support also changed the surface property; the negative charge on surface was lower than of MMCF. This resulted in the stronger electrostatic interaction between enzyme and support surface. As a consequence, the activity of HRP on Ag/SiO$_2$-8 was much lower than in absence of silver nanoparticles.

The HRP immobilized inside the pore of support (MCF, MMCF) had higher storage stability. Additionally, the HRP immobilized on MMCF, which was in the flexible form, had the highest activity during the observed period of time.

HRP immobilized on Ag/MCF and Ag/SiO$_2$ has been successfully applied on glassy carbon electrode. The amperometry showed that silver nanoparticles greatly enhance the current at electrode surfaces.

6.4 The suggestion for further research

Since it was shown in section 5.3.3, that Ag/MCF and Ag/SiO$_2$ could enhance electron rate at the surface of biosensor. It indicates that there is possibility to use these materials as an enzyme carrier. However, there are many performance factors need to be measured for representing the performance of this bioreceptor, such as selectivity, the concentration that can be measured (the detection limit), reproducibility, and life time, as well as the pH of the sample solution.

REFERENCE

[1] Lu G.Q. and Zhao X. S. *Nanoporous Materials Science and Engineering.* Singapore : World Sciencetific printers (s) Pte. Ltd., 2004.

[2] Takahashi, H., Li, B., Sasaki, T., Miyazaki, C., Kajino, T., and Inagaki, S. Immobilized enzymes in ordered mesoporous silica materials and improvement of their stability and catalytic activity in an organic solvent. *Micropor. Mesopor. Mater.* 44-45 (2001) : 755-762.

[3] Chong, A.S.M., Zhao, X.S., Kustedjo, A.T., and Qiao, S.Z. Functionalization of large-pore mesoporous silicas with organosilanes by direct synthesis. *Micrpor. Mesopor. Mater.* 72 (2004) : 33-42.

[4] Chong, A.S.M. and Zhao, X.S. Design of large-pore mesoporous materials for immobilization of penicillin G acylase biocatalyst. *Catal. Today.* 93-95 (2004) : 293-299.

[5] Zhao, A. X., Qiao, M.-Q., Yin, F., Shao, B., Wu, B.-Y., Wan, Y.-Y. Wang X. S., Qin, X., Li, S. Yu, L., and Chen, Q. Amperometric glucose biosensor based on self-assembly hydrophobin with high efficiency of enzyme utilization. *Biosens. Bioeletron.* 22 (2007) : 3021–3027.

[6] Díaz, J.F. and Balkus, Jr K.J. Enzyme immobilization in MCM-41 molecular sieve. *J. Mol. Catal. B: Enzym.* 2 (1996) : 115-126.

[7] Han, Y.J., Watson, J.T., Stucky, G.D., and Butler, A. Catalytic activity of mesoporous silicate-immobilized chloroperoxidase. *J. Mol. Catal. B: Enzym.* 17 (2002) : 1-8.

[8] He, J, Li X., Evans, D.G., Duan, X., and Li, C. A new support for the immobilization of penicillin acylase. *J. Mol. Catal B: Enzym.* 11 (2000) : 45-53.

[9] Chong, A.S.M. and Zhao, X.S. Functionalized nanoporous silicas for the immobilization of penicillin acylase. *Appl. Surf. Sci.* 237 (2004) : 398-404.

[10] Szymańska, K. Bryjak, J., Mrowiec-Bialoń, J. and Jarzębski, A.B. Application and properties of siliceous mesostructured cellular foams as enzymes

carriers to obtiain efficient biocatalysts. *Micropor. Mesopor. Mater.* 99 (2007) : 167-175.

[11] Solis, S., Painagua, J., Martínez, J., and Asomoza, M. Immobilization of papain on mesoporous silica: pH effect. *J. Sol-Gel Sci. Technol.* 37 (2006) : 125-127.

[12] Gómeza, A. Bódaloa, E. Gómeza, J. Bastidaa, A.M. Hidalgoa, and Gómeza, M. Immobilization of peroxidases on glass beads: An improved alternative for phenol removal. Enzym. Microb. Technol. 39 (2006) : 1016-1022.

[13] Enterzari, H. M., and Pétrier, C. A. combination of ultrasound and oxidative enzyme: sono-enzyme degradation of phenols in a mixture. Utrason. Sonochem. 12 (2005) : 283–288.

[14] Makrisa, D. P., and Rossiterb, J. T. An investigation on structural aspects influencing product formation in enzymic and chemical oxidation of quercetin and related flavonols. Food chem. 77 (2002) : 177-185

[15] Rosatto, S. S., Kubota, L. T., and Neto, G. O. Biosensor for phenol based on the direct electron transfer blocking of peroxidase on silica-titanium. *Analyt. Chimi. Acta.* 390 (1999) : 65-72.

[16] Mello, L.D., Sotomayor, M.D.P.T., and Kubota, L.T. HRP-based amperometric biosensorfor the polyphenols determination in vegetables extract. *Sens. Actua. B.* 96 (2003) : 636-645.

[17] Mello, L.D., Alves, A.A., Macedo, D.V., and Kubota, L.T. Peroxidase-base biosensor as a tool a fast evaluation of antioxidant capacity of tea. *Food Chem.* 92 (2005) : 515-519.

[18] Goradia, D., Cooney, J., Hodnett, B.K., and Magner, E. The adsorption characteristics, activity and stability of trypsin onto mesoporous silicates. *J. Mol. Catal.B: Enzym.* 32 (2005) : 231-239.

[19] Bai, Y., Yang, H., Yang, W., Li Y., and Sun, C. Gold nanoparticles-mesoporous silica composite used as an enzyme immobilization matrix for amperometric glucose biosensor construction. *Sens. Actuat. B.* 124 (2007) : 179-186.

[20] Xain, Y., Xian, Y., Zhou, L., Wu, F., and Jin, L. Encapsulation hemoglobin in ordered mesoporous silica:Influence factors for immobilization and bioelectrochemistry. *Electrochem. Comm.* 9 (2007) : 142-148.

[21] Lei, Z., and Fan, Y. Preparation of silver nanocomposites stabilized by an amphiphilic block copolymer under ultrasonic irradiation. *Mater. Letters.* 60 (2006) : 2256-2260.

[22] Park, J.-E., Atobe, M., and Fuchigami, T. Synthesis of multiple shapes of gold nanoparticles with controlled sizes in aqueous solution using ultrasound. *Ultra. Sonochem.* 13(2006) : 237-214.

[23] Pérez-Rodriquez, J.L., Wiewiora, A., Ramirez-Valle, V., Durán, A., and Pérez-Maqueda, L.A., Preparation of nano-pyrophyllite: Comparative study of sonication and grinding. *J. phys. Chem. Solids* 68 (2007) : 1225-1229.

[24] Gedanken, A. Using sonochemistry for the fabrication of nanomaterials. *Ultra. Sonochem.* 11 (2004) : 47-55.

[25] Awati, P.S., Awate, S.V., Shah, P.P. and Ramaswamy, V. Photocatalytic decomposition of methylene blue using nanocrystalline anatase titania prepared by ultrasonic technique. *Catal. Comm.* 4 (2003) : 393-400.

[26] Sariri, R. Sajedi, R.H. and Jararian, V. Inhibition of horseradish peroxidase activity by thiol type inhibitors. *J. Mol. Liq.*123 (2006) : 20-23.

[27] Takahashi, H., Li, B., Sasaki, T., Miyazaki, C., Kajino, T., and Inagaki, S. Catalytic activity in organic solvents and stability of immobilized enzymes depend on the pore size and surface characteristic of mesoporous silica. *Chem. Mater.* 12(2000) : 3301-3305.

[28] www. Toyobo.co.jp. 04 April, 2005.

[29] Lai, Y.-C., and Lin, S.-C. Application of immobilized horseradish peroxidase for the removal of *p*-chlorophenol from aqueous solution. *Process Biochem.* 40 (2005) : 1167–1174.

[30] Pandya, P.H., Jasra, R.V., Newalkar, B.L., and Bhatt, P.N. Studies on the activity and stability of immobilized α-amylase in ordered mesoporous silicas. *Micropor. Mesopor. Mater.* 77 (2005) : 67-77.

[31] Liu, Z-M, Tingry, S., Innocent, C., Durand, J., Xua, Z.,-K., and Seta P. Modification of microfiltration polypropylene membranes by allylamine plasma treatment Influence of the attachment route on peroxidase immobilization and enzyme efficiency. *Enzym. Microb. Technol.*39 (2006) : 868-876.

[32] Zhao, X. S., Bao, X.Y., Guo, W., and Lee, F.Y. Immobilizing catalysts on porous materials. *Mater. today* 9 (2006) : 32-39.

[33] Park, S.-E., Ryoo, R., Ahn, W.-S., and Lee, C. W., *Nanotechnology in Mesostructured Materials, Studies in Surface Science and Catalysis*. Elsevier Publishers, vol. 146, 2003.

[34] Lei, J., Fan, J., Yu, C., Zhang, L., Jiang, S., Tu, B., and Zhao, D. Immobilization of enzymes in mesoporous materials: controlling the entrance to nanospace. *Micropor. Mesopor. Mater*. 73 (2004) : 121-128.

[35] Yiu, H.H.P., Wright, P.A., and Botting, N.P. Enzyme immobilisation using siliceous mesoporous molecular sieves. *Micropor. Mesopor. Mater.,* 44-45 (2001) : 763-768.

[36] Beck, J.S., Vartuli, C., Roth, W. J., Leonowicz, M.E., Kresge, C. T., Schmitt, K. D., Higgins ,J.B., and Schlenker, J. L. A new family of mesoporous molecular sieves prepared with liquid crystal templates. *J. Am. Chem. So.* 114 (1992) : 10834-10843.

[37] Zhao, X. S., Lu, G.Q.(Max), and Millar, G. J. Advances in mesoporous molecular sieve MCM-41. *Ind. Eng. Chem. Res*. 35 (1996) : 2075-2090.

[38] Pinnavaia, T.J., and Thorpe, M.F. *Nanoporous materials*. New York : Plenumpress, 1995.

[39] Vartuli, J.C., Schmitt, K. D. Kresge, C.T., Roth, W.J., Leonowicz, M.E., McCullen, S.B., Hellring, S.D. Beck, J.S. Schlenker, J.L., Olson, D.H., and Sheppard, E.W. Effects of surfactant/silica molar ratios on the formation of mesoporous

molecular sieves: inorganic mimicry of surfactant liquid-crystal phases and mechanistic implications. *Chem. Mater*., 6 (1994) : 2317-2326.

[40] Lettow, J.S., Han, Y.J., Schmidt-Winkel, P., Yang, P., Zhao D., Stucky, G.D., and Ying J.Y. Hexagonal to mesocellular foam phase transition in polymer-templated mesoporous silicas. *Langmuir*. 11 (2000) : 8291-8295.

[41] Zhao, D., Feng, J., Huo, Q., Melosh, N., Fredrickson, G.H., Chmelka, B.F., and Stucky, G.D. Triblock copolymer syntheses of mesoporous silica with periodic 50 to 300 angstrom pores. *Science. 279* (1998) : 548-552.

[42] http://hyperphysics.phy-astr.gsu.edu/hbase/quantum/ imgqua/bragglaw.gif. 04 April, 2005.

[43] Sing, K. S. W., Everett, D. H., Haul, R. A. W., Moscoul, L., Pierotti, R. A., Rouquerol, J., and Siemieniewska T. Reporting physisorption data for gas/solid systems with special reference to the determination of Surface Area and Porosity. *Pure Appl. Chem.* 57 (1985) : 603—619.

[44] Nicolais L., and Caroltenuto G. *Metal-Polymer nanocomposites*. New Jersey USA: Johnwiley &sons, Inc. Hoboken. 2005.

[45] ASTM Standard D 4187-82, *Zeta Potential of Colloids in Water and Waste Water*, American Society for Testing and Materials, 1985.

[46] Shuler, M.L. and Kargi, F. *bioprocess Engineering*. New Jersey : Prentice Hall International Inc., 1992.

[47] Yiu, H. H. P., and Wright, P. A. Enzymes supported on ordered mesoporous solids : a special case of an inorganic–organic hybrid. *J. Mater. Chem.* 15 (2005) : 3690-3700.

[48] Andrade, J.D., Hlady, V.L. and Van Wagenen, R.A. Effects of plasma protein adsorption on protein conformation and activity *Pure Appl. Chem*. 56(1984) : 1345-1350.

[49] Veliky, I.A. and McLean, R.J.C. *Immobilized Biosystems Theory and Practical Application*. Glasgow, UK : Chapman and Hall, 1994.

[50] Soderquist M. E. and Walton, A.G. Structural changes in proteins adsorbed on polymer surface *J. Colloid Inter. Sci*.75 (1980) : 386-397.

[51] Bailey, J.E. and Ollis, D.F. *Biochemical Engineering Fundamentals*. 2nd edition. Singapore : McGraw-Hill Inc., 1994.

[52] Eggins, B.R. *Biosensors: An Introduction*. Chichester, UK: John Wiley & Sons Ltd, 1999.

[53] http://en.wikipedia.org/wiki/Cyclic_voltammetry. 04 April, 2005.

[54] Han, Y.-J., Stucky, G.D., Butler, A., Mesoporous Silicate Sequestration and Release of Proteins. *J. Am. Chem. Soc*. 121 (1999) : 9897-9898.

[55] Deere, J., Magne,r E., Wall, J.G., and Hodnett, K. Mechanistic and structural features of protein adsorption onto mesoporous silicates. *J. phys. Chem. B*. 106 (2002) : 7340-7347.

[56] Gimno-Kinsel, M.E., Groothuis, K., and Balkus,.Jr K.J. Photoluminescent properties of MCM-41 molecular sieves. *Micropor. Mesopor. Mater.* 20 (1998) : 67-76.

[57] Blanco, R. M., Terreros, P., Fernández-Pérez, M., Oter, C., and Diáz-González, G. Funcitonalization of mesoporous silica for lipase immobilization Charaterization of the support and the catalysts. *J. Mol. Catal. B: Enzym*. 30 (2004) : 83-93.

[58] Han, K., Wu, Z., Lee, J., Aha, I.S., Park, J.W., Min, B.R., and Lee, K. Activity of glucose oxidase entrapped in mesoporous gels. *Biochem .Eng. J*. 22 (2005) : 161-166.

[59] Chouyyok, W., Panprano,t J., Thanachayanants, C., and Prichanont, S. Effect of pH and pore characters of mesoporous silicas on horseradish peroxidase immobilization. *J. Mol. Catal. B: Enzym*. 56 (2009) : 246-252.

[60] Luan, Z.,Fournier, J.A., Wooten, J.B., and Miser, D. E. Preparation and characterization of(3-aminopropyl)triethoxysilane-modified mesoporous SBA-15 silica molecular sieves. *Micropor. Mesopor. Mater*. 83 (2005) : 150-158.

[61] Ren, C., Song, Y., Li Z., and Zhu, G. Hydrogen peroxide sensor based on horseradish peroxidase immobilized on a silver nanoparticles/cysteamin/gold electrode. *Anal. Bioanal. Chem*. 381 (2005) : 1179-1185.

[62] Xu, J.Z., Zhang, Y., Li G.X., and Zhu, J.J. An electrochemical biosensor constructed by nanosized silver particles doped sol-gel film. *Mater. Sci. Eng. C*. 24 (2004) : 833-836.

[63] Bai, Y.-X., Li, Y.-F., Yang, Y., and Yi, L.-X., Covalent immobilization of triacylglycerol lipase onto functionalizaed nanoscale SiO_2 spheres. *Process Biochem.* 41 (2006) : 770-777.

[64] Huang, H., Yuan, Q., and Yang, X., Preparation and characterization of metal-chitosan nanocomposites. *Colloids Surf. B: Biointer*. 39 (2004) : 31-37.

[65] Xu, Q., Mao, C., Liu, N.N., Zhu, J.-J., and Sheng, J. Direct electrochemistry of horseradish peroxidase based on biocompatible carboxymethyl chitosan-gold nanoparticle nanocomposite. *Biosen. Bioele.* 22 (2006) : 768-773.

[66] Xue, M.H., Xu, Q., Zhou, M., and Zhu, J.J. In situ immobilization of glucose oxidase in chitosan-gold nanoparticle hybrid film on Prussian Blue modified electrode for high-sensitivity glucose detection. *Electrochem. Comm.* 8 (2006) : 1468-474.

[67] Lin, T.-Y., Wu, C.-H., and Brennan, J.D. Entrapment of horseradish peroxidase in sugar-modified silica monoliths: Toward the development of a biocatalytic sensor. *Biosen. Bioele.* 22 (2007) : 1861-1867.

[68] Ren, X., Meng, X., Chen, D., Tang, F., and Jiao, J. Using silver nanoparticle to enhance current response of biosensor. *Biosen .Bioele.* 21 (2005) : 433-437.

[69] Adhyapak, P.V., Karandikar, P., Vijayamohanan, K., Athawale, A.A. and Chandwadkar, A.J. Synthesis of silver nanowires inside meoporous MCM-41 host. *Mater. Letters* 58 (2004) : 1168-1171.

[70] Zhu, W., Han, Y., and An, L. Silver nanoparticles synthesized from mesoporous Ag/SBA-15 composites. *Micropor. Mesopor. Mater.* 80 (2005) : 221-226.

[71] Park, J., Park J., and Shin, H. The preparation of Ag/mesoporous silica by direct silver reduction and Ag/functionalized mesoporous silica by in situ formation of adsorbed silver. *Mater. Letters* 61 (2007) : 156-159.

[72] Zhao, X.-G., Shi, J.-L, Hu, B., Zhang, L.-X., and Hua, Z.-L. In situ formation of silver nanopartilces inside pore channels of ordered mesoporous silica. *Mater. Letters* 58 (2004) : 2152-2156.

[73] Lin, J., Qu, W., and Zhang, S. Disposable biosensor based on enzyme immobilized on Au-chitosan-modified indium tin oxide electrode with flow injection amperometric analysis. *Analyt. Biochem.* 360 (2007) : 288-293.

[74] Mena, M.L., Yáñez-Sedeño, P., and Pingarrón, J.M. A comparison of different strategies for the construction of amperometric enzyme biosensors using gold nanoparticle-modified electrodes. *Analyt. Biochem.* 336 (2005) : 20-27.

[75] Zhang, S., Wang, N., Yu, H., Niu, Y., and Sun, C. Covalent attachment of glucose oxidase to an Au electrode modified with gold nanoparticles for use as glucose biosensor. *Bioelectrochemistry.* 67 (2005) : 15-22.

[76] Wu, Z., Chen, L., Shen, G., and Yu, R. Platinum nanoparticle-modified carbon fiber ultramicroelectrodes for mediator-free biosensing. *Sens. Actuat. B*. 119 (2006) : 295-301.

[77] Yang, M., Yang, Y., Liu, Y., Shen, G., and Yu, R. Platinum nanoparticles-doped sol-gel/carbon nanotubes composite electrochemical sensors and biosensors. *Biosen. Bioele.* 21 (2006b) : 1125-1131.

[78] Ye, J.S., Ottova, A., Tien, H.T., and Sheu, F.S. Nanostructured platinum-lipid bilayer compsite as biosensor. *Bioelectrochemistry.* 59 (2003) : 65-72.

[79] Tang, H., Chen, J., Yao, S., Nie, L., Deng, G., and Kuang, Y. Amperometric glucose biosensor based on adsorption of glucose oxidase at platinum nanoparticle-modified carbon nanotube electrode. *Analyt. Biochem.* 331 (2004) : 89-97.

[80] Lim, S.H., Wei, J., Lin, J., Li, Q., and You, J.K. A glucose biosensor based on electrodeposition of palladium nanoparticles and glucose oxidase onto Nafion-solubilized carbon nanotube electrode. *Biosen. Bioele.* 20 (2005) : 2341-2346.

[81] Okitsu, K., Mizukoshi, Y., Yamamoto, T.A., Maeda, Y., and Nagata, Y. Sonochemical synthesis of gold nanoparticles on chitosan. *Mater. Letters* 61 (2007) : 3429–3431.

[82] Park, J.-E., Atobe, M., and Fuchigami, T. Sonochemical synthesis of conducting polymer-metal nanoparticles nanocomposites. *Electrochim. Acta* 51 (2005) : 849-854.

[83] Zhang, J.-P., Chen, P., Sun, C.-H., and Hu, X.-J. Sonochemical synthesis of colloidal silver catalysts for reduction of complexing silver in DTR system. *Appl. Catal. A: Gen.* 266 (2004) : 49-54.

[84] Fujimoto, T., Mizukoshi, Y., Nagata, Y., Maeda, Y., and Oshima, R. Sonolytical preparation of various types of metal nanoparticles in aqueous solution. *Scripta Mater*. 44 (2001) : 2183-2186.

[85] Chen, W., Zhang, J., Shi, L., Di, Y., Fang, Q., and Cai, W. Characterization of sonochemically prepared silver-silica monolithic mesoporous nanocomposite. *Compos. Sci. Technol.* 63 (2003) : 1209-1212.

[86] Zhi, L., Zhao, T., and Yud, Y. Preparation of phenolic resin/silver nanocomposites via in situ reduction. *Scripta Materialia*. 47 (2002) : 875-879.

[87] Gac, W., Derylo-Marczewska, A., Pasiezna-Patkowska, S., Popivnyak, N., and Zukocinski, G. The influence of the preparation methods and pretreatment conditions on the properties of Ag-MCM-41 catalysts. *J. Mol. Catal. A: Chem.* 268 (2007) : 15-23.

[88] Chen, W., and Zhang, J. Ag nanopartilces hosted in monolithic mesoporous silica by thermal decomposition method. *Scripta Materialia*. 49 (2003) : 321-325.

[89] Bi, H., Cai, W., Shi, H., and Liu, X. Optical absorption of Ag oligomers dispersed within pores of mesoporous silica. *Chem. Phys. Letters* 357 (2002) : 249-254.

[90] Piquemal, J.Y., Viau, G., Beaunier, P., Bozon-Verduraz, F., and Fiévet, F. One-step construction of silver nanowires in hexagonal mesoporous silica using the polyol process. *Mate. Res. Bull.* 38 (2003) : 389-394.

[91] Lee, J.-M., Kim, D.-W., Jun, Y.-D., and Oh, S.-G. Preparation of silica-silver heterogeneous nanocomposite particle by one-pot preparation strategy suing polyol process: Size-controlled immobilization of silver nanoparticles. *Mater. Res. Bull.* 4 (2006) : 1407-1416.

[92] Srivastava, D.N., Perkas, N., Zaban, A., and Gedanken, A. Sonochemistry as a tool for preparation of porous metal oxides. *Pure Appl. chem.* 74 (2002) : 1509-1517.

[93] Suslick, K.S., Choe, S.B., Cichowlas, A.A., and Grinstaff, M.W., Sonochemical Synthesis of Amorphous Iron, *Nature* **353** (1991) : 414-416.

[94] Gedanken, A.,Tang, A. Wang, Y., Perkas, N., Koltypin, Y. Landau, M.V. Vradman, L., and Herskowitz, M. Using sonochemical methods for the preparation of mesoporous materials and for the deposition of Catalysts into the mesopores. *Chem. Eur. J.* 7 (2001) : 4547-4552.

[95] Cho, D. H., Change, T. S., Ryu, S. K., and Lee, Y. K. Characterization and catalytic activities of MoMCM-41. *Catal. Lett*. 64 (2000) : 227-232.

[96] Zhao, D., Huo, Q., Feng, J., Chmelka, B.F., and Stucky, G.D. Nonionic triblock and star diblock copolymer and oligomeric surfactant syntheses of highly ordered, hydrothermally stable, mesoporous silica structures. *J. Am. Chem. Soc.* 120 (1998) : 6024-6036.

[97] Halpin, B., Pressey, R., Jen, J., and Mondy, M. Purification and characterization of peroxidase isoenzymes from green peas (*Pisum sativum*). *J. Food Sci.* 54 (1989) : 644-649.

[98] Dai, Z., Xu, X., Lina, Wu, and Ju, H. Mesoporous materials promoting direct electrochemistry and electrocatalysis of horseradish peroxidase. *Electroanalysis*. 17 (2005) : 862-868.

[99] Montiel,C., Terrés, E., Domínguez,J-M., and Aburto, J. Immobilization of chloroperoxidase on silica-based materials for 4,6-dimethyl dibenzothiophene oxidation. *J. Mol. Cat. B: enzyme*. (2007) : 90-98.

[100] Rezwan, K., Meier, L.P., and Gauckle, L.J. Lysozyme and bovine serum albumin adsorption on uncoated silica and AlOOH-coated silica particles: the influence of positively and negatively charged oxide surface coatings. Biomaterials 26 (2005) : 4351–4357.

[101] Caramori, S.S., and Fernandes, K.F. Covalent immobilization of horseradish peroxidase onto poly (ethylene terephthalate) –poly (aniline) composite. *Process Biochem.* 39 (2004) : 883-888.

[102] Carrodo, K.A., Macha, S.M., and Tiede, D.M., Effects of Surface Functionalization and Organo-Tailoring of Synthetic Layer Silicates on the Immobilization of Cytochrome *c. Chem. Mater.* 16 (2004) : 2559-2566.

[103] Lei, Z., Zhang, L., and Wei, X., One-step synthesis of silver nanoparticles by sonication or heating using amphiphilic block copolymer as templates. *J. Colloid Inter. Sci.* 324 (2008) : 216-219.

[104] Ariga, K., Vinu, A., Hill J.P., and Mor, I. T. Coordination chemistry and supramolecular chemistry in mesoporous nanospace. *Coord. Chem. Rev.* 251 (2007) : 2562-2591.

[105] Weiping, C. and Lide, Z. Cai, W., and Zhang, L. Synthesis and structural and optical properties of mesoporous silica containing silver nanoparticles. *J. Phys. : Condens. Matter* 9 (1997) : 7257-7267.

[106] Guari, Y., Thieuleux, C., Mehdi, A,. Reyè, C., Corriu, R. J. P., Gomez-Gallardo, S., Philippot, K., Pethkar, A.V., Kularni, S.K., and Paknikar, K.M. Comparative studies on metal biosorption by two strains of Cladosporium cladosporioides. *Biores. Technol.* 80 (2001) : 211-215.

[107] Kotz, J.C., and Purcell, K.F. *Chemistry Chemical Reactivity*. 2 nd edition. Philadelphia: Saunders College Publishing. 1991.

[108] Mureseanu, M., Reiss, A. stefanescu, I., David, E., Parvulescu V., Renard G. and Hulea, V. Modified SBA-15 mesoporous silica for heavy metal ions remediation. *Chemosphere* 73 (2008) : 1499–1504.

[109] Sondi, I., Goia, D.V., and Matijević, E. Preparation of highly concentrated stable dispersions of uniform silver nanocomparticles. *J. Colloid Inter. Sci.* 260 (2003) : 75-81.

[110] Suber, L., Sondi, I., Matijević, E., and Goia, D.V. Preparation and the mechanisms of formation of silver particles of different morphologies in homogeneous solutions. *J. Colloid Inter. Sci.* 288 (2005) : 489-495.

[111] Long, D., Wu, G., and Chen, S. Preparation of oligochitosan stabilized silver nanoparticles by gamma irradiation. *Radiat. Phys. Chem.* 76 (2007) : 1126-1131.

[112] Merga, G., Wilson, R., Lynn, G., Milosavljevic, B.H., and Meisel, D. Redox catalysis on "naked" silver nanopartilces. *J. Phys.Chem. C* 111 (2007) : 12220-12226.

[113] Alvarez-Puebla, R.A., Arcco, E., and Goulet, P.J.G. Role of nanoparticles surface charge in surface-enhanced Raman scattering. *J. Phys. Chem.* B 109 (2005) : 3787-3792.

[114] Jiang, Z.J., and Liu, C.-Y. Seed-mediated growth technique for the preparation of a silver nanoshell on a silica sphere. *J. Phys. Chem.* B 107 (2003) : 12411-12415.

[115] http://en.wikipedia.org/wiki/Scherrer_Equation. 04 April, 2005.

[116] Ma, S., Lu, W., Mu, J., Liu, F., and Jiang, L. Inhibition and enhancement of glucose oxidase activity in a chitosand-based electrode filled with silver nanoparticles. Colloids and Surface A: Physicochem. *Eng. Aspects* 324 (2008) : 9-13.

[117] Wu, Z., Xiang, H., Kim, T., Chun, M.-S., and Lee, K. Surface properties of submicrometer silica spheres modified with aminopropyltriethoxysilane and phenyltriethoxysilane. *J. Colloid. Inter. Sci.* 304 (2006) : 119-124.

[118] Ma, S., Mu, J., and Jiang, L. Chitosan-Based Glucose Oxidase Electrodes Enhanced by Silver Nanoparticles. *J. Disper. Sci. technol.* 29 (2008) : 682-686.

[119] Wang, A., Wang, H., Zhou, C. Du, Z., Zhu, S., and Shen, S. Ag-induced efficient immobilization of Papain on silica spheres. *Chinese J. Chem. Eng*. 16 (2008) : 612-619.

[120] Ruzgas, T., Csoregi, E., Emneus, J., Gorton, L., and Marko-Varga, G. Review Peroxidase-modified electrodes: Fundamentals and application. *Analyt. Chimica Acta* 330(1996) : 123-138.

APPENDIX

APPENDIX
PUBLICATIONS

[1] Chouyyok, **W.,** Panpranot, J., Thanachayanant, C., and Prichanont, S. "Effects of pH and Pore Characters of Mesoporous Silicas on Horseradish Peroxidase Immobilization", *J. Mol. Catal. B: Enzym*. 56 (2009) : 246-252.

[2] Punwittayakool**,** S., **Chouyyok, W.,** and Prichanont, S. "Immobilization of Horseradish Peroxidase in the Composition Material of Mesoporous Silica and Chitosan", The 17th Thailand Chemical Engineering and Applied Chemistry Conference, October 29-30, 2007, Chiang Mai, Thailand.

VITAE

Miss Wilaiwan Chouyyok was born on November 15th, 1975 in Phatthalung, Thailand. She received the Bachelor's Degree of Science from the Department of Agricultural Industry, King Mongkut's Institute of Technology Ladkrabang in 1998. After graduation, she enteredstudy for a Master's Degree with a major in Chemical Engineering at the Department of Chemical Engineering, Faculty of Engineering, Chulalongkorn University and completed the program in 2002. In 2004, she continued her Doctoral Degree in Department of Chemical Engineering, Faculty of Engineering, Chulalongkorn University.